We thank the reviewer for the careful reading of the manuscript and the fruitful comments. Please find below our point-by-point replies:

I. General Comments

GC1. The current model setup is not clear to the reviewer and section 2.1 on the model setup needs to be improved for clarity. I guess the PISCES ecosystem model is run off-line with physical transport, T, and S fields taken from a physical ocean only simulation. I guess the ocean only simulation is forced with repeated time-varying surface temperature and salinity fields taken from observational data for years 1948 to 2009. In my opinion section 2.1 needs a rewrite and should be structured in a much better way. The description of the setup of the model used to get the forcing fields (circulation, T, S?) to drive PISCES and the spin up and drift of this part of the model chain should be clearly separated from the setup of PISCES.

- PISCES model is run off-line for this work, with the physical transport, temperature, and salinity fields taken from a physical ocean NEMO simulation. This NEMO simulation was driven five times (310 years) for the years 1948 to 2009 (Skyllas et al., 2019). For all PISCES offline simulations, we used the same 1-year physical ocean forcing. This one year was calculated as a multi-year daily mean over the 5th iteration 1948-2009 of the 310-year NEMO simulation. This way we removed interannual variability and any long-term trend in the physical forcing but conserved the full seasonal cycle on a daily basis. To avoid confusion, we rewrote Sect. 2 adding further analyses by including separately a description of the forcing data (Sect. 2.1.1) and a description of the PISCES model setup (now Sect. 2.1.2):
  "2.1.1 Physical Ocean forcing
  The dynamical physical outputs used to force PISCES for this study are produced by the physical ocean model NEMO, following the protocol of the OMIP simulation (Ocean Modelling Intercomparison Project; Orr et al., 2017). OMIP aims at harmonizing forcing fields of boundary conditions, as well as validation and analysis procedures among different ocean models. Atmospheric forcing fields are from the CORE II forcing (Coordinated Ocean-ice Reference Experiments - Phase II; Large & Yeager, 2009). CORE II provides a 62-year interannual forcing for the period 1948-2009. The physical model is initialized with gridded observational data from the World Ocean Atlas 2013 and then ran for 310 years by repeating the 62-year CORE II forcing. The necessary physical variables to force the offline biogeochemical model PISCES (see Table S1) are taken from the last 62-year iteration. To avoid, however, any long-term trends from spin up, the multi-year (1948-2009; i.e., the 5th iteration of the 310-year run) mean of daily forcing fields was calculated. The resulting mean 1-year forcing thus contains the mean seasonal cycle and was (repeatedly) applied to drive all simulations with the biogeochemical PISCES offline model. All biogeochemical simulations were initialized and forced with the same physical fields from the average 1-year forcing derived from the OMIP run. Thus, all the PISCES offline simulations are drift-free in physical variables. More details of the OMIP protocol can be found in Orr et al. (2017) and a first validation of the OMIP run is provided by Skyllas et al. (2019)."

"Table S1. Physical forcing fields provided at a daily time step.

Water flux into seawater	*$kg/m^2/s$*
Mixed layer depth	*m*
Surface net downward shortwave flux	*W/m^2*
Wind speed	*m/s*
Ice concentration	*%*

Water flux due to freezing/melting	$kg/m^2/s$
Tracer diffusive fluxes along the bottom boundary layer	m^3/s
River runoff	$kg/m^2/s$
Ocean vertical salt diffusivity	m^2/s
Horizontal divergence transport	*1/s*
Seawater salinity	*g/kg*
Seawater potential temperature	*°C*
Effective ocean transports	m^3/s

GC2. Simulated changes in nutrient concentrations and productivity are relatively modest. The question arises whether the difference in simulated surface nutrient concentrations (Fig. 2) and productivity (Fig. 6) between PI, present and future periods are only due to differences in the deposition fields as implied by the manuscript or also influenced by other factors. Namely, model drift and, potentially also very important, differences in the physical fields used to force PISCES between the three period of interests could be responsible for some of the differences. I am not sure and I may be wrong, but I have the impression that the physical fields used to force PISCES are taken from different nominal years of the ocean only simulations and therefore different ocean circulation fields could explain part of the simulated differences in nutrient concentrations and productivity. I also miss the mentioning of a true control run with constant deposition and identical forcing as the standard transient runs with time-varying deposition. This would allow the authors to correct for drifts and changes related to physical forcing. As modelled changes are relatively small, this appears particularly important.

- We thank the reviewer for attracting our attention to this issue. Indeed, all simulations of this work were performed with the same forcing data. The only difference among the simulations was the atmospheric nutrient inputs to the ocean; thus, the differences in oceanic surface concentrations and productivity between PAST, PRESENT, and FUTURE periods are only due to the respective deposition fields considered by PISCES. We agree with the reviewer that a true control run that would correspond to a simulation with constant PI deposition and identical forcing as the transient simulation with time-varying deposition presented in the paper would be the appropriate way to show that the model drift in our simulations is low. For this, we now include a control run (i.e., with constant preindustrial deposition and identical forcing as the standard transient runs) that used for the drift correction of model results, i.e., the nutrient concentrations and marine productivity fields that are presented in the manuscript. The model drifts are calculated here using the linear detrend operator of the CDO (climate data operators) software. Although the impact is minimal thus without changing at all our conclusion, we have also updated all figures based on the resulted drift corrections and we added the following part in the new Sect. 2.1.2, i.e., "*To account, however, for potential drifts, a control simulation as for STD but using only preindustrial (i.e., the year 1850) atmospheric nutrients (N, P, and Fe) inputs into the global ocean is also performed. For example, Fig. S1 demonstrates that for the main ocean basins the drift is minimal after 1850 and clearly below the signal imposed by the altered nutrient deposition. This holds even for the Southern Ocean where the impact of atmospheric deposition is typically weak due to the absence of neighbored emission sources. Nevertheless, all model results presented in this work have been adjusted by subtracting the drift of the control run from STD.*"

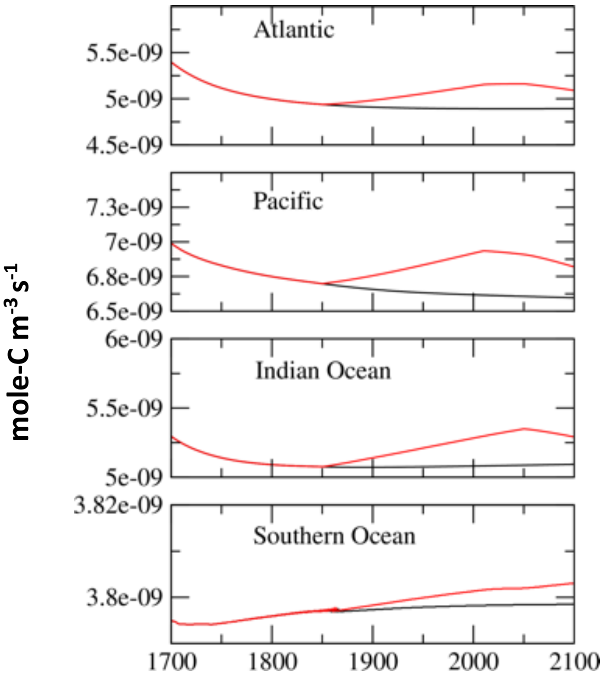

Figure S1: Area averaged annual mean primary production in mole-C m^{-3} s^{-1} for the main ocean basins. Red lines indicated primary production rates for the STD simulation and black lines the CTRL simulation, respectively.

GC3. Further, I am wondering whether the four figures with 27 maps used to compare simulated with observed fields are really that relevant for this study. They distract from the other, very nice and important figures. Surface nutrient and productivity fields for PISCES have been compared with observations in earlier studies. These simulated fields result predominantly from physical transport of nutrients within the ocean and from the PISCES model itself, whereas the role of atmospheric deposition is rather marginal. The comparison in these four figures tells us, in my opinion, not much about the topic of this study – atmospheric nutrient deposition. They may be included in an appendix and the corresponding text can, in my view, be drastically shortened.

- We agree with the reviewer that the model evaluation part may distract the reader from the main conclusions of this work. For this, we now moved all model evaluation figures and the respective discussion to the supplement.

GC4. On the other hand, I miss some assessment how changes in deposition influence surface nutrients or productivity regionally. Is this due to local effects/deposition? Or is there an influence of ocean surface transport in bringing deposited material to other regions? I have not firm recommendation, but some analysis would be useful. I could imagine to correlate changes in deposition fields with changes in simulated fields or to run factorial simulations with deposition varying only in certain regions, though this may be too CPU expensive.

- Indeed, to really distinguish the local depositional forcing and the second-order effect of advection of unutilized nutrients on the local productivity would require several additional sensitivity simulations, not currently feasible with available resources. However, we note that in areas where a specific nutrient is not limiting, advection to remote places is highly likely. For the revised version, further analysis has been carried out to investigate and demonstrate this for e.g., the North Pacific in the new section 3.2.1 as well as in the new Discussion Section (i.e., Sect. 5 in the new version of the manuscript). Besides, an additional sensitivity simulation was performed with a constant P deposition, which demonstrated the importance of iron and nitrate compared to phosphorous.

GC5. I miss a figure that shows time series of the prescribed transient evolution of globally averaged deposition of N, P, Fe, from 1850 to 2100. Potentially one could show in this figure also the share of inorganic and organic forms or different sources. This figure should also include a time serie(s) representing the evolution of the applied physical forcing (e.g. global mean sea surface temp or SAT). In this way, the reader could quickly understand how and what is varied in the simulations and this figure would complement the table and current Fig. 1

- We agree with the reviewer that such a figure would be useful in case of a transient evolution of nutrient deposition fields and physical forcing. However, as we stated in Sect. 2, the nutrient inputs to the ocean for PAST, PRESENT, and FUTURE periods are due to an atmospheric simulation using the emission for the years 1850, 2010, 2050, and 2100, respectively. In more detail, the available atmospheric nutrient deposition inputs to the ocean are based on anthropogenic and biomass burning emissions along with the resulted atmospheric chemistry impacts on the gas- and particulate-phases for the single years 1850, 2010, and 2100. Note, however, that a transient simulation of atmospheric tracers from 1850-2100 would require extremely high computational power for the atmospheric chemistry and transport model (which is extremely cost-intensive due to a high number of chemical tracers to be advected and an extremely short time step required for atmospheric models). Therefore, we followed the coordinated CMIP protocol to investigate the effects of atmospheric chemistry AerChemMIP (Collins et al., 2017; https://gmd.copernicus.org/articles/10/585/2017/gmd-10-585-2017.pdf) which recommends only single year emission forcings defined for a limited number of 4 to 6 different year between 1850-2100. Furthermore, compared to the ocean, the atmosphere is comparably well mixed and biomass burning, as an additional source, will be in equilibrium within maximal a couple of months in the atmosphere. The applied physical forcing is kept constant for all simulations of this study, and the whole period (PAST, PRESENT, and FUTURE). This is now clearly stated in Sect. 2.1.1 (see also our reply in GS1).
However, we now provide a new figure in the Supplement that shows the globally averaged atmospheric deposition data simulated by CTM and applied for PISCES. The following text is added in the manuscript (Sect. 2.2): "*An example of the globally averaged N, Fe, and P atmospheric deposition data as simulated be CTM and applied in PISCES is presented in Fig. S2. Hence, the here discussed simulations should be considered as idealized sensitivity experiments to estimate the response on the ocean surface biogeochemical properties to changed atmospheric deposition.*"

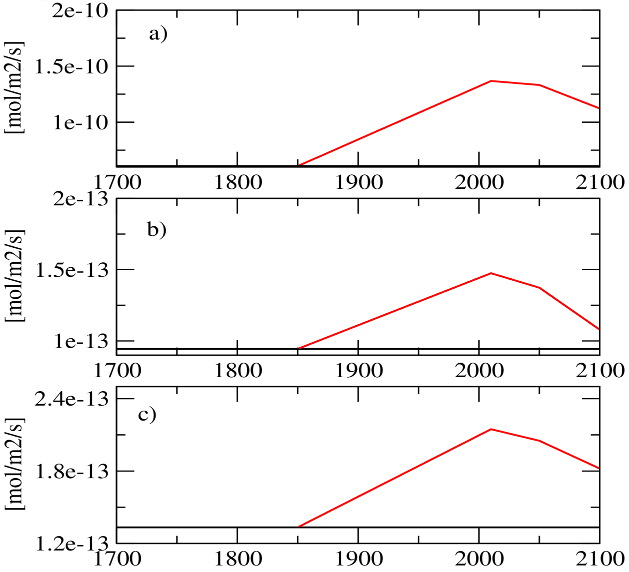

Figure S2: Globally averaged atmospheric deposition fluxes (red lines) of a) nitrogen, b) phosphorous, and c) iron in mol m^{-2} s^{-1}, as simulated by the atmospheric chemistry and transport model and taken into account in PISCES. The black line indicates forcing for the control run under preindustrial conditions (i.e., year 1850).

II. Specific Comments

SC1. P1, l9: Immediately when reading the abstract one starts to wonder what kind of physical ocean model is used to power PISCES. Please clarify that PISCES is coupled offline (?) to a forced ocean only simulation.

- We propose to add the following sentence in the abstract: '*PISCES, as part of the EC-Earth model suite, runs here in offline mode using prescribed dynamical fields as simulated by the ocean model NEMO.*'

SC2. P1, l9: Please mention how atmospheric CO_2 and climate change is included.

- As our study focuses on nutrient cycling and productivity which in NPZD models are independent of atmospheric CO_2 (or dissolved inorganic carbon in the water), we think it's better not to mention the atmospheric CO_2 mixing ratio in the abstract since it is not a central topic of our study, i.e., the effect on acidity and carbon fluxes is not in the focus here. All the simulations are forced by preindustrial pCO_2 and this is now clearly stated in the revised manuscript, both in the model description and the Summary sections, i.e., "*Moreover, the atmospheric CO_2 mixing ratio is set to the preindustrial value of 284.7 ppm, to effectively isolate the impact of atmospheric deposition on the marine biogeochemistry parameters.*"

  Overall, climate change is not considered here. Our idealistic approach allows us to isolate the effect of atmospheric chemistry and transport changes on productivity undisturbed from any other physical changes and longer-term variability. With climate change included, the conclusion drawn in this study would not be possible or, less robust. However, a detailed discussion on how climate change would affect our results is provided in the new Discussion section now.

SC3. P3, l29: Is it correct to say that Fe-containing combustion aerosols are mainly deposited in the Pacific and Southern Ocean? Or do you mean that combustion aerosols play a larger role (compared to dust) in these regions?

- We agree with the reviewer. This part now reads as: '*However, the aerosols from natural and combustion sources tend to be deposited in different regions of the oceans. For example, the subtropical North Atlantic Ocean and the Arabian Sea receive the majority of Fe originated from natural dust aerosols, in contrast to the Pacific and Southern oceans where the Fe-containing combustion aerosols play a more important role compared to atmospheric dust (Hamilton et al., 2020; Ito et al., 2019b).*'

SC4. P5, l19-22: I do not understand what the authors want to say here. Is PISCES now fully coupled online to NEMO and the EC-Earth ESM or rather forced offline with an OMIP simulation? I think it should read: "The state-of-the art biogeochemistry PISCES model is here run "offline" with prescribed transport and T, and S fields (see sec. 2.1). The version of PISCES implemented within NEMO and the European Earth System Model EC-Earth is used in this study. PISCES simulates the . . .

- This part now reads as: "*The state-of-the-art biogeochemistry model PISCES (Aumont et al., 2015), enabled here within the framework of the European Community Earth System Model EC-Earth (http://www.ec-earth.org/), is here used in offline modus to investigate the impact of atmospheric deposition fluxes of N, Fe and P on the marine productivity. PISCES (Pelagic Interactions Scheme for Carbon and Ecosystem Studies volume 2), as a part of the Nucleus for European Modelling of the Ocean (NEMO), includes a detailed representation of the lower trophic levels of marine ecosystems.*"

  Moreover, a new section (i.e., Sect. 2.1.1) that describes in detail the forcing data used to run PISCES is now added (please see our reply to SC1).

SC5. P6, l5: please specify the physical output used to force PISCES.

- Please see our reply to GC1.

SC6. P6, l6: which OMIP simulation?

- Please see our reply to GC1.

SC7. P6, l6: Please specify how the 1948 to 2009 forcing is aligned in the spin-up of PISCES and the transient simulation from 1850 to 2100.

- Please see our reply to GC1.

SC8. P6, l7: I guess this refers to the spin up for ocean model without PISCES? Please clarify.

- Please see our reply to GC1.

SC9. P6, l8-l10: again – to which simulation or model does this initialization apply?

- Please see our reply to GC1.

SC10. P6, l8-l10: I guess there are still substantial drifts in O_2, N, Si, P and Alk after such a short spin up of 300 years only. Please specify how large the drifts are.

- For this work, we analyzed the results from 1851 to 2100 (namely, PAST: 1851–1870 average, PRESENT: 2001–2020 average, and FUTURE: 2081–2100 average). For the revised version, however, we also performed a control simulation with constant preindustrial deposition inputs (N, Fe, and P) and identical forcing as the STD and ORG transient runs. This new simulation is used for the drift corrections of the model results (please see also our reply to GC2). According to the new control simulation, however, the resulted drifts in surface properties are low and can be considered in equilibrium, without changing our conclusions. Regarding the oceanic concentrations of O_2, N, Si, P, and Alk, we present below the relative differences between the drift-corrected and the uncorrected annual mean oceanic concentrations of i) O_2, ii) N, iii) Si, iv) P, v) Fe and vi) Alk, for depths from the surface up to ~100m.

i)

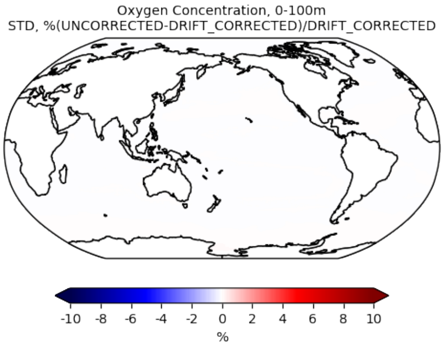

ii)

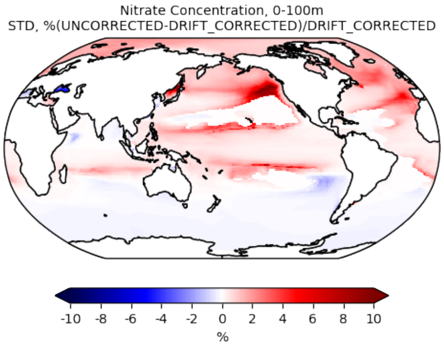

iii)

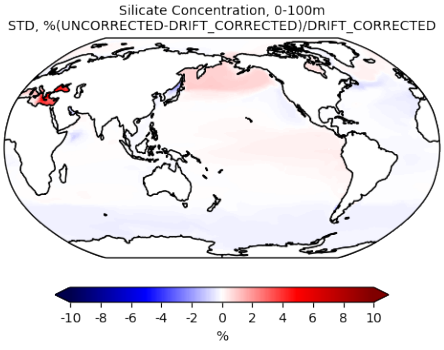

iv)

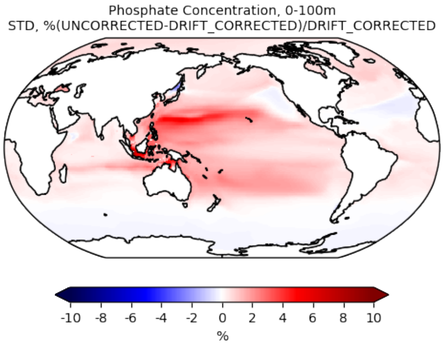

v)

vi)

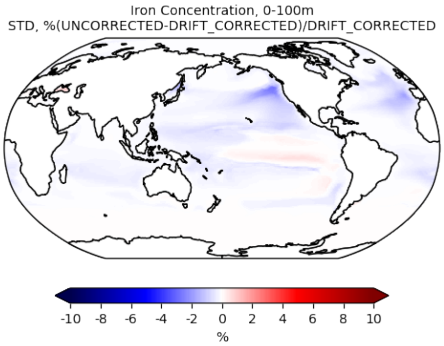

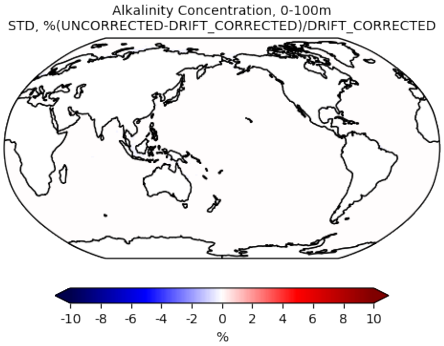

According to the above plots, it is obvious that for O_2 and Alkalinity the drifts are minimal, i.e., ~0.01% and -0.15%, respectively for their global average concentrations. For Si and Fe, the drifts are also very low i.e., ~ -0.15% and -0.07%, respectively, for their annual mean concentrations, whereas for the (closely related in the model) N and P, the drifts are calculated somehow higher compared to other fields (regionally up to 10% in the Pacific Ocean). Nevertheless, for their global average concentrations, the drifts are calculated equal to ~ -0.08% and 0.04%, respectively. Note that we present here the mean relative differences of the oceanic concentrations for the period 1851-1870 (hence after 200 years of spin-up) and 0-100m depths.

For the revised version, we also calculated the drifts for vii) Primary Production and viii) Nitrogen Fixation. Again, the drifts as relatively low for the PAST period (i.e., after 200 years spin-up). The global annual mean primary production and nitrogen fixation change due to drift corrections of about 0.11% and -0.04%, respectively. In more detail, the “uncorrected” primary production equals to 45.64 Pg-C yr^{-1}, and the drift-corrected equals to 45.59 PgC yr^{-1}, thus a difference ~ 0.05 Pg-C yr^{-1} for the PAST period. Respectively, the “uncorrected” N-Fixation equals to 111.87 Tg-N yr^{-1}, and the drift-corrected equals to 111.92 Tg-N yr^{-1}, a difference roughly 0.05 Tg-N yr^{-1}.

vii)

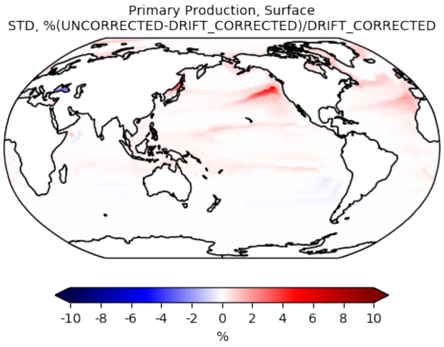

viii)

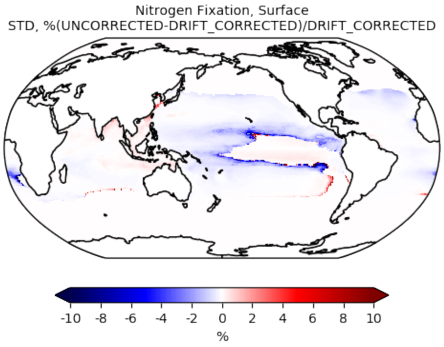

All in all, we conclude here that there is not a substantial drift in our simulations. However, we agree with the reviewer’s comment that it is scientifically more appropriate to account for any potential model drifts when present our results, and for this, in the revised version all results are corrected (please see also our reply to GC2). The following part is added in the model description section: “*To account, however, for potential drifts in the deeper ocean layers, a control simulation as for STD but using only preindustrial (i.e., the year 1850) atmospheric nutrients (N, P, and Fe) inputs into the global ocean is also performed. For example, Fig. S1 (see Sup. Mat.) demonstrates that for the main ocean basins the drift in vertically integrated primary production is minimal and clearly below the signal imposed by the altered nutrient deposition after 1850. This holds even for the Southern Ocean where the impact of atmospheric deposition is typically weak due to the absence of neighbored emission sources. Nevertheless, all model results presented in this work have been adjusted by subtracting the drift of the control run from STD.*”

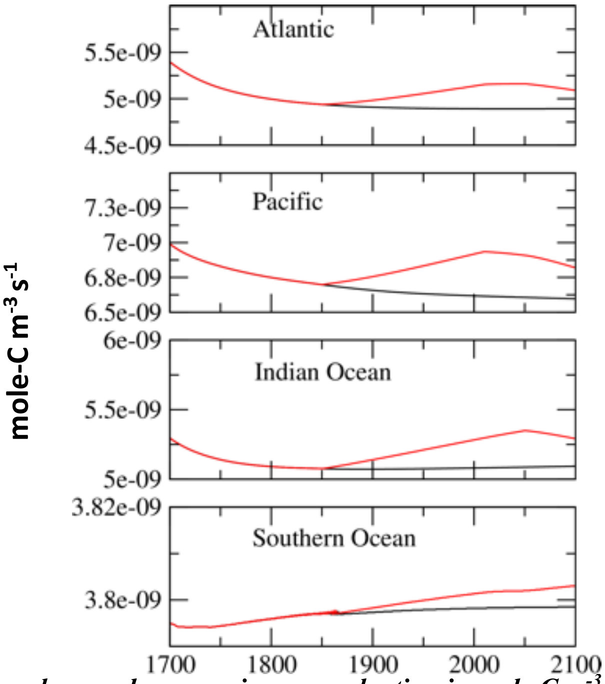

Figure S3: Area averaged annual mean primary production in mole C m^{-3} s^{-1} for the main ocean basins (Atlantic, Pacific, Indian and Southern Oceans). Red lines indicate primary production rates for the STD simulation and black lines the CTRL simulation, respectively.

SC11. P6, l8-10: Is there any initialization of DIC or DOM?

- The following part is now added: "*For the initialization of the ocean biogeochemical fields, the climatological fields of oxygen, nitrate, silicate, and phosphate from the World Ocean Atlas 2009 (WOA; Garcia et al., 2010a, 2010b) along with dissolved inorganic carbon (DIC) and alkalinity from the Global Ocean Data Analysis Project (GLODAP; Key et al., 2004) were adopted.*"

SC12. P6: What is the role of global warming/climate change in these simulations?

- To effectively isolate the impact of atmospheric deposition into the ocean, we did not account for any global warming/climate change. This is now clarified in the new Sect. 2.1.2.

SC13. P6: Has a true control run with constant dust deposition and same physical forcing be applied for the 1850 to 2100 period? The drift in critical variables should be quantified.

- We now include a "true" control run with constant preindustrial (the year 1850) deposition fields to remove any potential drifts from our results. Please see our reply to GC2.

SC14. P6, l29: I find the labeling of the first simulation as "CTRL" very misleading. For me this is the standard simulation with time-varying deposition forcing. Please select another name for this simulation.

- We agree with the reviewer. We changed the name of the first simulation from CTRL to STD.

SC15. P7, l5: Here a second spin-up is mentioned. The structure of the section is confusion, switching between a first spin-up (of the ocean model), transient PISCES simulation, a second spin up (for PISCES?) and again transient simulation. Please streamline the structure of section 2.1

- We improved this section and added further analyses. Please see our reply to GC1.

SC16. P7, l7: No indication is given how this drift is quantified and for which period it holds and whether this is for the global average or for each horizontal grid cell. Please specify.

- Please see our reply to GC2.

SC17. P6, l7: Is the physical forcing to PISCES identical for the three periods (past, present, future). If not, what would be the implication of differences in the physical forcing?

- Yes, the physical forcing is identical all periods as stated and for all runs. This is now clearly documented in the revised text. Please see our reply to GC1.

SC18. Section 2: A figure showing the time series of global mean deposition of P, N, and Fe would be really useful.

- The global mean deposition of P, N, and Fe are kept constant before 1850. However, after the 200 years spin-up period (1651 until 1850), the atmospheric deposition input data for the STD and ORG simulations were linearly interpolated from preindustrial to present-day conditions (i.e., the year 2010) to smoothly capture the transition from past to the modern conditions (e.g., Krishnamurthy et al., 2009). Respectively, the deposition data from the present day were linearly interpolated to the projected estimates (i.e., the years 2050 and 2100). Please see also our reply to GC5.

SC19. Section 2.2 A note how these atmospheric deposition fluxes compare with the riverine input would be helpful.

- The following sentences are added in the manuscript:
    - Sect. 2.1.1*: The river supply of N in the model is 36 Tg-N yr*$^{-1}$.
    - Sect. 2.1.2*: For comparison, we note that the total riverine Fe supply in the model equals 1.45 Tg-Fe yr*$^{-1}$.
    - Sect. 2.1.3*: Note also that in the model, DP of roughly 3.7 Tg-P yr*$^{-1}$ *is also delivered to the ocean by rivers.*

SC20. Section 2.2. A note how these atmospheric deposition fluxes compare with export (or new) production of P, Fe, N (as particulate and dissolved organic forms)

- The export production in the model for the present-day (STD simulation) is calculated to ~7.54 Pg-C yr^{-1}. Accounting however for the Redfield ratio used in the model (i.e., C/N/P = 122/16/1), the export production for N and P, it would correspond to 1.15 Pg-N yr^{-1} and 0.16 Pg-P yr^{-1}, respectively. Moreover, according to the explicit model calculation, the export production for Fe is about 0.79 Tg-Fe yr^{-1}.

SC21. P11, l29: Is production limited by light as suggested here or also be Fe?

- Yes, the production is also limited by light, as we also stated in the manuscript, i.e., "*PISCES includes two types of phytoplankton, namely nanophytoplankton and diatoms, and it simulates the chlorophyll concentrations and the growth of phytoplankton based on the availability of nutrients (i.e., DP, DN, and DFe for nanophytoplankton and DP, DN, DFe, and DSi for diatoms), temperature and light.*" Moreover, we now provide a new figure which presents the factors that are important in limiting productivity in our model (Fig. 4), i.e., the limitations for nanophytoplankton production by nutrients (N, P), light, and iron.

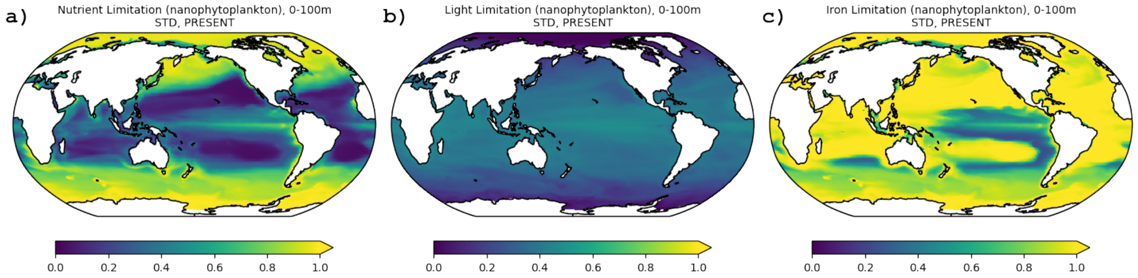

Figure 4: Limitation for nanophytoplankton production by nutrients (N, P right), light (middle), and iron (left). Low values indicate the high limitation imposed by the property.

SC22. P17, l8: Please state how PISCES is forced and what circulation fields are used.

- Please see our reply to GC1.

SC23. P17, l14-20: Part of this text should be mirrored in section 2 where the model setup is described. For example, the mentioning of salinity restoring comes somewhat at a surprise as it is not clear from section 2 that restoring boundary conditions are applied. Similarly, you talk about a prolongation of the OMIP simulation using an RCP8.5 scenario run. Again, this seems not to be described in the method section. Please provide a complete description of the model setup in section 2.

- We acknowledge that there is a basic misunderstanding in this part. For this work salinity restoring was only applied during the OMIP run from which the forcing for the offline model was generated (please see also our reply to GC1). The salinity of the biogeochemical offline runs is kept, however, constant, representing only a seasonal cycle on a daily basis. Since the prolongation of the run for the RCP8.5 scenario is not that relevant for this study, this statement is now removed from the text to avoid any further confusion.

SC24. P20: It would be very useful for the community if the deposition files would be made available, e.g. as NetCDF files, to the community. I miss a corresponding data availability statement.

- We thank the reviewer for this suggestion. The deposition fields will be freely accessible to the community through the Zenodo. A relevant statement is added to the Data availability section at the end of the manuscript.

We thank the reviewer for the careful reading of the manuscript and all the fruitful comments and suggestions. Please find below our point-by-point replies:

I. General Comments

GC1. While the authors systematically validated their present day simulation against observations and described the effects of their new atmospheric nutrient deposition fields on surface ocean nutrient concentrations, as well as the rates of primary production and nitrogen fixation, I found that the quantity and organization of the material eclipsed crucial results, and that the depth of the analysis that was presented was somewhat limited. Since the title emphasizes global oceanic productivity, I was expecting significantly more discussion about the emergent rates of primary production and nitrogen fixation (currently ~1 page combined). That biological productivity/nitrogen fixation is relatively stable at the global scale while more significant changes occur regionally implies a compensatory mechanism, which is not really explored. I was looking for more information supported by encompassing and generalizing diagnostics than the numerous supplied maps could provide:

We appreciate the aforementioned valuable and constructive suggestions. Meanwhile, additional simulations were performed, and a deeper analysis of the results allowed more substantial insight into the questions raised by the reviewer. Altogether, this leads to a major revision of the manuscript taking up all the reviewers' suggestions and leading to substantial improvements.

- **How does the ratio of the atmospheric supply of nutrients change regionally/globally?**

  The figure below (middle) shows the N/P ratio of atmospheric deposits relative to the Redfield ratio for the PRESENT and the changes in PAST and FUTURE periods. As can be seen for PRESENT atmospheric fluxes supply, nearly everywhere a surplus of nitrogen compared to phosphorus is demonstrated. By contrast, the same plot for surface water concentrations indicates a deficiency by nitrogen (in agreement with observational evidence). In both FUTURE and PAST periods, the atmospheric N/16P ratio is lowered which would favor N-fixation in warm water regions if not counteracted for by other processes.

  <u>**Atmospheric deposition ratios**</u>

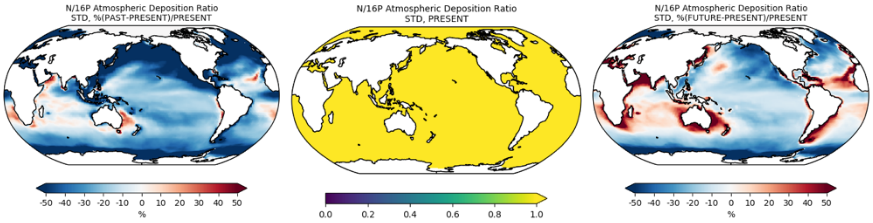

  Atmospheric nutrient deposition fluxes relative to the Redfield ratio for PRESENT (middle; values >1.0 denotes excess of nitrogen compared to phosphorus) and the relative changes for PAST (left) and FUTURE (right) for the STD simulation.

Oceanic Concentration Ratios

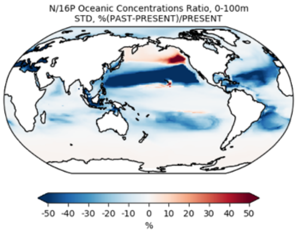

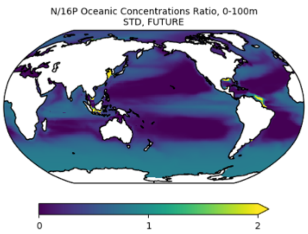

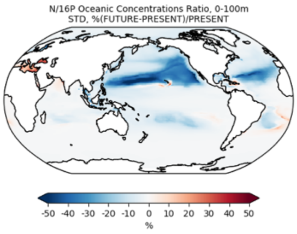

The implications for both productivity and N-fixation and are now discussed in the new Sect. 3.3.1 in the revised version of the manuscript, e.g., "*In regions with significant macronutrient limitations, the elemental ratio of deposited N:P can be, however, important. To estimate the relative impact of the changes in this ratio, we calculated the modeled nitrogen concentrations relative to the model's Redfield ratio (Fig. 5a). For PRESENT, the model exhibits almost everywhere a deficiency with respect to nitrogen (except for some coastal areas). This is in good agreement with data from WOA which likewise indicates a predominant nitrogen deficiency almost everywhere (Fig. 5b). Next, the N:P ratio relative to the Redfield as supplied by atmospheric deposition for PRESENT (middle) together with the changes in PAST and FUTURE (Fig. S8b) is calculated. Hence, a strong excess of N compared to P for modern times is indicated. As a consequence of the model's nitrogen deficiency (Fig. 5a), this atmospheric nitrogen excess maintains higher productivity than without the atmospheric supply. For preindustrial times, the atmospheric N:P ratio is almost everywhere reduced, thus increasing the N-deficiency. Hence, rather the lowered atmospheric nitrogen inputs than the lowered phosphorous inputs in PAST and FUTURE are responsible for the diminished productivity in these experiments. To further demonstrate this, we carried out an additional sensitivity simulation (namely PIP simulation) where, phosphorous atmospheric deposition fluxes kept constant at preindustrial levels, while the other studied atmospheric inputs (i.e., N and Fe) varied as for the STD simulation. As expected, the effect on phosphate concentrations (Fig. S9b) and productivity (Fig. S9d) in this sensitivity simulation remain extraordinarily low, i.e., the relative difference to STD is almost everywhere below 1%. This overall demonstrates that the changes in phosphorus do not play a significant role in marine productivity from preindustrial to future periods.*"

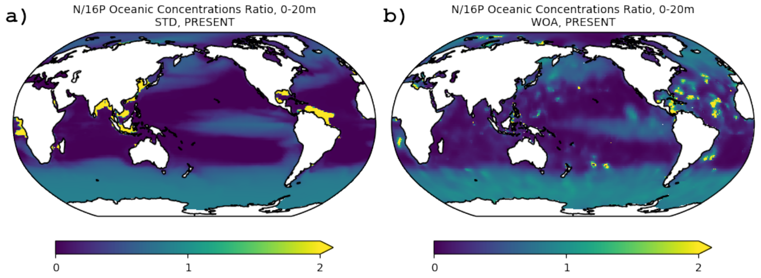

Figure 5: Molar oceanic ratios N:16P averaged in the upper 20m for PRESENT, as calculated by the model (left) and based on World Ocean Atlas (WOA; Garcia et al., 2010b) data (right). Values >1.0 denote overshoot of N vs P relative to the Redfield ratio (C:N:P =122:16:1); blue areas indicate a surplus of P or deficiency of N.

Please find a more detailed discussion in the revised manuscript.

- **How does the combination of these resources promote or inhibit production vs diazotrophy?**

  The answer is complex since it varies regionally. In PAST most of the emitted nitrogen is deposited in cold water regions where the effect on N-fixation is low, while in some warm water regions iron deposition declines and further limits N-fixation by diazotrophs. In the North Pacific iron seems to be the key driver of found changes with cascading effects involving declining diatom production, nutrient accumulation in the subpolar gyre, and advective nutrient transport to remote regions.

  These interesting findings, however, are now detailly discussed in the revised manuscript, i.e., "*PISCES models two phytoplankton functional types: 1) the nanophytoplankton producing calcareous shells and 2) the diatoms producing siliceous shells (Aumont et al., 2015). In the high latitudes, a large part of productivity is related to siliceous diatoms (e.g., Malviya et al., 2016; Uitz et al., 2010) which is accounted for in the model by low nanophytoplankton to diatoms ratios (Fig. 6b). Accordingly, the overwhelming part of productivity reduction in the northernmost Pacific (Fig. 3d) is related to the decline of diatoms. This is well reflected by the increase of the nanophytoplankton to diatoms ratio for PAST relative to PRESENT (Fig. 6a). In turn, this leads to enhanced silicate concentrations in the North Pacific (Fig. 7a). Part of the unutilized silicate is advected southward via the North Pacific Current and the California Current leading also to elevated concentrations along the western coast of North America (Fig. 7a). A further consequence of the strongly diminished productivity is an accumulation of nitrogen in the subpolar gyre of the North Pacific (Fig. 2a). The nitrogen anomaly is strongest in the southwestern area of the gyre and part of the excess nitrogen is injected into the northern California Current. As a result, a strong positive and wedge-shaped productivity anomaly develops in front of western Canada in PAST (see Fig. 3d). The positive anomaly is caused by the increased production of nanophytoplankton productivity (not shown) which dominates in this region (Fig. 6b); north of the wedge lowered iron limits productivity while south of the wedge nitrate is limiting. Altogether, this reflects a slight shift from diatom production to nanophytoplankton in the eastern Pacific north of 40 °N, as indicated by a decline of ~10% of the nanophytoplankton to diatoms concentrations in the upper 20 m (see Fig. 7b).*

  Apart from the northernmost Pacific, the decline in diatom production leads almost everywhere to slightly increased silicate concentrations in PAST (Fig. 7a). Productivity changes in the Southern Ocean remain low (Fig. 3d) for PAST. The reason for this is the strong light limitation around Antarctica (Fig. 4b) and the deep mixed layer which suppresses productivity and subsequently builds up a large pool of unutilized nutrients. Part of the unutilized nutrients is advected further north into the Southern Ocean, driving productivity there. Accordingly, the reduced deposition of nitrogen and iron in this area (Figs. 1a,d) have only a slight impact on productivity. Consequently, this region is relatively robust against external nutrient input maintaining stable productivity. A similar effect is seen for the North Atlantic where vigorous exchange with Arctic waters takes place across the Norwegian-Greenland Sea. By contrast, in the subpolar North Pacific, the import of unutilized nutrients from the Arctic is hampered, as the water exchange with polar waters is limited by the shallow Bering Strait and the Aleutian Arc. Therefore, the North Pacific appears most sensitive to external nutrient inputs."

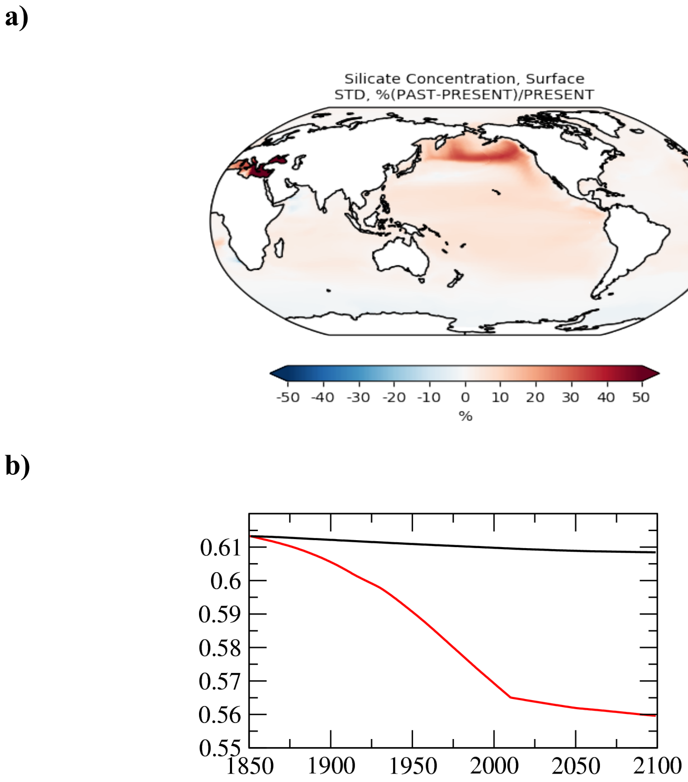

Figure 7: a) PAST to PRESENT relative differences (%) of silicate surface oceanic concentrations of as calculated by the model for the STD simulation; b) Seawater concentration ratio of nanophytoplankton to diatoms in the upper 20m, averaged over the NW Pacific (east of 200°E and north of 40°N). The red line indicates primary production rates for the STD simulation and the black line for the CTRL simulation, respectively.

- **Are phytoplankton (or diazotrophs) consuming critical resources "upstream" that inhibit "downstream" productivity via scarcity or changing nutrient ratios?**

Indeed, we found indications for this in the mid to high latitude North Pacific, where a decline in iron lowers productivity, which leads to enrichment of nitrogen which is subsequently transported southeastward where these waters cause a positive anomaly in nanophytoplankton. A comprehensive analysis is now given in the revised version (see also our reply to the previous comment), e.g.," *The North Pacific turns out to be most sensitive to iron deposition. For the preindustrial period, the lowered input of iron to this region leads to a strong decline of siliceous diatom production leading to an enrichment of silicate, nitrogen, and phosphorus. In turn, this leads to enhanced equatorward transport of nutrients resulting in elevated production rates of calcareous nanophytoplankton in the south-eastern North Pacific. Overall, the North Pacific appears most sensitive to external nutrient deposition mainly due to two reasons: 1) the strongest deposition changes take place in the northern mid to high latitudes, and 2) that compared to the Southern Ocean and the North Atlantic, the exchange with cold and nutrient-enriched polar waters is limited by land by the shallow Bering Strait and the Aleutian arc. By contrast, the southern high latitude ocean contains a large amount of unutilized nutrients that are advected further north (to mid-latitudes) making this region more robust against changes in external nutrient input. In agreement, however, with observational evidence from WOA, PISCES exhibits a widespread surplus of nitrogen compared to phosphorous and with respect to the Redfield ratio. Therefore, the applied changes in phosphorus inputs have nearly no impact on primary production in the model. Note that this applies even to the warm water regions, where reductions* *in atmospheric iron supply limit nitrogen fixation by diazotrophs in both PAST and FUTURE periods.*"

- **Are unutilized nutrients (e.g. Southern Ocean iron in the future) transported away from the surface to reemerge elsewhere and stimulate productivity remotely?**

  Yes, we found the Southern Ocean (and as well the North Atlantic) to be more robust against changes in atmospheric deposition than the N. Pacific. In the Southern Ocean, extremely cold temperatures around Antarctica (thermal isolation due to the ACC) and the widespread lack of iron further delimit productivity and thus nitrogen-enriched water are advected equatorward and maintain vigorous productivity in mid-latitudes where the iron limitation is of minor importance. The additional Fe around Antarctica in FUTURE is deposited around the coast where strong light limitation exists (we show this in the revised version. Therefore, the effect on productivity is low and nutrients are advected equatorward and maintain more or less stable production in the mid-latitudes.

  In the North Pacific injection of nutrient-enriched Arctic waters is effectively suppressed by the shallow Bering Strait and the Aleutian volcanic arc while in the North Atlantic exchange with Arctic waters is maintained by the Norwegian current and East Greenland Current.

  Please find for more details in the revised manuscript, e.g., "*This work documents an overall low impact of atmospheric nutrient deposition scenarios on total marine primary production on a global scale. This is because much of modern productivity is driven by nutrients already recycled in the euphotic zone or by nutrient import from the deep ocean (such as in upwelling regions). Additionally, atmospheric transport appears rather important, as a significant part of nutrient deposition takes place in the northern high latitudes, where light conditions and temperature further limit productivity. Accordingly, even substantial reductions of nitrogen, phosphorus, and iron, ranging between 36 and 51% during the preindustrial period result in an only modest decline of primary production of about 3%. However, substantial local productivity changes of up to 20% were found in regions today limited by nutrients. The strongest sensitivity against atmospheric nutrients is found for the oligotrophic subtropical gyres of the North Atlantic and North Pacific. In these regions, good light conditions and warm temperatures together with low nutrient concentrations predominate. Additional atmospheric nutrient input to this region immediately results in production by increasing the biogenic turnover.*

  The North Pacific turns out to be most sensitive to iron deposition. For the preindustrial period, the lowered input of iron to this region leads to a strong decline of siliceous diatom production leading to an enrichment of silicate, nitrogen, and phosphorus. In turn, this leads to enhanced equatorward transport of nutrients resulting in elevated production rates of calcareous nanophytoplankton in the south-eastern North Pacific. Overall, the North Pacific appears most sensitive to external nutrient deposition mainly due to two reasons: 1) the strongest deposition changes take place in the northern mid to high latitudes, and 2) that compared to the Southern Ocean and the North Atlantic, the exchange with cold and nutrient-enriched polar waters is limited by land by the shallow Bering Strait and the Aleutian arc. By contrast, the southern high latitude ocean contains a large amount of unutilized nutrients that are advected further north (to mid-latitudes) making this region more robust against changes in external nutrient input. In agreement, however, with observational evidence from WOA, PISCES exhibits a widespread surplus of nitrogen compared to phosphorous and with respect to the Redfield ratio. Therefore, the applied changes in phosphorus inputs have nearly no impact on primary production in the model. Note that this applies even to the warm water regions, where reductions in atmospheric iron supply limit nitrogen fixation by diazotrophs in both PAST and FUTURE periods."

- **Are there teleconnections associated with regions of enhanced export and enriched deep water nutrients upwelling elsewhere?**

  Advection by deep waters is generally slow, and significant effects will probably emerge on multi-centennial time scales. Furthermore, diffusive mixing takes place with nutrient-rich deep waters. This makes it difficult to detect in our scenarios. In general, the export of nutrients can take place in regions where light and temperature limit productivity (further constraints relate to iron). The below figure displays exemplary the degree of light limitation for calcareous nanophytoplankton.

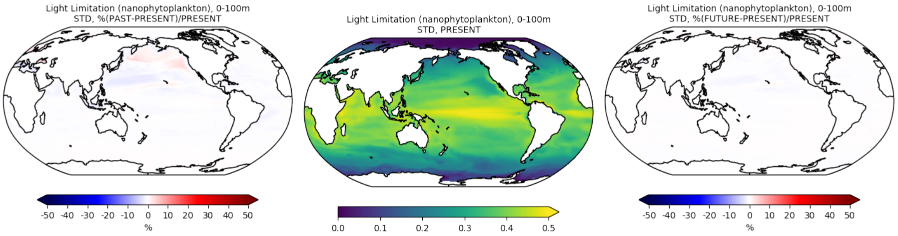

  Low values indicate the predominance of light limitation. Outside the polar regions where light/temperature dominates changes reflect mainly changes forced by altered productivity due to the self-shading effect. In the North Pacific light limitation clearly declines in PAST due to the more effective iron limitation. This leads to enhanced nitrogen transports southwards in regions with predominant N-limitation and subsequently enhanced productivity there.

  In the revised version limitations are discussed in a broader and more comprehensive context including changes in other limiting factors (i.e., nutrients, light, Fe). Please find for more details in the revised manuscript, e.g., “ *Despite the relatively strong changes in total atmospheric nutrient supply from PAST to FUTURE (Table 1), the impact of atmospheric nutrients on the global productivity rates remains low in the model. This is not unexpected, however, as the atmospheric nutrient supply constitutes only a small fraction of the total ocean nutrient inventory. In addition, oceanic regions that are not nutrient-limited today are less sensitive to external nutrient supply. Finally, a large part of primary production is regenerated by remineralized nutrients from particulate organic matter (mainly detritus) in the upper ocean layer.*

  To further identify the oceanic regions that are particularly sensitive to changes in external nutrient inputs, the limiting factors for local productivity in the model are investigated (Fig. 4). Note that we here focused primarily on changes in PAST compared to PRESENT because, in most of the cases, the changed depositional fluxes in FUTURE are roughly in the same direction as in PAST (but lower in magnitude). Figure 4a displays limitations due to nitrogen or phosphorus. High values indicating low limitation are seen in regions that are subject to intense upwelling, like in the equatorial divergence zones or the western margins of NW and southern Africa and South America (coastal upwelling). Accordingly, these regions are less sensitive to atmospheric deposition as nutrients are supplied from deep ocean layers. Lower nutrient limitation is likewise seen in the mid to high latitudes where limitations by temperature and light (Fig. 4b) limit the growth rates. Exceptions are the North Pacific, the Southern Ocean, and the equatorial Pacific where iron limitation matters (Fig. 4c). Consequently, the model’s nutrient sensitivity is largest in the subtropics, in particular in the subtropical gyres where good light conditions and warm waters support high growth rates paralleled by diminished nutrient supply from depth due to Ekman pumping. Furthermore, these regions are far from land nutrient sources and so, a major part of total primary production relates to regenerated production (not directly forced by external nutrient supply). This makes the subtropical gyres sensitive to changes in the external atmospheric nutrient.”

  Please find a more detailed discussion in the revised manuscript.

- **What about silicate (Si) fluxes?**

  Si atmospheric deposition fluxes into the ocean do not change from PAST to FUTURE since they are solely based on present-day dust deposition fields, as simulated from the CTM for the year 2010 (see also our reply in SC8). The atmospheric Si inputs are calculated by assuming a constant fraction of 30.8% Si by weight in the dust. 7.5% of the deposited Si is assumed soluble and thus entered in the dissolved silicate pool of the model upon deposition.

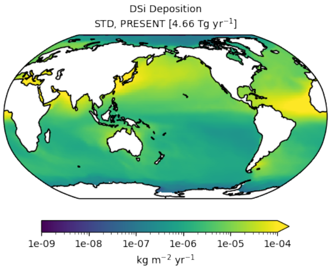

  Simulated changes in PAST and PRESENT oceanic concentrations are therefore related to changed productivity patterns (mainly diatoms). The figures below confirm that due to the lowered productivity in PAST, Si concentrations increase almost everywhere, but stronger in the N-Pacific, and further transport out of the subpolar gyre along the California Current (see below left).

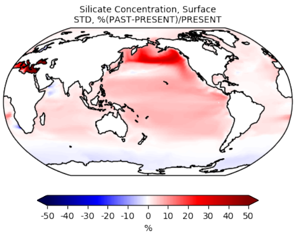

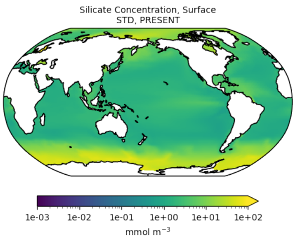

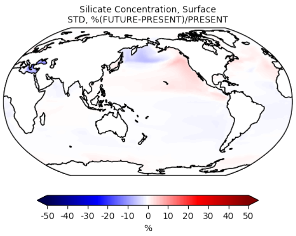

- **How did the composition of phytoplankton functional groups (diatoms vs other phytoplankton) change?**

As an example, we here compare the ratio of nanophytoplankton to diatoms concentration with the iron limitation term in the respective experiments. The above figure shows the ratio of nanoplankton: diatoms (middle) and changes in PAST and FUTURE experiments. The pattern is strongly determined by iron limitation with the strongest impact in the North Pacific where iron and silicate consuming diatoms are diminished compared to nanophytoplankton.

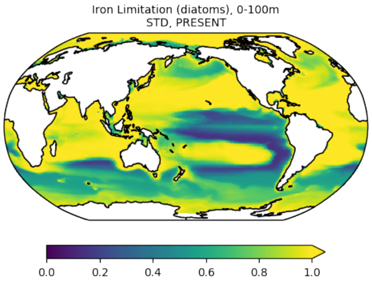

  This likewise explains the higher silicate concentrations in the PAST. The weaker response in the FUTURE with partly decreased iron limitation is related to higher iron inputs in this region compared to PAST and PRESENT. These figures and the respective discussion are now included in the revised manuscript. The following text is added in the revised manuscript: "In the high latitudes, a large part of productivity is related to siliceous diatoms (e.g., Malviya et al., 2016; Uitz et al., 2010) which is accounted for in the model by low nanophytoplankton to diatoms ratios (Fig. 6b). Accordingly, the overwhelming part of productivity reduction in the northernmost Pacific is related to the decline of diatoms. This is well reflected by the increase of the nanophytoplankton to diatoms ratio for PAST relative to PRESENT (Fig. 6a). In turn, this leads to enhanced silicate concentrations in the North Pacific.

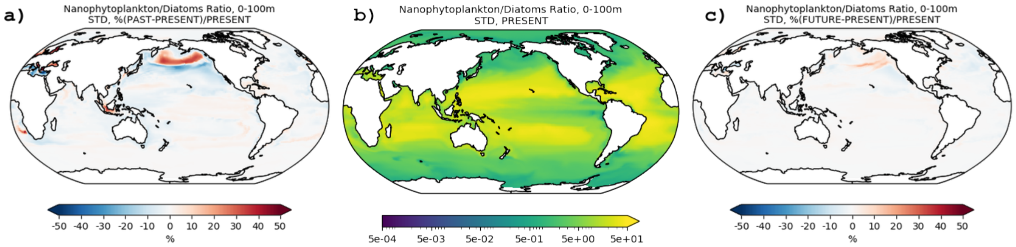

Figure 6: Nanophytoplankton to diatoms oceanic concentrations ratio averaged in the upper 100m for PRESENT (middle), and relative changes for PAST (left) and FUTURE (right) for the STD simulation.

- **Is production limited by a top-down grazing pressure, or a bottom-up resource limitation?**

  Both are true. Grazing by zooplankton delimits phytoplankton production and is most effective during intense blooms. In turn, in oligotrophic regions, the lack of nutrients limits production as well.

- **Some of these issues were touched upon when explaining the counterintuitive higher oceanic P concentrations simulated for the preindustrial era despite lower P deposition, which I found really interesting.**

  Indeed, our simulations demonstrate that the increase in P deposition fluxes into the global ocean from PAST to PRESENT is of minor importance for oceanic productivity. As a result, the present-day phosphate oceanic concentrations are calculated lower, compared to preindustrial times. To further demonstrate this, we performed an additional simulation as for STD, but keeping the DP deposition inputs to preindustrial (PI) levels (namely PIP). As expected, we get almost identical present-day oceanic phosphate concentrations and for primary productions as well. This indicates that marine biogeochemistry is more important in controlling phosphorus concentrations at the surface ocean than the direct atmospheric deposition of phosphorus, as we stated in the manuscript. The following text is added in the revised manuscript: "*As expected, the effect on phosphate concentrations (Fig. S9b) and productivity (Fig. S9d) in this sensitivity simulation remain extraordinarily low, i.e., the relative difference to STD is almost everywhere below ~1%. This overall demonstrates that the changes in phosphorus do not play a significant role in marine productivity from preindustrial to future periods.*"

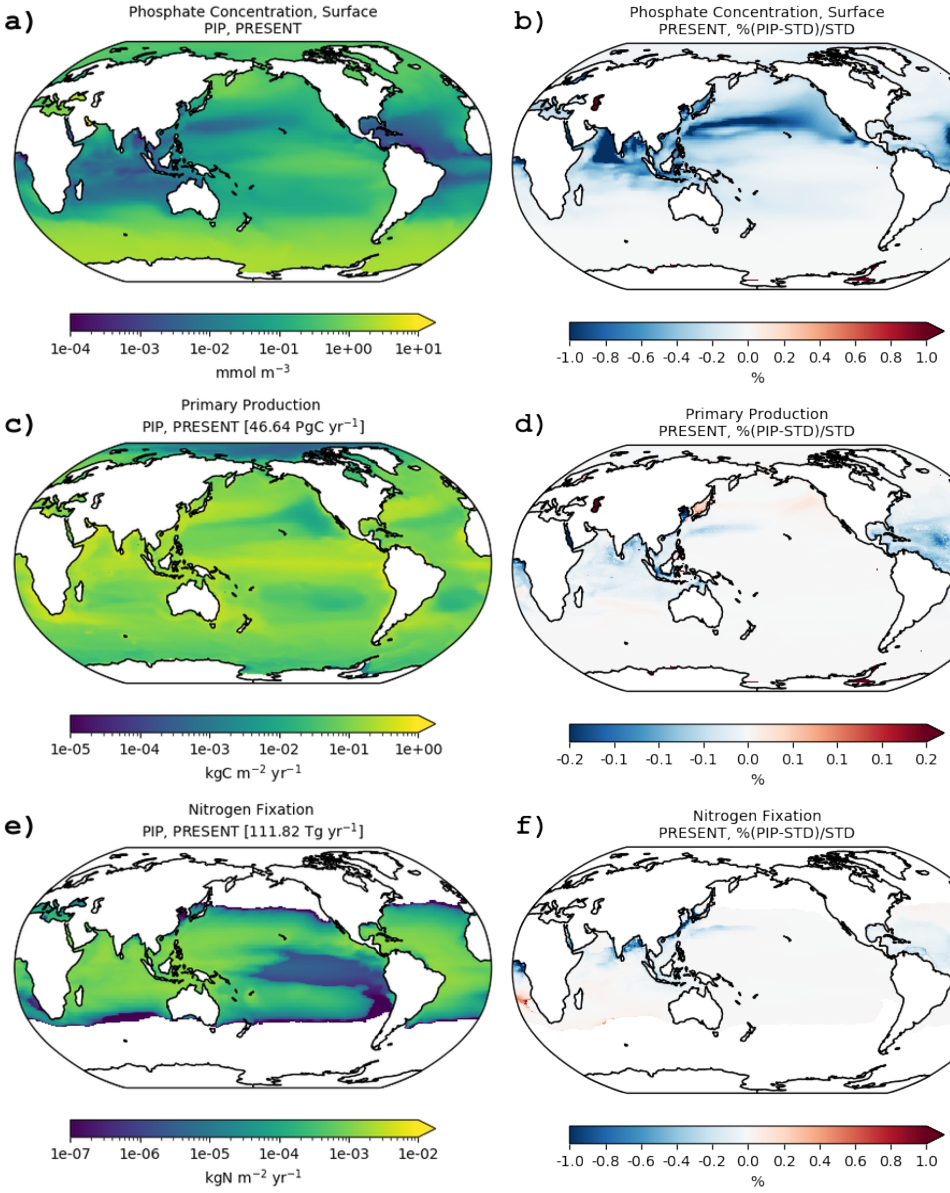

Figure S1: Surface oceanic concentrations (mmol m^{-3}) of phosphate (top row), primary production rates (kg-C m^{-2} yr^{-1}) (middle row), and nitrogen fixation (kg-N m^{-2} yr^{-1}) (bottom row), as calculated by the model for PRESENT for the sensitivity PIP simulation (i.e., as for STD, but keeping phosphorus atmospheric deposition to preindustrial levels) (left column), and the respective relative differences (%) to the STD simulation (right column).

GC2. There are many "moving parts" associated with this study that some idealized experiments might help disentangle the mechanistic role of atmospheric nutrient deposition on ocean biogeochemistry and production. Perhaps substitution experiments with the newly derived N, P, or Fe deposition singly swapped with remaining "standard" PISCES inputs (or combinations of two substituted out of three).

- We agree that more sensitivity experiments would be beneficial for a deeper analysis. This approach is limited, however, by the available resources. Nevertheless, we carried out an additional sensitivity simulation where phosphorous deposition fluxes kept constant at preindustrial levels while all other atmospheric inputs (i.e., N and Fe) changed. This run allows new insight on the importance of N and P macronutrients which is presented in the revised version. Please see our overall reply to SC1.

GC3. I appreciated the signposting of the manuscript structure at the end of the introduction, but I thought the paper would benefit from having separate "results" and "discussion" sections, with integrative diagnostics in the former, and more emphasis on explaining the changes in emergent ocean properties and comparisons with previous studies such as Krishnamurthy in the latter. At the moment, the key messages are very much buried within the qualitative/semi-quantitative description of the results.

- We agree with the reviewer and for this, the manuscript has undergone a major revision, including now a more detailed analysis. As suggested, we separated the discussion from the results in the revised version of the manuscript. For this, the discussion of productivity has completely rewritten and is substantially expanded now. Respectively, in the revised version, the conclusions are rewritten more concisely.

GC4. I also think that the model-data comparisons, although reassuring, interrupted the flow of presentation. One could create a new section on model validation, but I would recommend moving the material and figures to Supplementary information.

- Indeed, our aim was not to repeat the work of previous studies but to show, in short, that our version of the model reproduces the main features from the observations. Thus, a separate section of a model evaluation would be very limited and out of the scope of this work. However, we agree with the reviewer that the model-evaluation figures may interrupt the presentation of this work and for this, the model evaluation part has now moved to the Supplementary material of the revised version, as suggested.

GC5. One comparison that may have been really interesting to include is a comparison of the "CTRL" run to a vanilla PISCES simulation, with the standard atmospheric nutrient fluxes.

- A comparison with the standard atmospheric inputs in PISCES would be of course interesting, but we believe that the value of this study lays on providing new data set of atmospheric deposition inputs for the preindustrial, the present, and future based on realistic atmospheric chemistry and physics (i.e., based on a state-of-the-art atmospheric transport and chemistry model) and plausible scenarios for the future and past. For the standard PISCES configuration, the Fe and P deposition inputs to the ocean are based on the same dust deposition file and based on constant nutrient content and solubilities on the deposited dust aerosols. In contrast, for this work, we provide deposition fluxes based on a detailed mineralogy dataset, online mineral dissolution processes, and atmospheric chemistry for three periods (i.e., namely the years 1850, 2010, and 2100). Such a comparison would be meaningful only for the present-day deposition fields. However, for this work, we intend to rather focus on differences between different periods. Nevertheless, in the case of such a comparison, we do not expect fundamental differences at least on a global scale, as also denoted by current model evaluation compared to previous studies. Though, regional changes could be more important. All in all, we did not provide a comparison with a standard input simulation in this work, since this would be out of the scope of this work.

II. Specific Comments

SC1. P3, line 20: "no-linearly" typo.

- Changed to "*non-linearly*"

SC2. P4, line 13: "It has also been suggested. . ." citation needed, unless it's Krishnamurthy et al. (2010) in which case rephrase for clarity.

- This part is rephrased as "*Krishnamurthy et al. (2010) also suggested that the simultaneous anthropogenic N and Fe deposition can increase oceanic productivity by 1.5 Pg-C yr-1, corresponding overall to a reduction of atmospheric pCO2 level by ~2.2 ppm by the year 2100.*"

SC3. P6, line 7: "five iterations" I think it would be more precise to say you ran the model for 300 years, repeating the 60 year physical forcing five times. Five iterations could technically imply a spin-up of 5x2700s.

- We agree with the reviewer that this statement may be confusing. We rewrote this part by adding a new subsection (i.e., Sect. 2.1); please see also our reply to GC1 of Reviewer #1.

SC4. P6, line 9: Which versions of WOA and GLODAP did you use (if not WOA2013 and GLODAPv2). How was DIC initialized? Also from GLODAP?

- This part is now read as: "*For the initialization of the ocean biogeochemical fields, the climatological fields of oxygen, nitrate, silicate, and phosphate from the World Ocean Atlas 2009 (WOA; Garcia et al., 2010a, 2010b) along with dissolved inorganic carbon (DIC) and alkalinity from the Global Ocean Data Analysis Project (GLODAP; Key et al., 2004) were adopted.*"

SC5. P6, line 25: "no extra optimizations for the iron scavenging parameters" The specific iron cycle configuration is of critical importance to understanding the effect of changing iron input, please can you give more details about this? Did you use particle dependent scavenging? How is organic ligand complexation parameterized (constant or variable ligand concentration)?

- We agree with the reviewer that the iron cycle configuration is of high importance for Fe and other nutrients oceanic concentrations. Since we are mostly focused here on the differences on productivity and nutrients oceanic concentrations solely due to different atmospheric input parameterizations, the simple chemistry model of PISCES (i.e., based on one ligand (L) dissolved inorganic Fe and dissolved complexed iron (FeL)) is just used and not, for example, the complex chemistry scheme that is also available in the model (i.e., ln_fechem = F), as developed by Tagliabue and Arrigo (2006) and Tagliabue and Völker (2011), which is based on five iron species and two ligands and better match with observations. The ligand concentration in the ocean for this work is kept constant, equal to 0.6 nmol L^{-1} and the scavenging rate by dust is equal to 150 d^{-1} mg^{-1} L (see Table 1 in Aumont et al., 2015).

  We propose to add the following part in the manuscript: "*For this work, the simple chemistry scheme based on one ligand (L) dissolved inorganic Fe and dissolved complexed iron (FeL) is used. Additionally, the ligand concentration in the ocean, is kept constant, equal to 0.6 nmol L^{-1} and the scavenging rate by dust is equal to 150 d^{-1} mg^{-1} L (see Aumont et al., 2015 and ref. therein).*"

SC6. P7, lines 1-12: Timeseries of the model nutrient sources would clarify how the experiment was run i.e. I think you did one transient run 1651-2100 and analyze the nutrient concentrations/ecosystem response at three 20-year average periods. In addition, it would be great to show the temporal evolution of globally/regionally-averaged nutrient concentrations and emergent diagnostics during this run. This got me thinking about

whether the "present day" actually represents the peak in atmospheric nutrient deposition, or if that was earlier (70's, 80's or 90's)? There was no real justification for choosing the 2001-2020 average given.

- The revised manuscript (supplement) contains now time series with globally averaged depositional inputs for P, N, and Fe which clarifies how the model was forced. We also reformulated the description of the experiment in the text. The time series clearly demonstrates that the period 2000-2020 is the one with the highest deposition fluxes into the ocean, i.e.,

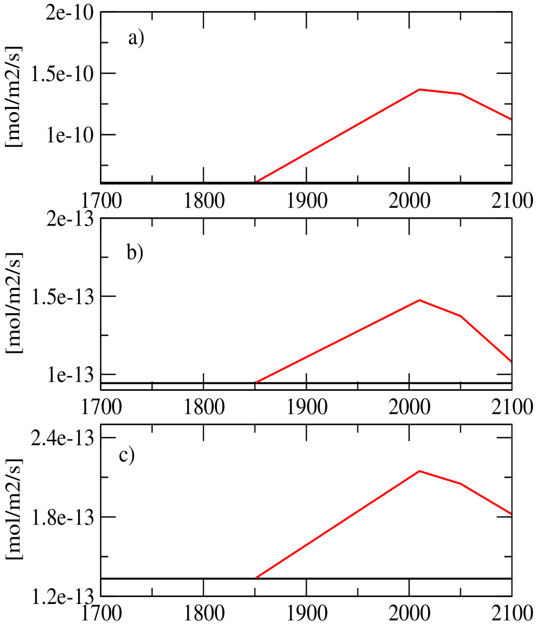

Figure S2: Globally averaged atmospheric deposition fluxes (red lines) of a) nitrogen, b) phosphorous, and c) iron in mol m^{-2} s^{-1}, as taken into account in PISCES. The black line indicates forcing for the control run under preindustrial conditions (i.e., year 1850).

- Indeed, we here performed simulations from 1651-2100, using the first 200 yrs. (i.e., 1651-1850) as a spin-up period for our experiments. For the analysis of the results, we used three 20-year average periods, corresponding to PAST, PRESENT, and FUTURE periods. The simulations with the atmospheric chemistry model comprise yearly simulations for years 1850, 2010, and 2050/2100 (using ACCMIP emissions from Lamarque et al, 2013). The reason is that the atmospheric CTMs are among the most expensive models, so the performance of transient runs over multi centennials is practically impossible. However, considering the typical residence time of tropospheric aerosols of only a few days a 1-year simulation is by far sufficient to bring the atmosphere in equilibrium. Note that for all CTM simulations a one-year spin-up is performed. Afterward, for the ocean depositional forcing, a linear interpolation between the years of the atmospheric run is applied. A more detailed explanation is now provided in the revised version, in the new Sect. 2.2. i.e.,
"*Simulations with the atmospheric transport and chemistry model are, nevertheless, extremely expensive. Therefore, limitations in available computational resources made it necessary to reduce the CTM simulations to representative single years for 1) the preindustrial state (before 1850), 2) the present-day state (representing the year 2010), and 3) a mid-century (2050), as well as, an end of century (2100) state. However, as the typical residence time of tropospheric aerosols is in the order of a few days, the atmospheric depositional fields used in PISCES represent a well equilibrated atmospheric chemistry and deposition flux, without the need of time transient simulations.*

For the ocean biogeochemistry model spin up (i.e., from 1651 to 1850) the preindustrial field (the year 1850) was applied. After the 200 years spin-up period, the atmospheric deposition input data for the STD and ORG simulations were linearly interpolated from preindustrial to present-day conditions (i.e., the year 2010) to smoothly capture the transition from past to the modern conditions (e.g., Krishnamurthy et al., 2009). Respectively, the deposition data from the present day were linearly interpolated to the projected estimates (i.e., the years 2050 and 2100). Note that for all temporal and spatial interpolations of this work, as well as for the drift calculations applied for this work, the Climate Data Operators (CDO v.1.9.8) software, as provided by the Max Planck Institute for Meteorology, is here used (https://code.mpimet.mpg.de/projects/cdo/embedded/cdo.pdf; last access 29/02/2020). An example of the globally averaged N, Fe, and P atmospheric deposition data as simulated by the CTM and applied in PISCES is presented in Fig. S2. Overall, the here discussed simulations should be considered as idealized sensitivity experiments to estimate the response on the ocean surface properties to changed atmospheric deposition."

SC7. P7, line 12: Will these datasets be available online for ESM groups to experiment with?

- We thank the reviewer for this comment. The atmospheric deposition datasets used for this study (past, present, and future) will be available in Zenodo. A relevant statement is added to the Data availability section at the end of the manuscript.

SC8. P11, line 18: How do dust and aerosol emissions, that are not considered, vary over the time period in question? I think this is touched upon in the "summary".

- The deposition data we used for this study come from a CTM simulation using anthropogenic and biomass burning emissions (gases and aerosols) for the past (1850), present (2010), and future projected (2050/2100) eras. However, due to the nature of CTMs (i.e., offline models), these simulations do not consider changes of the meteorology for the preindustrial era or projected meteorology. Thus, dust emissions that are wind-driven, besides the impact of land-use changes, do not vary in these simulations either. Overall, changes in the deposition fields applied in PISCES for this study, represent changes in nutrient concentrations due to anthropogenic and biomass burning emissions as well as the respective impact of atmospheric chemistry (i.e., atmospheric processing). To make more clear, the following part is now added in the new discussion section (i.e., now Sect. 5): "*All changes in nutrient deposition fluxes here accounted for are solely driven by changes in the anthropogenic and biomass burning emissions, along with the changes in insoluble to soluble conversions rates due to atmospheric processing. Thus, the atmospheric deposition fields used in this study did not account for any changes in dust and bioaerosol emissions. Instead, they were kept constant to the present-day atmosphere (i.e., the year 2010), although several studies suggest that dust fluxes may be sensitive to climate change and the land-use changes (e.g., Ginoux et al., 2012; Mahowald et al., 2010; Prospero and Lamb, 2003), and thus could be an important driver of the atmospheric nutrient cycles.*"

SC9. P11, line 26: "cooler water temperatures. . ." caused also by high latitude upwelling?

- The main effect is the cooler mean climate in the high latitudes. The imprint upwelling (N-Pacific) or deep (and convective) mixing (e.g. Labrador Sea North Atlantic) also affects the pattern of SST in the model.

SC10. P12, line 5: "leads to more efficient export." N supply may certainly lead to increased rates of export in nitrate-limited oligotrophic regions, but if the nutrients are

drawn down to the same low levels, for example in the gyres, is the export actually more efficient?

- We agree with the reviewer. We replaced the word "efficient" with "*increased*".

SC11. P12, line 33: It would be an even more convincing model-data comparison if the authors took advantage of the extensive GEOTRACES iron dataset (https://www.geotraces.org/geotraces-intermediate-data-product-2017/) with 6 years of cross calibrated additional data from a concerted international effort.

- For this work, we only chose the previous GEOTRACES version because it facilitates comparison with previous studies (e.g., Aumont et al. 2015). As also stated in GC4, we use here the GEOTRACES dataset to demonstrate that our simulations produce realistic oceanic concentrations compared to previous studies, and for this, in the revised version we moved the model evaluation in the supplement (please see our reply in GC4).

SC12. P13, line 21-25: side note about Redfield ratios might be better placed with the model set up.

- The following sentence has been added to the new Sect. 2.1 (i.e., model set-up): "*The model simulates the biogeochemical cycles of carbon and the main nutrients (N, P, Fe, and Si) and includes external nutrient sources from atmospheric deposition, rivers, sea ice, sediment dissolution, and hydrothermal vents, and a constant Redfield ratio (i.e., C:N:P = 122:16:1) for growth of phytoplankton*".

SC13. **P14, line 14: Why does nitrogen fixation decrease?**

- We agree with the reviewer that this should be better explained. For this, we have analyzed it in more detail in the revised manuscript and further relate it to the decreased iron concentration in the PAST (and the FUTURE experiments), i.e., "*Note, however, that nitrogen fixation in PISCES is restricted to warm waters (i.e., above 20 °C). Therefore, the strong reductions of nitrogen deposition in the mid to high latitude North Pacific in PAST have no direct impact on nitrogen fixation. In the subtropical Pacific reduced nitrogen fixation rates mainly reflect the diminished iron input (Fig. 1d). On a global scale, the model calculates overall only a small decrease (~0.2%; Table 1) in preindustrial nitrogen fixation rates compared to present-day, mainly as a result of the decreased soluble iron inputs in the subtropical North Pacific (Fig. 1d). For the future conditions, the model likewise calculates a modest decrease in the global nitrogen fixation (~1%; Table 1) along with decreased iron inputs to the ocean (Figs. 1c,f, respectively) resulting overall in some lower rates of up to 10% in the Equatorial Pacific Ocean (Fig. 3c).*"

SC14. P14, line 22: "with the projected decrease of the global inorganic nitrogen and iron inputs. . ." Nitrogen fixation should be promoted by lower N:P ratio (i.e. decreased N and increased P) so is the lower fixation rate due to iron limitation? Is it possible to show maps of resource limitation from the model for phytoplankton/diazotrophs, e.g. the limiting terms in Equation 6 in Aumont et al. (2015)?

- This is true; in PAST simulation, nitrogen concentrations slightly increase or do not change while phosphate increases strongly. Only iron decreases, overall demonstrating the importance of iron deposition. We have unfortunately not outputted the limitation term for diazotrophs (only for nanophytoplankton and diatoms).

SC15. P15, line 32: "all dissolved organic matter is assumed to be instantaneously remineralized. . ." I think this is incorrect. Equation 32 in Aumont et al. (2015) shows how dissolved inorganic matter (for carbon and other species related by fixed Redfield ratios) is separately modeled as a pool supplied by phytoplankton and zooplankton exudation and remineralized aerobically or anaerobically by bacteria over a timescale of the order of months to years.

- We thank the reviewer for attracting our attention to this issue. We rephrased this part as: "*Note that as for the riverine organic fractions in the model (see Aumont et al., 2015), we assume here an instant transformation of the atmospheric dissolved organic nitrogen (DON) and organic phosphorus (DOP) inputs to the respective inorganic fractions in the water column.*"

SC16. P16, line 19: "in contrast to the rather balanced nitrogen fixation rates. . ." a 2% change in primary production also sounds rather balanced to me.

- We agree with the reviewer and we removed this part.

SC17. P16, line 20-28: 15-20% increases occur relatively widely in the ocean, so what causes the counterbalancing decline in productivity? Why are the decreases confined to these bands in the Pacific?

- In ORG increased iron input in the sub-polar gyre increases diatom production leading to more consumption of nitrate. Subsequent transport of nitrogen diminished waters further to the south cause a decrease in productivity further south. In the tropical north Pacific, we find a small zonal dipole pattern of decreased (north) and increased (south). The boundary between decreased and increased bands matches the sharp boundary from iron limitation to non-iron limitation (see example below). We suppose increased iron input south (where iron limitation is) stimulates the production and diminishes nitrogen. Advective mixing of the N-diminished waters with water further north decreases productivity leading to the dipole pattern as presented in the old Figure 4 (i.e., in the submitted version).
  This analysis is now included in the revised version, i.e., "*Primary production increases almost in all ocean basins for the ORG simulation (Fig. 8d), except some parts of the Subpolar Pacific Ocean. In particular, higher rates are calculated in the subpolar Atlantic Ocean (up to 15%). In the N-limited oceanic regions, the increased ORG atmospheric nitrogen deposition (Fig. S3b) directly increases the production rates (Fig. 8d). Such a case is the western subtropical North Pacific, where atmospheric N deposition supports an extra production of up to 15%. The production rates are also increased in the subtropical South Pacific and Atlantic Oceans up to nearly 20% in the ORG simulation. In total, the primary production increased from ~46.7 Pg-C yr-1 for the STD to ~47.8 Pg-C yr-1 for the ORG (Table 1). Figure 8d points out to regions in the Pacific where production decreased. For the North Pacific, however, this represents the same mechanism as described above for the differences in primary production rates between PAST and PRESENT. For the ORG simulation, the increased iron input in the Pacific subpolar gyre increases diatom production leading to higher consumption of nitrate (Fig. S10b). Subsequent transport of nitrogen diminished waters further to the south cause a decrease in productivity further south. The boundary between decreased and increased bands matches the sharp transition from iron limitation to nitrogen limitation (Figs. 4a,c). Increased iron input south of the boundary (i.e., where iron limits) stimulates the production and diminishes nitrogen. However, the advective mixing of the N-diminished waters with waters further north decreases productivity north of the boundary (i.e., where N limits). Overall, the result is the dipole pattern as demonstrated in Fig. 8d.*"

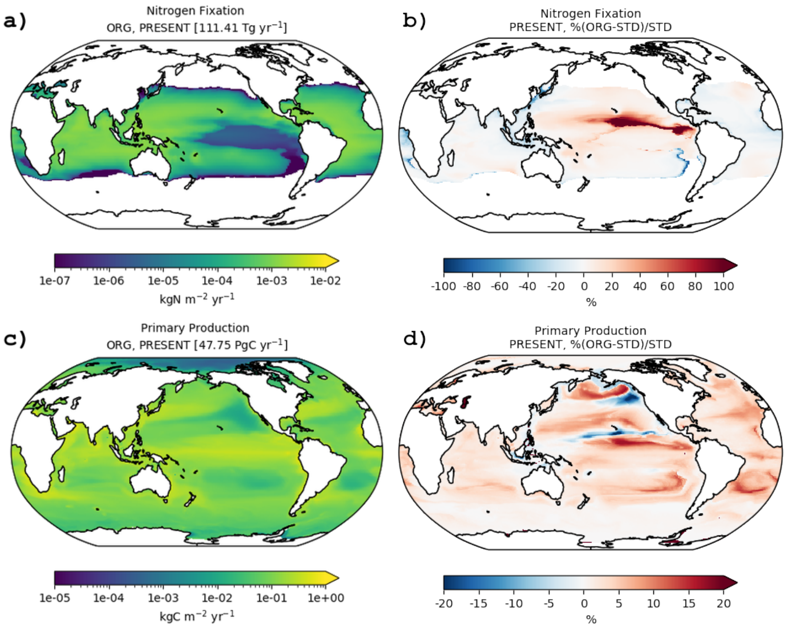

Figure 8: Nitrogen fixation (kg-N m^{-2} yr^{-1}) and primary production (kg-C m^{-2} yr^{-1}) rates as calculated by the model (a,c) for the ORG simulation for PRESENT (2001–2020 average), and the respective relative (%) differences (b,d) compared to the STD simulation.

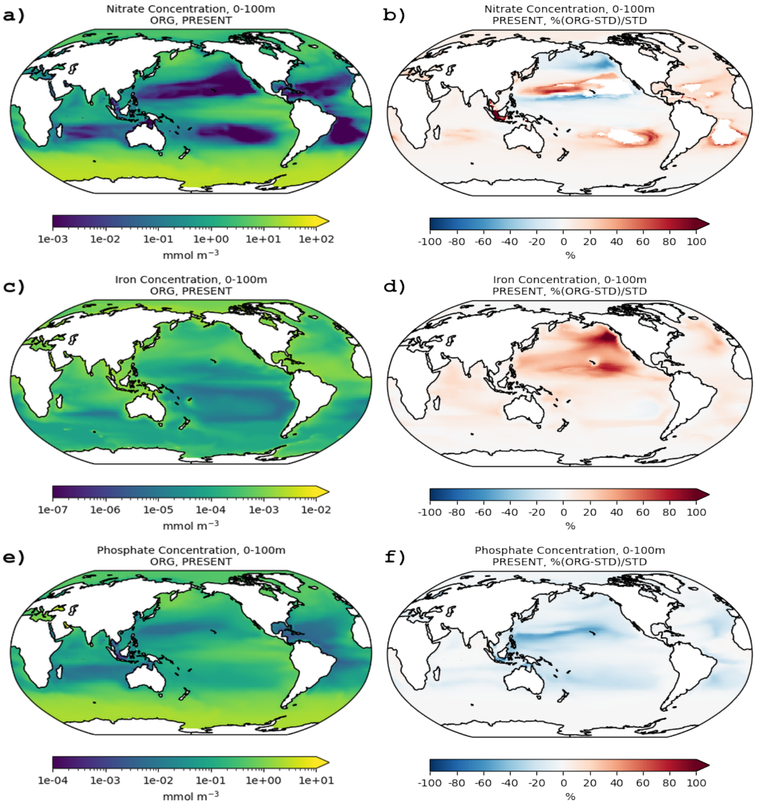

Figure S3: Oceanic concentrations averaged over the upper 100m (left column) of nitrate (a), iron (c) and phosphate (e) as calculated by the model for the ORG simulation for PRESENT (2001–2020 average), and the respective percentage differences (b,d,f) compared to the STD simulation (right column).

SC18. P17, line 13-20: Salinity restoring and mixed layer dynamics was never mentioned in the main text, so surprised to see it prominently in the "Summary" section.

- For this work salinity restoring was only applied during the OMIP run from which the physical ocean forcing for the offline PISCES runs were generated. The salinity of the biogeochemical offline runs is, however, constant, representing only the yearly cycle on a daily basis. To avoid any confusion, we removed this part from the text, since the prolongation of the run for the RCP8.5 scenario is not that relevant for this study. Note, however, that a complete description of the forcing data used for this study is now added in Sect. 2.1 in the revised version.

SC19. Figures: It would be preferable to use a perceptually uniform color palette for the CTRL maps, as opposed to the rainbow/jet colormap currently shown (see here for details: https://blogs.egu.eu/divisions/gd/2017/08/23/the-rainbow-colour-map/, not to mention the accessibility issue surrounding red/green vision deficiency).

- We thank the reviewer for attracting our attention to this issue. We replotted all figures using standard perceptually uniform colormaps, such as Viridis, (see https://bids.github.io/colormap/)

An explicit estimate of the atmospheric nutrient impact on global oceanic productivity

Stelios Myriokefalitakis[1], Matthias Gröger[2], Jenny Hieronymus[3] and Ralf Döscher[3]

[1] Institute for Environmental Research and Sustainable Development (IERSD), National Observatory of Athens, Penteli, Greece
[2] Leibniz Institute for Baltic Sea Research Warnemünde (IOW), Rostock, Germany
[3] Swedish Meteorological and Hydrological Institute (SMHI), Norrköping, Sweden

Correspondence to: Stelios Myriokefalitakis (steliosm@noa.gr) and Matthias Gröger (matthias.groeger@io-warnemuende.de)

Abstract. State-of-the-art global nutrient deposition fields are here coupled to the biogeochemistry model PISCES to investigate the effect on ocean biogeochemistry in the context of atmospheric forcings for preindustrial, present, and future periods. PISCES, as part of the EC-Earth model suite, runs in offline mode using prescribed dynamical fields as simulated by the ocean model NEMO. Present-day atmospheric deposition fluxes of inorganic N, Fe, and P into the global ocean are accounted equal to ~40 Tg-N yr^{-1}, ~0.28 Tg-Fe yr^{-1}, and ~0.10 Tg-P yr^{-1}. Preindustrial atmospheric nutrient deposition fluxes are lower compared to present-day (~51%, ~36%, and ~40% for N, Fe, and P, respectively). However, the impact on global productivity is low (~3%) since a large part of marine productivity is driven by nutrients recycled in the upper ocean layer or other local factors. Prominent changes are, nevertheless, found for regional productivity. Up to 20% reductions occur in oligotrophic regions such as the subtropical gyres in the northern hemisphere under preindustrial conditions. In the subpolar Pacific, reduced preindustrial Fe fluxes lead to a substantial decline of siliceous diatom production and subsequent accumulation of Si, P, and N, in the subpolar gyre. Further southward transport of these nutrient-enriched waters leads to strongly elevated production of calcareous nanophytoplankton further south and southeast, where iron no longer limits productivity. The North Pacific is found most sensitive to variations in depositional fluxes, mainly because the water exchange with nutrient-rich polar waters is hampered by land bridges. By contrast, large amounts of unutilized nutrients are advected equatorward in the Southern Ocean and North Atlantic making these regions less sensitive to external nutrient input. Despite the lower aerosol N:P ratios with respect to the Redfield ratio during the preindustrial period, the nitrogen fixation decreased in the subtropical gyres mainly due to diminished iron supply. The projected future changes in air pollutants under the RCP8.5 emission scenario result in a modest decrease of the atmospheric nutrients inputs into the global ocean compared to present-day (~13%, ~14%, and ~20% for N, Fe, and P, respectively), without significantly affecting the projected primary production in the model. Sensitivity simulations further show that the impact of atmospheric organic nutrients on the global oceanic productivity turns out roughly as high as the present-day productivity increase since preindustrial times when only inorganic nutrients' supply is taken into account in the model. On the other hand, variations in atmospheric phosphorus supply have almost no effect on productivity in the model.

Style Definition: None

Formatted: Superscript

Deleted: over

Formatted: Not Superscript/ Subscript

Deleted: The resulting globally integrated primary production of roughly 47 Pg-C yr^{-1} is well within the range of satellite-based estimates and other modeling predictions. …

Deleted:), resulting here in a lower marine primary

Deleted: by ~3% globally. Future changes

Deleted: bioaccessible

Deleted: input

Deleted: %

Deleted: The global mean nitrogen-fixation rates changed only marginally from preindustrial to future conditions (111±0.6 Tg-N yr^{-1}). With regard to the atmospheric inputs to the ocean, sensitivity model …

Deleted: indicate

Deleted: contribution of

Deleted: organic fraction results in an increase in primary production by about 2.4%. This estimate is …

Deleted: equal to the

Deleted: of emissions and atmospheric processing on the oceanic biogeochemistry since preindustrial times in the model, when only the inorganic fraction of the nutrients is considered. Although the impact of the atmospheric organic nutrients may imply a relatively weak response of marine productivity on a global scale, stronger regional effects up to ~20% are calculated in the oligotrophic subtropical gyres. Overall, this work provides a first explicit assessment of the contribution of the organic forms of atmospheric nutrients, highlighting the importance of their representation in biogeochemistry models and thus the oceanic productivity

Formatted: Justified

1 Introduction

Marine primary production is a critical component of the global carbon cycle and important for sustaining the habitability on Earth, although vulnerable to environmental changes (e.g., Steinacher et al., 2010). For example, an estimated decline of subarctic productivity has been reported to accompany the warming of the last 150 years (Osman et al., 2019). Global warming induced by greenhouse gas emissions has increased ocean stratification, reducing the supply of nutrients from subsurface waters and inhibiting the growth of phytoplankton in the surface ocean (Behrenfeld et al., 2006). Thus, the role of nutrient supply by atmospheric deposition will likely be more important in a warmer climate. Several studies have documented the importance of primary production on the surface ocean CO_2 concentrations (e.g., Falkowski et al., 2000; Gruber, 2004; Gruber et al., 2009; Le Quéré et al., 2013; Smith, 2019) via carbon uptake and sinking of the particulate organic matter to the deeper ocean. However, significant uncertainties remain in the projected production among state-of-the-art model simulations, which can range between 2 and 20% for the coupled model intercomparison project phase 3 (CMIP3) and CMIP5 models (Fu et al., 2016; Steinacher et al., 2010), mainly due to the different responses of phytoplankton production to changes in water temperature and stratification (Gröger et al., 2013; Laufkötter et al., 2016; Steinacher et al., 2010).

During primary production, the growth of the phytoplankton functional types (e.g., diatoms and nanophytoplankton) results in a newly formed particulate organic matter within the euphotic zone. These processes are limited however by light, temperature, and nutrients' availability. Nutrient inputs to the euphotic upper ocean result from internal ocean dynamics, such as upwelling or external sources, i.e., input by rivers and atmospheric deposition. Effects of riverine inputs have been widely investigated and are mostly restricted along the coasts or in marginal shelf basins (e.g., Behrenfeld et al., 2006; Gröger et al., 2013; Holt et al., 2012). Hence, the atmospheric deposition is the only external supply that can reach distal open ocean regions far remote from land.

Human activities have heavily perturbed the atmospheric chemical composition (e.g., Mahowald et al., 2017), but the impact of atmospheric composition on marine biogeochemistry, and consequently on the oceanic carbon- and nutrient cycles, is rather complex and still not fully understood. Among other species deposited into the open ocean, nitrogen (N), iron (Fe), phosphorus (P), and silicon (Si) are the nutrients that significantly limit the marine phytoplankton growth rates and thus directly impact on ocean-atmosphere carbon fluxes, in particular where nutrients are the growth-limiting factor for phytoplankton.

Atmospheric nitrogen inputs to the global ocean are mainly derived from anthropogenic combustion and agricultural sources over densely populated regions (Duce et al., 2008). So far, it is widely accepted that the marine biota primarily utilizes the inorganic nitrogen in its oxidized form (i.e., nitrogen oxides (NOx), nitric acid (HNO_3) and particulate nitrate (NO_3^-)), as well as in its reduced form (i.e., ammonia (NH_3) and particulate ammonium (NH_4^+)) (e.g., Duce et al., 1991). However, there is evidence that the dissolved organic nitrogen (DON) inputs (e.g., from rivers along the coasts) can likewise be also efficiently utilized (e.g., Aumont et al., 2015). In the atmosphere, the global organic nitrogen (ON) cycle has been demonstrated to have a strong (~45%) anthropogenic component (Kanakidou et al., 2012). Kanakidou et al. (2016) calculated that 20%–25% of the

Formatted: Font color: Black

Deleted: but

Deleted: , highlighting thus

Formatted: Default Paragraph Font

Deleted: to the ocean

Deleted: export

Field Code Changed

Deleted: e.g.,

Deleted: nano-phytoplankton

Deleted: -

Deleted: and

Deleted: the

Formatted: Justified

nitrogen deposition is in the form of ON, overall with DON deposition to be about 25% of the total dissolved nitrogen deposition to the global ocean.

Present-day atmospheric nitrogen input to the oceans is estimated to be roughly 39-68 Tg-N yr^{-1} (e.g., Duce et al., 2008; Kanakidou et al., 2016; Krishnamurthy et al., 2007; Wang et al., 2019), and the global oxidized and reduced nitrogen flux has increased from preindustrial values of ~13 Tg-N yr^{-1} to about 40 Tg-N yr^{-1} in modern times (Kanakidou et al., 2016). Moreover, the aforementioned studies suggested that nearly half of nitrogen emissions are transformed into aerosols in the atmosphere, with the nitrogen-containing aerosols having increased by approximately 2.5 times since preindustrial times. This resulted in a doubling of atmospheric soluble N deposition in the ocean due to human activities alone. Atmospheric nitrogen deposition may also significantly impact on the surface water inorganic N/P ratios and thus further influence global nitrogen fixation rates (Moore and Doney, 2007), i.e., the reduction of gaseous N_2 to ammonium as catalyzed by nitrogenase. Krishnamurthy et al. (2007) demonstrated that compared to preindustrial conditions, present-day inorganic nitrogen inputs to the oceans from anthropogenic sources could so far be partially compensated by the decreased nitrogen fixation, resulting thus in a modest effect on primary production. For future conditions, however, Wrightson and Tagliabue (2020) showed that the CMIP5 models project a general decrease in N_2-fixation by diazotrophs under the Representative Concentration Pathway (RCP) 8.5 emission scenario, although the complexity in response to climate change at a regional scale among the different models.

The most important atmospheric source for marine nutrients (such as Fe, P, and Si) in the open ocean is the mineral dust deposition. Dust aerosols are usually subject to intensive atmospheric processing during their long-range transport over remote oceanic regions. Changes in the properties of mineral aerosols during atmospheric transport involve chemical interactions with air masses (i.e., aerosol aging) that lead to different coatings of dust particles by sulfate (SO_4^{2-}), NH_4^+, NO_3^-, and organics (e.g., oxalic acid). In particular, pollutants from strong acids, such as the sulfuric (H_2SO_4) and nitric (HNO_3) acids, that coat deliquesced minerals, potentially transform part of their contained insoluble forms (e.g., hematite, apatite) into soluble forms (e.g., Fe(II), Fe(III), PO_4^{-3}) during atmospheric processing (e.g., Nenes et al., 2011; Shi et al., 2011). This process is further enhanced in the presence of organics such as the oxalic acid, that converts part of the insoluble Fe-containing minerals to soluble organic Fe-complexes, under favored atmospheric conditions (e.g., Paris et al., 2011; Paris and Desboeufs, 2013). However, according to future emission scenarios (van Vuuren et al., 2011), the sources of the main acidic atmospheric species such as the nitrogen oxides (NOx) and sulfur (SOx) are expected to decrease by 34–59% and 75–88%, respectively, from 2010 to 2100, but ammonia (NH_3) will increase by 3–55%. This heterogeneity in the projection of acidic and alkaline emissions is expected to non-linearly perturb the atmospheric aerosol acidity (Weber et al., 2016), making overall the atmosphere-ocean interactions even more complex.

Iron is utilized by marine phytoplankton mainly in its dissolved form, although the actual bioavailability may substantially differ from the soluble forms of the deposited nutrients into the ocean (Meskhidze et al., 2019). For example, Rubin et al. (2011) showed that in the tropical and subtropical Atlantic Ocean, some marine organisms (e.g., the *Trichodesmium*) can directly access the mineral (insoluble) particulate iron. Dissolved Fe (DFe) from anthropogenic combustion and biomass burning processes can contribute significantly to the atmospheric inputs into the ocean (e.g., Barkley et al., 2019; Hamilton et

Deleted: with

Deleted: having

Deleted: the

Deleted: authors

Deleted: processed

Deleted: ; overall, corresponding to

Deleted: ~2 times increase

Deleted: also

Deleted: increase the atmospheric acidity via the formation of

Deleted: and eventually

Deleted: no

Deleted: Both iron and phosphorus are

Deleted: their

Deleted: forms

Deleted: access

Deleted: In addition, emissions of dissolved

Deleted:) and dissolved P (DP

Deleted: (e.g., Barkley et al., 2019; Matsui et al., 2018).

Formatted: Justified

al., 2020; Matsui et al., 2018). However, the aerosols from natural and combustion sources tend to be deposited in different regions of the oceans. For example, the subtropical North Atlantic Ocean and the Arabian Sea receive the majority of Fe originated from natural dust aerosols, in contrast to the Pacific and Southern oceans where the Fe-containing combustion aerosols play a more important role compared to atmospheric dust (Ito et al., 2019b).

Present-day global atmospheric DFe and dissolved P (DP) deposition fluxes into the ocean are calculated in the range 0.2–0.4 Tg-Fe yr^{-1} (Ito et al., 2019a; Myriokefalitakis et al., 2018) and 0.10-0.17 Tg-P yr^{-1} (Mahowald et al., 2008; Myriokefalitakis et al., 2016), respectively. Myriokefalitakis et al. (2016) presented a comprehensive description of the organic forms of P (i.e., soil's organic matter, OP associated with anthropogenic combustion and biomass burning emissions, as well as from primary biological aerosol particles). They also demonstrated that DOP can contribute to DP more than 50% over the equatorial oceanic regions. Compared to the present day, DP and DFe emissions may have increased by roughly 3 and 6 times respectively, since 1850 (Myriokefalitakis et al., 2015, 2016). Wang et al. (2014) further showed that DP emissions increased due to the extended use of biofuels in the energy production sector in developing countries as well as emissions due to extensive deforestation in South America and Southeast Asia. By contrast, a significant increase for DFe emissions before the 1990s due to coal combustion is demonstrated, followed-up by a decline due to the implementation of air-pollution abatements (Wang et al., 2015b).

The primary production is strongly linked to nitrogen and iron acquisitions by marine biota. However, surface oceanic nutrient concentrations are strongly impacted by atmospheric deposition on a regional scale. Nitrogen atmospheric inputs were shown to have a significant effect on marine productivity, export production, and carbon uptake in Low-Nutrient-Low-Chlorophyll (LNLC) regions. The impact of N and P atmospheric deposition in strong oligotrophic regions, such as the Eastern Mediterranean, may lead to an increase in present-day primary production by up to 35% (Christodoulaki et al., 2013), resulting overall in a total phytoplanktonic biomass increase by 16% since preindustrial times (Christodoulaki et al., 2016). Marine global primary production rates are currently estimated in the order of 44 - 67 Pg-C yr^{-1}, based on biogeochemistry calculations and satellite-based estimates (e.g., Aumont et al., 2015; Behrenfeld et al., 2005; Gröger et al., 2013; Krishnamurthy et al., 2007, 2009, 2010; Steinacher et al., 2010). Krishnamurthy et al. (2009) suggested that the simultaneous anthropogenic N and Fe deposition can increase oceanic productivity by 1.5 Pg-C yr^{-1}, corresponding overall to a reduction of atmospheric pCO$_2$ level of 2.2 ppm by the year 2100. The impact of soluble iron deposition on the carbon export efficiency, although highly uncertain, indicates overall that the Southern Ocean is more sensitive in the projected fire emissions changes compared to other oceanic regions (Hamilton et al., 2020). Assuming, however, a complete assimilation of anthropogenic nitrogen by carbon fixation, a new marine biological production up to 0.3 Pg-C yr^{-1} could be supported (Duce et al., 2008). Although P deposition may account for only a small fraction of production (Krishnamurthy et al., 2010), an increase in Fe and P deposition can further enhance the N$_2$-fixation in LNLC oceans (Mahowald, 2011; Moore et al., 2013b).

A large portion of the global ocean, especially the subtropical gyres, is depleted in nitrate and phosphate, and consequently, sustain low productivity (e.g., Moore et al., 2013a). About 40% of the global ocean is estimated to be N-limited (Krishnamurthy et al., 2009; Wang et al., 2015a), with most of the remaining to be Fe-limited. The relative larger increases in N than P

Deleted: ; for

Deleted: are mainly deposited

Deleted: calculated

Deleted: Primary production is currently estimated in the order of 44 - 67 Pg-C yr^{-1}, based on biogeochemistry calculations and satellite-based estimates (e.g., Aumont et al., 2015; Behrenfeld et al., 2005; Gröger et al., 2013; Krishnamurthy et al., 2007, 2009, 2010; Steinacher et al., 2010). The primary production is, however, strongly linked to nitrogen and iron acquisitions by marine biota, with modelling estimates to indicate an increase for present-day values since preindustrial times (Krishnamurthy et al., 2009). The surface oceanic nutrient concentrations, however, are strongly impacted by the

Deleted: It has been also

Deleted: by ~2.2 ppm by the year 2100 (Krishnamurthy et al., 2010). Assuming, however,

Deleted: can

Deleted: also

Deleted: export

Deleted:

Deleted: a low growth of phytoplankton and other marine organisms…

Formatted: Justified

deposition in many oceanic regions of the globe cause shifts from N to P limitation (Krishnamurthy et al., 2009; Moore et al., 2013a). On the other hand, many studies suggest that anthropogenic Fe deposition is the most important factor for carbon uptake (Krishnamurthy et al., 2010; Okin et al., 2011), mainly due to its positive effect on productivity in High-Nutrient-Low-Chlorophyll (HNLC) regions. Accordingly, the essential role of iron in oceanic productivity is well established (Tagliabue et al., 2017) and currently routinely included in marine biogeochemistry models (Aumont and Bopp, 2006; Hajima et al., 2019; Hamilton et al., 2020; Ito et al., 2019b; Moore et al., 2001; Tagliabue et al., 2014, 2016). A further effect of iron is that it can stimulate nitrogen fixation (Camarero and Catalan, 2012; Schulz et al., 2012) because N_2-fixing species (diazotrophs) have elevated Fe requirements (Kustka et al., 2002). For example, the N_2-fixation is found to be suppressed due to iron-limitations in the eastern tropical Pacific (Wang et al., 2019). Hamilton et al. (2020) further demonstrated that changes in iron deposition fluxes into the global ocean may affect up to 70% the marine nitrogen cycle via increases in denitrification and nitrogen fixation rates. Present-day global nitrogen fixation is currently estimated in the range of ~111-163 Tg-N yr^{-1} (e.g., Aumont et al., 2015; Krishnamurthy et al., 2009; Wang et al., 2019). Wang et al. (2019) suggested that roughly half of the export production in the subtropical gyres is due to the nitrogen from microbial fixation and external inputs, such as rivers and atmospheric deposition. Regarding the atmospheric inputs, however, the aforementioned study demonstrated based on inversion calculations a potential decrease (~10%) of N_2-fixation, as a response to the elevated present-day nitrogen emissions.

The present study aims to analyze the impact of a comprehensive representation of atmospheric inputs to oceanic productivity. For this, a state-of-the-art marine biogeochemical model is used to integrate the recent knowledge of the atmospheric nutrient deposition fluxes into the ocean, driven by natural and combustion emissions, along with further processing during atmospheric transport. The outlined variable composition and varying sources of the deposited nutrients (i.e., N, Fe, and P) used in this work, have been recently modeled with a state-of-the-art atmospheric chemistry and transport model based on preindustrial, present, and future emissions. The description of the biogeochemical model and the parameterizations used in the atmospheric chemistry transport model, which determines the atmospheric deposition fields of this work, are presented in Sect. 2. A detailed description of the regional changes in deposition fluxes and the linked atmospheric processes controlling them is also provided. In Sect. 3, the modeled nutrient oceanic concentrations are presented, and the relevant biogeochemical processes, such as the nitrogen fixation and the primary production, are discussed and also compared to estimates from observations and other modeling studies. The role of present-day air pollutants on nutrients' atmospheric deposition is also discussed, via the comparison of experiments that are forced from atmospheric inputs of preindustrial and projected anthropogenic and biomass burning emission scenarios. The impact of the atmospheric nutrients' organic fraction on the global oceanic productivity is assessed in Sect. 4. Moreover, the implications of our findings concerning the above biogeochemistry parameters are discussed in Sect. 5. Finally, the main conclusions are summarized in Sect. 6, together with proposed directions for future marine biogeochemistry studies.

Deleted: fluxes

Deleted: Many

Deleted: the potential to increase productivity in High-Nutrient-Low-Chlorophyll (HNLC) regions. On the other hand, a number of studies argue that anthropogenic N deposition is equally important for ocean biogeochemistry (Duce et al., 2008; Wang et al., 2015a). The essential role of iron in oceanic productivity is, however,

Deleted: modelling studies

Deleted: (e.g., Aumont and Bopp, 2006; Hajima et al., 2019; Ito et al., 2019b; Moore et al., 2001; Tagliabue et al., 2014, 2016). Nitrogen fixation rates are also sensitive to atmospheric Fe inputs

Deleted: since N_2-fixing species (diazotrophs) have elevated Fe requirements. For example, the N_2-fixation is

Deleted: With regard to

Deleted: also

Deleted: by

Deleted: aim of the

Deleted: is

Deleted: detailed

Deleted: the

Deleted: the contribution of the

Deleted: processing

Deleted: related to the calculations of

Deleted: comprehensive

Deleted: calculated

Deleted: presented

Deleted: modelling

Deleted: here

Deleted: In particular, the

Deleted: of the deposited nutrients in

Deleted: also

Deleted: . Finally

Deleted: 4

Formatted: Justified

2 Model description

The state-of-the-art biogeochemistry model PISCES (Aumont et al., 2015), enabled within the framework of the European Community Earth System Model EC-Earth (http://www.ec-earth.org/), is here used in offline modus to investigate the impact of atmospheric deposition fluxes of N, Fe, and P on the marine productivity. PISCES (Pelagic Interactions Scheme for Carbon and Ecosystem Studies v. 2), as a part of the Nucleus for European Modelling of the Ocean (NEMO), includes a detailed representation of the lower trophic levels of marine ecosystems. The model simulates the biogeochemical cycles of carbon and the main nutrients (N, P, Fe, and Si), assuming a constant Redfield ratio (i.e., C:N:P = 122:16:1) in organic matter and living biomass. The external nutrient sources from atmospheric deposition, rivers, sea ice, sediment dissolution, and hydrothermal vents are also considered. PISCES includes two types of phytoplankton, namely calcareous nanophytoplankton and siliceous diatoms, and it simulates the chlorophyll concentrations and the phytoplankton growth based on nutrients' availability (i.e., DP, DN, and DFe for nanophytoplankton and DP, DN, DFe, and DSi for diatoms), temperature and light. Phytoplankton can be grazed by zooplankton or enters directly into the detritus pool. All particulate organic matter sinking to the bottom undergoes remineralization and the nutrients formerly incorporated during photosynthesis are released again. Thus, PISCES simulates the full inorganic carbon cycle including the biological and the carbonate counter pump. At the ocean surface, air-sea gas exchanges for carbon dioxide, oxygen, and nitrogen are parameterized following Wanninkhof (1992). The model has been successfully tested against the response of oceanic productivity to dust (e.g., Guieu et al., 2014) and climatic variability (e.g., Schneider et al., 2008).

2.1 Model set-up

2.1.1 Physical Ocean forcing

The dynamical physical outputs used to force PISCES for this study were produced by the physical ocean model NEMO, following the protocol of the OMIP simulation (Ocean Modelling Intercomparison Project; Orr et al., 2017). OMIP aims at harmonizing forcing fields of boundary conditions, as well as validation and analysis procedures among different ocean models. Atmospheric forcing fields are from the CORE II forcing (Coordinated Ocean-ice Reference Experiments - Phase II; Large & Yeager, 2009). CORE II provides a 62-year interannual forcing for the period 1948-2009. The physical model is initialized with gridded observational data from the World Ocean Atlas 2013 (Locarnini et al., 2013; Zweng et al., 2013) and then ran for 310 years by repeating the 62-year CORE II forcing. The necessary physical variables to force the offline biogeochemical model PISCES (see Table S1 in the Sup. Mat.) were taken from the last 62-year iteration. To avoid, however, any long-term trends from the spin-up, the multi-year (1948-2009; i.e., the 5th iteration of the 310-year run) mean of daily forcing fields was calculated. The resulting mean 1-year forcing, thus, contains the mean seasonal cycle and is (repeatedly) applied to drive all simulations with the biogeochemical PISCES offline model. All biogeochemical simulations are initialized and forced with the same physical fields from the average 1-year forcing derived from the OMIP run. Thus, all the PISCES

Deleted: here

Deleted: (ESM)

Deleted: EC-Earth is

Deleted: global ESM, with the ECMWF Integrated Forecast System (IFS) and

Deleted:) as core components, with PISCES (as part of NEMO) to include

Deleted: PISCES (Pelagic Interactions Scheme for Carbon and Ecosystem Studies volume 2)

Deleted:) and includes

Deleted: .

Deleted: growth of

Deleted: to enter

Deleted: in the deeper ocean

Deleted: nutrient

Deleted: is

Deleted: (Guieu et al., 2014)

Field Code Changed

Deleted: Biogeochemistry

Formatted: Normal

Formatted: Ohne, Font: Times New Roman

Deleted: set-up

Formatted: Justified

offline simulations are drift-free in physical variables. More details of the OMIP protocol can be found in Orr et al. (2017) and a first validation of the OMIP run is provided by Skyllas et al. (2019).

2.1.2 The ocean biogeochemistry model

For this study, PISCES uses a ~1° horizontal resolution with a latitudinal grid refinement in the tropics and 75 layers for the ocean (i.e., ORCA R1) and a timestep of 2700 sec. For the initialization of the ocean biogeochemical fields, the climatological fields of oxygen, nitrate, silicate, and phosphate from the World Ocean Atlas 2009 (WOA; Garcia et al., 2010a, 2010b) along with dissolved inorganic carbon (DIC) and alkalinity from the Global Ocean Data Analysis Project (GLODAP; Key et al., 2004) are adopted. The default N, Fe and P atmospheric nutrient inputs of PISCES in the EC-Earth configuration have been replaced for this work by state-of-the-art monthly mean atmospheric deposition fields recently published in the literature. Note that the default PISCES configuration (Aumont et al., 2015) uses yearly resolution N deposition fluxes of ~67 Tg-N yr^{-1} into the global ocean (Duce et al., 2008) assuming that all deposited N into the ocean to be dissolved. Respectively, the Fe, P, and Si atmospheric inputs were calculated from the same (monthly resolution) dust deposition field. Specifically, for the Fe atmospheric input, the Fe content in dust was set to 3.5%, and its soluble fraction was derived based on the simulated monthly resolved Fe solubility fields (Luo et al., 2008; Mahowald et al., 2009) overall, resulting in a soluble Fe input to the ocean of ~0.15 Tg-Fe yr^{-1}. For the P atmospheric input, the P content in dust was set globally to 750 ppm and with a constant solubility of 10% (Mahowald et al., 2008), resulting in a DP deposition flux of ~0.02 Tg-P yr^{-1} in the global ocean. Finally, for Si atmospheric inputs, a constant fraction of 30.8% in dust was set, assuming that 7.5% of the deposited total Si as soluble (~6.35 Tg-Si yr^{-1}) and, thus, upon deposition entered in the dissolved silicate pool of the model.

In contrast to previous studies (e.g., Aumont et al., 2015), the new N, Fe, and P atmospheric deposition fields considered here (see Sect. 2.2) are all calculated based on:

1) emissions of natural and combustion nutrient containing aerosols,
2) detailed atmospheric gas- and aqueous-phase chemical schemes, and
3) mineral dissolution processes due to atmospheric acidity and organic ligand (oxalic acid) in aerosol water and cloud droplets.

Note that, as for the default PISCES configuration, Si deposition fluxes into the ocean are only based on the new dust deposition fields coupled in the model. Moreover, for this work, no extra optimizations for the iron scavenging parameters have been applied, since the default PISCES configuration already considers a variable iron solubility on the dust deposition inputs (Aumont et al., 2015). However, the simple chemistry scheme available in PISCES is here used, which is based on one ligand (L) dissolved inorganic Fe and one dissolved complexed iron (FeL). The ligand concentration in the ocean is kept constant, equal to 0.6 nmol L^{-1} and the scavenging rate by dust is equal to 150 d^{-1} mg^{-1} L (see Aumont et al., 2015 and ref. therein). For clarity, we further note that the ocean and biogeochemistry modules used for this study may slightly differ from the version recently used in EC-Earth CMIP6 simulations since at the time the simulations were carried out the final version of EC-Earth was still not released.

Formatted: Font: Bold

Deleted: global timestep of 2700 sec. The model is here forced by dynamical physical outputs from an OMIP simulation (Ocean Modelling Intercomparison Project; Orr et al., 2017), with a repeated interannual (1948-2009) forcing. For the spin up, five iterations were carried out to ensure that the upper ocean biogeochemistry is drift free (Skyllas et al., 2019). For the initialization of the ocean biogeochemical fields, the climatological fields of oxygen, nitrate, silicate, and phosphate from the World Ocean Atlas

Deleted: and alkalinity from the Global Ocean Data Analysis Project (Key et al., 2004) were adopted. ¶
The default N, Fe and P atmospheric inputs of PISCES in the EC-Earth configuration have been replaced for the present study by state-of-the-art monthly mean atmospheric deposition fields, recently published in the literature.

Deleted: is

Deleted: (

Deleted:)

Deleted: %

Moved down [1]: In contrast to previous studies (e.g., Aumont et al., 2015), the new

Deleted: atmospheric deposition fields considered here are all calculated based on:

Moved (insertion) [1]

Deleted: Note that no extra optimizations for the iron scavenging parameters have been applied for this work, since the default model set-up already considers a variable iron solubility on the dust deposition inputs…

Formatted: Justified

Two transient simulations from 1651 to 2100 are here performed to study the impact of nutrients (N, P, and Fe) atmospheric input on global marine productivity:

1) a standard (STD) simulation accounting for the inorganic fractions of the deposited atmospheric nutrients (N, P, and Fe) into the global ocean, and
2) a sensitivity (ORG) simulation, as for STD but also accounting for the organic fractions of the deposited atmospheric nutrients (N, P, and Fe).

We here present results for the preindustrial (PAST: 1851–1870 average), present-day (PRESENT: 2001–2020 average), and future projected (FUTURE: 2081–2100 average) periods. For all PISCES simulations, the first 200 yrs. (i.e., 1651-1850) are not interpreted but considered as a spin-up to reach a quasi-equilibrium state in the model with a well-ventilated upper ocean. Moreover, the atmospheric CO_2 mixing ratio is set to the preindustrial value of 284.7 ppm, to effectively isolate the impact of atmospheric deposition on the marine biogeochemistry parameters. All monthly atmospheric inputs of nutrients are prescribed to the model, with the deposition fluxes for the spin-up fixed at the levels calculated with the anthropogenic and biomass burning emissions of the year 1850. To account, however, for potential drifts in the deeper ocean layers, a control (CTRL) simulation as for STD but using only preindustrial (i.e., the year 1850) atmospheric nutrients (N, P, and Fe) inputs into the global ocean is also performed. Figure S1 (see Sup. Mat.) demonstrates that for the main ocean basins the drift in vertically integrated primary production is minimal and clearly below the signal imposed by the altered nutrient deposition after 1850. This holds even for the Southern Ocean where the impact of atmospheric deposition is typically weak due to the absence of neighboring emission sources. Nevertheless, all model results presented in this work have been adjusted by subtracting the drift of the control run from STD.

2.2 The atmospheric nutrient inputs

All atmospheric nutrient inputs coupled to PISCES are derived from the offline global atmospheric Chemistry-Transport Model (CTM) TM4-ECPL. The CTM is driven by the ECMWF (European Centre for Medium-Range Weather Forecasts) Interim reanalysis project (ERA-Interim) meteorology (Dee et al., 2011) for the year 2010, and uses a horizontal resolution of 3° in longitude by 2° in latitude, with 34 hybrid layers up to 0.1 hPa. The CTM simulates the gas-phase chemistry along with the major non-methane volatile organic compounds, as well as all major aerosol components, such as dust, sea-salt, organic aerosols (OA), black carbon (BC), SO_4^{2-}, NH_4^+, and NO_3^-. The thermodynamic equilibrium model ISORROPIA II (Fountoukis and Nenes, 2007) is used to estimate the water content and the acidity of hygroscopic aerosols, accounting also for the impact of crustal materials (i.e., Ca^{2+}, Mg^{2+}, K^+, Na^+, Cl^-) from mineral dust and sea-salt (Myriokefalitakis et al., 2015). The in-cloud acidity is mainly controlled in the model by strong acids, i.e., sulphuric acid H_2SO_4/SO_4^{2-}, methanesulphonic acid (MSA/MS$^-$), and HNO_3/NO_3^-, and bases (NH_3/NH_4^+), accounting also for the dissociation of hydrated CO_2, sulfur dioxide (SO_2), and oxalic acid (Myriokefalitakis et al. 2011). The CTM further considers the multiphase chemistry secondary aerosol production in cloud droplets and aerosol water (Myriokefalitakis et al., 2011), as well as the secondary organic aerosol (SOA) formation via gas-to-particle partition over land and oceanic regions (e.g., Myriokefalitakis et al., 2010). The anthropogenic (including

Deleted: 1851

Deleted: were

Deleted: control

Deleted: (CTRL)

Deleted: (ORGF),

Deleted: CTRL

Deleted: analyze

Deleted: Note also that the ocean and biogeochemistry modules used here may slightly differ from the version recently used in EC-Earth CMIP6

Formatted: Ohne

Deleted: since at the time the simulations were carried out the final version of EC-Earth was still not released.¶
For the revised atmospheric deposition rates, a spin-up period of

Deleted: is here

Formatted: Font color: Black

Deleted: for each simulation,

Deleted: and a minimal model drift (i.e., <0.01% difference in the vertically integrated primary production). The

Deleted: were

Deleted: After the spin-up period, the deposition data were employed as external forcings, linearly interpolated from preindustrial (i.e., the year 1851) up to present-day conditions (i.e., the year 2010) to smoothly capture the transition from preindustrial to the modern conditions as in Krishnamurthy et al. (2009). Respectively, the deposition data from the present day were also linearly interpolated to the projected estimates (i.e., the year 2100). Note that for all temporal and spatial interpolations of this work, the Climate Data Operators (CDO v.1.9.8) software as provided by the Max Planck Institute for Meteorology is used (https://code.mpimet.mpg.de/projects/cdo/embedded/cdo.pdf; last access 29/02/2020). For all simulations, the atmospheric CO_2 mixing ratio is set to the pre-industrial value of 284.7 ppm, to effectively isolate the impact of atmospheric deposition on the marine biogeochemistry parameters.

**Deleted: Atmospheric parameterizations¶
For this work, all**

Formatted: Space Before: 12 pt

Deleted: –

Deleted: re–analysis

Deleted:

Deleted: sulphur

Deleted: For the present study, the

Formatted: Justified

ships and aircraft emissions) and biomass burning emissions from the historical Atmospheric Chemistry and Climate Model Intercomparison Project (ACCMIP) database (Lamarque et al., 2013) are used in the CTM, and the Representative Concentration Pathways 8.5 (RCP8.5) scenario (van Vuuren et al., 2011) is applied for the future CTM emissions. For all CTM simulations, a spin-up period of one year is applied. Note that we use here nutrient atmospheric deposition fields based on simulations with the latest updates of the CTM, as recently published by Kanakidou et al. (2020), which are all based on an improved on-line dust emission scheme (Tegen et al., 2002). As a result, the global dust source for all simulations is here equal to ~1287 Tg yr^{-1} for the year 2010, well comparable to a multimodel estimate of ~1257 Tg yr^{-1} as reported by Huneeus et al. (2011). For example, the global annual mean Si deposition input rate to the global ocean, which is solely related to the dust deposition, is accounted here to about 4.7 Tg-Si yr^{-1} and in the range of other estimations when a solubility of 7.5% is considered (e.g., see Krishnamurthy et al., 2010). Nevertheless, some small differences on the total amount of deposited nutrients over the ocean compared to previously published results (e.g., Kanakidou et al., 2016; Myriokefalitakis et al., 2015, 2016) are expected, due to the various updates of the code, the different year of simulation, or even the different definitions of the oceanic regions due to the applied horizontal analysis in PISCES (i.e., the ORCA R1).

Simulations with the atmospheric transport and chemistry model are, nevertheless, extremely expensive. Therefore, limitations in available computational resources made it necessary to reduce the CTM simulations to representative single years for 1) the preindustrial state (before 1850), 2) the present-day state (representing the year 2010), and 3) a mid-century (2050), as well as, an end of century (2100) state. However, as the typical residence time of tropospheric aerosols is in the order of a days, the atmospheric depositional fields used in PISCES represent a well equilibrated atmospheric chemistry and deposition flux, without the need of time transient simulations.

For the ocean biogeochemistry model spin up (i.e., from 1651 to 1850) the preindustrial field (the year 1850) was applied. After the 200 years spin-up period, the atmospheric deposition input data for the STD and ORG simulations were linearly interpolated from preindustrial to present-day conditions (i.e., the year 2010) to smoothly capture the transition from past to the modern conditions (e.g., Krishnamurthy et al., 2009). Respectively, the deposition data from the present day were linearly interpolated to the projected estimates (i.e., the years 2050 and 2100). Note that for all temporal and spatial interpolations of this work (as well as, for the drift corrections), the Climate Data Operators (CDO v.1.9.8) software, as provided by the Max Planck Institute for Meteorology, is here used (https://code.mpimet.mpg.de/projects/cdo/embedded/cdo.pdf; last access 29/02/2020). An example of the globally averaged N, Fe, and P atmospheric deposition data as simulated by the CTM and applied in PISCES is presented in Fig. S2. Overall, the here discussed simulations should be considered as idealized sensitivity experiments to estimate the response on the ocean surface biogeochemical properties to changed atmospheric deposition.

2.2.1 Nitrogen

For the calculation of the atmospheric nitrogen deposition fluxes, the CTM uses primary emissions of NOx, NH$_3$, marine amines, and emissions of particulate organic nitrogen (ON) from natural and anthropogenic sources (Kanakidou et al., 2012, 2016, 2018). The particulate ON is linked to the OA tracers using varying N:C molar ratios (Kanakidou et al., 2012), as well

Deleted: also used

Deleted: conditions.

Deleted: the latest updates of

Deleted: presented in

Deleted: However, some small differences on the total amount of deposited nutrients over the ocean are expected

Deleted: ,

Formatted: Font: +Body (Times New Roman)

Deleted: cycle

Deleted: ¶

Formatted: Justified

as to the SOA formation under high NOx-to-VOC conditions (Myriokefalitakis et al., 2010; Tsigaridis et al., 2006). Amines of marine origin in the gas phase are also considered to form amine salts (Myriokefalitakis et al., 2010). A more detailed description of the N-cycle parameterization in the CTM can be found in Kanakidou et al. (2016, 2018).

Figure 1b presents the annual mean spatial distribution of dissolved nitrogen deposition as considered in PISCES for the STD simulation. The present-day DIN deposition fluxes into the global ocean are estimated to be ~40 Tg-N yr^{-1} (Table 1). DIN deposition (oxidized and reduced inorganic nitrogen) shows the highest fluxes downwind industrial areas of the Northern Hemisphere and the tropical biomass burning regions due to the enhanced NOx emissions, as well as downwind Europe, China, and Indonesia, reflecting overall the high strength of NH$_3$ emissions in these regions. DIN deposition exceeds $1 \cdot 10^{-3}$ kg-N m^{-2} yr^{-1} downwind the eastern United States, Europe, India, China, and Indonesia (Fig. 1b). Some low DIN deposition fluxes over the remote ocean are related to the recycling of the marine NH$_3$ sources. Moreover, when the ON is accounted for the dissolved nitrogen deposition, as considered in the ORG simulation (Fig. S3a), much higher nitrogen deposition fluxes are calculated in the tropics mainly due to the large contribution by primary biogenic particles, the biomass burning emissions, along with the ON production during SOA formation (Fig. S3b). For comparison, we note that the total river supply of bioaccessible nitrogen in the model is roughly 36 Tg-N yr^{-1} (Aumont et al., 2015). Note, however, that the total present-day dissolved nitrogen deposition estimate (~58 Tg-N yr^{-1} for the ORG simulation; Table 1) is lower compared to the N deposition fluxes (~67 Tg-N yr^{-1}) as taken from Duce et al. (2008) and used in previous PISCES configurations (Aumont et al., 2015).

Deleted: 1

Deleted: CTRL

Deleted: ORGF

Deleted: S1a

Deleted: S1b

Deleted: clarity

Deleted: for the ORGF simulation,

Deleted: ON is assumed as readily

Deleted: in the PISCES, following the previous assumptions for the atmospheric …

Deleted: inputs to

Deleted: ocean

Deleted: for the ORGF simulation

Deleted: account for ~

Compared to the present day, almost all ocean basins (except some parts of the South Indian and the South Pacific Ocean) display a substantially lower (>50%) nitrogen deposition flux during the preindustrial era (Fig. 1a). Inorganic nitrogen inputs to the ocean have significantly increased for present-day along the coasts of the African, Australian, and the South American continents, downwind densely populated areas in the northern hemisphere, such as the east coast of North America and Europe, as well as regions with intensive agriculture downwind the coast of East and South Asia (Kanakidou et al., 2016). Globally, present-day atmospheric inorganic nitrogen inputs to the ocean have increased by a factor of ~2 since 1850 (Table 1) due to the respective increase of NH$_3$ and NO$_x$ emissions. The projected atmospheric DIN inputs to the ocean indicate also a decrease (~15%), although much less significant compared to preindustrial times (Table 1) since the reduction in NOx emissions is projected to be compensated by the continuing increase in NH$_3$ emissions. Note that the preindustrial ON deposition fluxes into the ocean are estimated to be roughly of the same magnitude as the inorganic nitrogen oceanic input (i.e., ~15 vs. ~20 Tg-N yr^{-1}; Table 1). Projections under the RCP8.5 scenario, however, indicate that NHx emissions will gain in importance, resulting overall in a weaker contribution of the oxygenated inorganic nitrogen to the atmospheric deposition into the ocean for future conditions.

Deleted: although

Deleted:), projections

2.2.2 Iron

The global atmospheric Fe deposition fluxes are parameterized in the CTM considering primary Fe emissions associated with minerals in dust and combustion processes. The Fe content of dust minerals is based on detailed mineralogy maps (Nickovic et al., 2012), accounting also for an initial soluble Fe content in the mineral emissions (Ito and Xu, 2014), overall resulting in

Deleted: cycle is

Formatted: Justified

a mean Fe content of about 3.2% in dust emissions. For the Fe-containing combustion aerosols, the CTM accounts for emissions from biomass burning, coal, and oil combustion (Ito, 2013; Luo et al., 2008) with dissolved Fe contents of 12% for biomass-burning, 8% for coal combustion, and 81% for oil combustion from shipping Fe emissions. The CTM further accounts for acid- and organic ligand-solubilizations of dust aerosols, in both aerosol water and cloud droplets, as well as, for the aging (i.e., the conversion of insoluble to soluble) of the Fe-containing combustion aerosols via atmospheric processing. More details on the atmospheric Fe-cycle set-up can be found in Myriokefalitakis et al. (2015, 2018), along with updates from Kanakidou et al. (2020).

Figure 1e presents the annual mean spatial distribution of dissolved iron deposition fluxes, as considered from PISCES for the STD simulation. DFe deposition fluxes into the ocean present strong spatial variability (Fig. 1e) with an annual flux of ~0.28 Tg-Fe yr^{-1} for the STD and ~0.35 Tg-Fe yr^{-1} for the ORG simulation (Table 1), both estimates are well in the range of the mean DFe deposition flux into the ocean (0.2-0.4 Tg-Fe yr^{-1}), as derived from the GESAMP model intercomparison study (Myriokefalitakis et al., 2018). For comparison, we note that the total riverine Fe supply in the model equals 1.45 Tg-Fe yr^{-1} (see Aumont et al., 2015 and ref. therein). The highest annual mean DFe deposition fluxes into the ocean (Fig. 3c) occur downwind dust source regions with significant deposition rates to also be found in the outflow of tropical biomass burning regions (i.e., Central Africa and Indonesia), reflecting the importance of combustion processes. Annual mean DFe deposition rates of ~10^{-5} kg-Fe m^{-2} yr^{-1} are considered for the tropical Atlantic Ocean, as well as, for the Indian Ocean under the influence of the Arabian and Indian peninsulas. For the Southern Ocean, the DFe atmospheric inputs (up to ~10^{-6} kg-Fe m^{-2} yr^{-1}) are mainly associated with the Patagonian, the Southern African, and Australian deserts. Figure S3c further presents the annual mean DFe deposition fluxes into the ocean when the organic fraction is considered. The organic bound Fe is produced in the CTM during the organic-ligand dust dissolution processes (i.e., as Fe(II/III)-oxalato complexes), and further accounted for a fixed 0.1% fraction in Fe-containing combustion aerosols (Kanakidou et al., 2018; Myriokefalitakis et al., 2018). Note that although this estimate is highly uncertain due to the lack of observational data, and it overall appears to contribute modestly to the global DFe atmospheric input to the ocean (~0.07 Tg-Fe yr^{-1}), the deposition of organic bound Fe aerosols can be potentially important (~up to 40%) in the remote tropical Pacific and the Southern Ocean (Fig. S3d) where the atmospheric Fe concentrations are extremely low and are mainly occurring due to biomass burning and anthropogenic (i.e., ship) combustion emissions (Ito et al., 2019a).

The CTM calculates increases in DFe deposition rates since preindustrial times, as stronger Fe combustion emissions and a more efficient dust dissolution rate due to the more acidic modern environment occur in the modern era; overall, accounting for about 1.5 times higher DFe atmospheric input to the global ocean for present-day (Table 1). On the other hand, the derived DFe in the ocean for the future atmosphere is calculated ~14% lower than present-day conditions (Table 1), owing to the projected changes in anthropogenic emissions and air-quality. For the preindustrial era, the largest differences in atmospheric DFe deposition fluxes compared to present-day are considered in the Northern Indian, the North Pacific, and the tropical North Atlantic Oceans (Fig. 1d). Lower PAST atmospheric DFe deposition fluxes compared to present-day are simulated in remote oceanic regions away from dust plumes, in the tropical and subtropical Pacific Ocean, also due to the increased present-day

Deleted: of about 3.2%.

Deleted: water

Deleted: ageing

Deleted: (Myriokefalitakis et al., 2015, 2018)

Deleted: CTRL

Deleted: CTRL

Deleted: ORGF

Deleted:)

Deleted: The highest annual mean DFe deposition fluxes into the ocean (Fig.

Deleted: high

Deleted: S1c

Deleted: model

Deleted: ,

Deleted: also

Deleted: the combustion emissions by considering here

Deleted: 01

Deleted: it

Deleted: S1d),

Deleted: ,

Deleted: accounts for

Deleted: changes in anthropogenic emissions and air-quality are projected to weaken, with

Deleted: to be

Deleted: the

Deleted:).

Deleted: is also

Formatted: Justified

atmospheric processing. The combustion source of DFe turns out, however, to be rather important near industrial and biomass burning sources, such as downwind South and East Asia, where dust emissions are lower. For the future emissions, however, smaller changes are derived, with a general decrease of the atmospheric DFe input in most parts of the global ocean (Fig. 1f), except for some increases in the Eastern North Pacific Ocean and over the very low atmospheric Fe concentrations regions in the remote Southern Ocean. Nevertheless, the demonstrated increases in the past (and future) deposition fluxes over remote oceanic regions with low atmospheric Fe concentrations, such as the Southern Ocean or downwind strong biomass burning and anthropogenic coal combustion regions, are due to both the changes in emission strengths and the impact of atmospheric processing on the dissolved Fe lifetime (Myriokefalitakis et al., 2018).

Deleted: the

Deleted: calculated

Deleted: Note, however, that

Deleted: calculated

Deleted: relative

2.2.3 Phosphorus

Formatted: Tab stops: Not at 10.45 cm

The atmospheric P-cycle is calculated based on emissions of insoluble mineral-P, phosphate, and insoluble and soluble organic P (OP), with the resulted DP deposition fluxes in the CTM being driven by natural (i.e., dust, bioaerosols, sea spray and, volcanic aerosols) and combustion P-containing aerosol emissions. Acid solubilization of dust particles (i.e., conversion from mineral P to phosphate) takes place in both aerosol water and cloud droplets, along with the conversion from insoluble to soluble OP aerosols during atmospheric processing. The CTM accounts for two P-containing insoluble minerals (the fluoroapatite and the hydroxyapatite) in dust based on soil mineralogy maps (Nickovic et al., 2012), as well as for OP present in soil's organic matter (Kanakidou et al., 2012). A solubility of 10% is applied to all P-containing dust emissions in the CTM. For P-containing combustion aerosols, the CTM accounts for anthropogenic (i.e., for fossil fuel, coal, waste, and biofuel) and biomass burning emissions, based on observed P/BC mass ratios (Mahowald et al., 2008). Sea-spray and volcanic aerosols account for a rather low DP global source, in contrast to bioaerosols which are estimated to contribute significantly to DOP. The naturally emitted OP by bioaerosols is overall represented by bacteria, fungi, and pollen (Myriokefalitakis et al., 2017). More details on the P-cycle representation in the CTM can be found in Myriokefalitakis et al. (2016).

Deleted:

Deleted: In addition, the acid

Deleted: particles

The present-day global annual DIP deposition flux into the global ocean for the STD simulation accounts for ~0.10 Tg-P yr^{-1} (Table 1), presenting also a strong spatial variability (Fig. 1h). The highest DIP deposition input rates occur downwind the major dust source regions (~$5\cdot10^{-6}$ kg-P m^{-2} yr^{-1}) owing to the phosphate content in dust emissions. High DIP deposition fluxes (~$1\cdot10^{-6}$ kg-P m^{-2} yr^{-1}) also occur downwind heavily forested regions (i.e., Amazonia, Central Africa, and Indonesia) due to the enhanced biomass burning sources. The combustion of anthropogenic origin further contributes to the DIP deposition flux into the ocean, such as downwind the South and East Asia (~$1\cdot10^{-6}$ kg-P m^{-2} yr^{-1}). Notable deposition rates are also illustrated away from dust sources, such as in the Northern Atlantic and Pacific Ocean (~$5\cdot10^{-7}$ kg-P m^{-2} yr^{-1}), due to the mineral P solubilization during atmospheric transport and somewhat lower rates occur in the Southern Ocean. Moreover, the consideration of organic fraction to atmospheric DP inputs to the global ocean (Fig. S3e) results in a ~50% increase in the global DP deposition flux (Table 1), but stronger regional increases of up to 80% can be also seen (Fig. S3f). Note also that in PISCES, DP fluxes of roughly 3.7 Tg-P yr^{-1} is also delivered to the ocean by rivers (Aumont et al., 2015).

Deleted: CTRL

Deleted: Moreover, consideration of organic fraction in atmospheric DP inputs (Fig. S1e) results in a ~50% increase in the global DP deposition flux (Table 1) and a significant increase of up to 80% can be also seen (Fig. S1f).

Formatted: Justified

An increase in the global DIP deposition of ~40% is considered here for present-day (i.e., 0.06 Tg-P yr^{-1}) compared to preindustrial conditions, and a modest decrease of ~20% is projected for the year 2100 (i.e., 0.08 Tg-P yr^{-1} under the RCP8.5 scenario), as shown in Table 1. The regional differences for the preindustrial times appear, however, to be stronger (up to 60 %; Fig. 1g), especially downwind highly populated regions of the Northern Hemisphere, in the Atlantic and Pacific Oceans. DIP deposition fluxes are also projected to decrease over the midlatitudes of the Northern Hemisphere where human activities dominate under the RCP8.5 scenario, with the largest changes up to 40% downwind of China and Australia. Significant changes (~20 %) are also illustrated in the Arabian Sea and the Bay of Bengal due to the expected increases in population (Fig. 1i).

Deleted: the

Deleted: for

Deleted:)

Deleted: Regional

Deleted: Note here that since the CTM neglects any changes in dust and bioaerosol emissions that occurred in the past or are expected in the future, all changes in DP deposition fluxes accounted in PISCES are solely driven by changes in the anthropogenic and biomass burning emissions, along with the changes in insoluble to soluble conversions rates due to atmospheric processing.

3 Results

Deleted: and discussion

3.1 Oceanic nutrient concentrations

Nitrate: The simulated annual mean nitrate surface concentrations in the seawater for the present-day and the relative differences for past and future eras are presented in Fig. 2. The present-day surface nitrate distribution shows high concentrations along the equatorial divergence where nutrients are upwelled, and solar insolation supports good light conditions throughout the year. In the high latitudes, cooler water temperatures and seasonally damped light conditions reduce nutrient consumption by biological productivity, resulting overall in elevated annual mean nutrient concentrations. High surface concentrations are also calculated in the high latitude Southern Ocean where the deep convection around Antarctica maintains high nutrient transports to the surface and productivity is limited by a thick mixed layer, lower water temperatures, and reduced light conditions. Elevated nutrient concentrations are likewise simulated in the Eastern Equatorial Pacific, and the Subarctic North Pacific, i.e., the well-known HNLC regions. All in all, this reflects a reasonable simulation of the abiotic oceanographic drivers in the model. A comparison between the simulated present-day surface nitrate concentration and the compiled data from the World Ocean Atlas is given in Fig. S4.

Deleted: lowers phytoplankton growth

Deleted: processes in the model

Formatted: Default Paragraph Font

Increased atmospheric nitrogen deposition fluxes from the preindustrial to the modern era (Table 1) result in a respective increase in surface nitrate concentrations in almost all oceanic regions, with some exceptions in the Eastern Equatorial and the subpolar Pacific Ocean (Fig. 2a). In remote oceanic areas, far from any coastal or riverine nutrient supply and thus strongly nutrient-limited, the higher present-day inorganic nitrogen and iron atmospheric inputs compared to the preindustrial era (Figs. 1a,d) increase primary production (see also Sect. 3.3). This may, overall, lead to increased export of the surface seawater nitrogen to the deeper ocean in the form of sinking biogenic particles in these oligotrophic oceanic regions (e.g., Krishnamurthy et al., 2007, 2010). For the future conditions, however, the model calculates both negatives and positive changes in the surface nitrate concentrations, resulting from an overall decrease (~4%) of the global inorganic nitrogen oceanic input (from atmospheric deposition and N$_2$-fixation) (Table 1). Indeed, for the future era, a decrease in almost all oceanic regions is calculated, except for the coastlines of Southeast Asia, Africa, and South America (Fig. 1c).

Deleted: results

Deleted: and

Deleted: (

Deleted: also

Deleted: Fe

Deleted:),

Deleted: results in an

Deleted: in

Deleted: a more efficient

Formatted: Justified

Iron: Figure 2 also presents the annual mean surface concentrations of iron for present-day in STD simulation along with the respective past and future relative differences. Present-day surface iron distribution (Fig. 2e) shows high concentrations in the subtropical North Atlantic Ocean and the Arabian Sea, with the lowest surface concentrations being calculated in the Eastern Equatorial Pacific and the Southern Ocean. A secondary maximum in iron concentrations is calculated in the Subarctic North Pacific. In general, iron concentrations in the model are low, especially in the Southern Ocean, the Eastern Equatorial Pacific, and the Subarctic North Pacific. Higher concentrations are found along the coasts or over the continental margins. For the past (Fig. 2d) and future (Fig. 2f) conditions, the model generally calculates lower iron surface concentrations, reflecting overall the respective decreases in DFe deposition fluxes into the ocean (Figs. 1d,c, respectively). Consequently, the strongest declines are found in the northern hemisphere, especially in the mid to high latitude Pacific and Atlantic. An exception is the NW Pacific where higher iron input in FUTURE (Fig. 1f) results in elevated oceanic iron concentrations. A comparison of the simulated present-day surface oceanic iron concentration with available DFe oceanic observation data (Tagliabue et al., 2012) is given in Fig. S4.

Phosphate: The annual mean present-day phosphate surface concentrations as calculated for the STD simulation together with the respective relative differences for past and future eras are presented in Figs. 2g-i. In general, the phosphate concentrations show similar distributions as the dissolved inorganic nitrogen. The surface phosphate distribution in the model shows high concentrations along the equatorial divergence where nutrient-rich deep water is upwelled, as well as in the high latitudes, with the highest surface concentrations to be simulated in the Southern Ocean. A secondary maximum is calculated in the Eastern Equatorial Pacific and the Subarctic North Pacific; both regions are subject to large scale oceanic upwelling of deep waters. Note that in general, phosphate concentrations in deep waters are higher than at the surface where nutrients are removed by biotic productivity and exported by sinking particulate organic matter to the deeper ocean. However, due to the constant Redfield Ratio (i.e., C:N:P = 122:16:1) applied in the model (Aumont et al., 2015), the phosphorus cycle is closely related to that of nitrogen, as both are subjected to the same large-scale physical processes and circulation in the ocean. An exception is the N_2-fixation that acts as an additional external source for inorganic nitrate in the model. A comparison of the simulated surface phosphate concentration with observational data is given in Fig. S6.

Despite the roughly 1.7 times increase in the phosphate deposition inputs to the ocean from preindustrial to the modern era (Table 1), the preindustrial surface phosphate oceanic concentrations are calculated 20-50% higher in most oceanic regions (Fig. 2g), except for the Southern Ocean where no significant change is calculated. Accordingly, although the projected decrease of the global phosphate input (Table 1), higher phosphorus surface oceanic concentrations are simulated for the future, up to ~20% (Fig. 2i). The main reason for these elevated phosphate concentrations is the decreased primary production almost everywhere (Figs. 3d,f). Indeed, as nitrogen is the limiting factor for phytoplankton in the open ocean, the primary production rates have been lowered according to lower nitrogen deposition rates. Accordingly, less phosphate consumption by phytoplankton growth takes place and this outcompetes the effect of lowered P deposition, leading to relatively higher phosphate concentrations. The effect of the decreased productivity on phosphate concentrations would be, however, even stronger if it was not being partly compensated by higher N_2-fixation rates. Overall, this points to the marine biogeochemical

Deleted: Figure 3 illustrates the comparison between the simulated present-day surface nitrate concentration and the compiled data from the World Ocean Atlas (WOA; Garcia et al., 2010b) for two seasons: the boreal winter (December, January, and February; DJF) and the boreal summer (June, July, and August; JJA). Generally, the model compares quite well with the nitrate surface observations. However, compared to the WOA compilation (Figs. 3a,b) the modelled nitrate concentrations (Figs. 3c,d, respectively) are lower in the northern high latitudes for both seasons (~5-10 mmol/m^3), especially in the Subpolar Pacific Ocean (up to 30 mmol/m^3) during DJF. This is likely related to the model's too shallow mixed layer thickness (not shown) and as a consequence, the transport of nutrients and from deeper layers to the surface is likewise underestimated during the winter season. On the other hand, the surface nitrate concentrations are somewhat overestimated in the Southern Ocean for both seasons (Figs. 3e,f). This is also the case when the model uses PISCES defaults atmospheric deposition fields and it might be related to deficiencies in the model's abiotic processes. In addition, as also explained by Aumont et al. (2015), the WOA climatology may be biased toward lower values since most of the observational data have been collected during the productive season in that region.¶

Deleted: further

Deleted: as calculated

Deleted: CTRL

Deleted: present

Deleted: in

Deleted: in

Deleted: , and as also seen in other modelling studies

Deleted: , with the highest oceanic

Deleted: to be calculated

Deleted: in general

Deleted: ¶
Figure 4 presents the comparison of the modelled with observed

Deleted: concentrations in the upper 100m, for two seasons (DJF and JJA). The

Deleted: (Figs. 4a,b) are taken from Tagliabue et al. (2012) (https://www.bodc.ac.uk/geotraces/data/historical/; last access 29/02/2020). The model simulates reasonably the observed oceanic iron concentrations for both seasons, for the CTRL simulation (Figs. 4c,d). The observed low oceanic DFe concentrations are well ... [1]

Deleted: 4d). Low dissolved iron concentrations of about 0.1 nM (i.e., 1nM = 10^{-9} moles per liter) are simulated and observed in the ... [2]

Deleted: CTRL

Deleted: which

Deleted: Although

Deleted: Despite

Deleted: also

Deleted:

Deleted: 6d

Formatted: Justified

processes as an essential factor in controlling the phosphorus concentrations at the surface ocean rather than depositional fluxes (see also Sect. 3.3.1).

3.2 Nitrogen fixation

For the STD simulation, the nitrogen fixation is calculated to about 112 Tg-N yr^{-1} for the present day (Table 1). The respective relative differences compared to past and future periods are also presented in Figs. 3a-c. Compared to modern times, the model calculates a significant decrease (up to 20%) in nitrogen fixation in the tropical and subtropical Pacific and the subtropical Atlantic Ocean for the preindustrial era. On the contrary, downwind land sources such as the Bay of Bengal and Indonesia, nitrogen fixation is higher for the preindustrial conditions, due to the lower nitrogen deposition fluxes accounted by the model (see Sect. 2.2.1). Finally, the nitrogen fixation rates present very low differences in the Equatorial Pacific, Equatorial Atlantic, and the Southern Indian Ocean (0-10%) away from land sources (Fig. 3a). Note, however, that nitrogen fixation in PISCES is restricted to warm waters (i.e., above 20º C). Therefore, the strong reductions of nitrogen deposition in the mid to high latitude North Pacific in PAST have no direct impact on nitrogen fixation rates. In the subtropical Pacific reduced nitrogen fixation rates mainly reflect the diminished iron input (Fig. 1d). On a global scale, the model calculates overall only a small decrease (~0.2%; Table 1) in preindustrial nitrogen fixation rates compared to present-day, mainly as a result of the decreased soluble iron inputs in the subtropical North Pacific (Fig. 1d). For the future conditions, the model likewise calculates a modest decrease in the global nitrogen fixation (~1%; Table 1) along with decreased iron inputs to the ocean (Figs. 1c,f, respectively) resulting overall in some lower rates of up to 10% in the Equatorial Pacific Ocean (Fig. 3c).

3.3 Primary production

The present-day annual mean primary production together with the relative differences to past and future periods are presented in Figs. 3d-f. The primary production distribution in the open ocean shows high rates along the equatorial divergence and in the high latitudes, where nutrients concentrations are high. The decreased nitrogen deposition during preindustrial conditions compared to present-day results in lowered primary production rates almost in all oceanic regions. A projected modest decrease of primary production rates is calculated by the model (Fig. 3f), owing also to the lower (~14%) dissolved iron deposition fluxes implemented from present to future conditions (Fig. 1f).

The present-day modeled globally integrated production (~47 Pg-C yr^{-1}; Table 1) is lower compared to satellite-based estimates from SeaWiFS (Behrenfeld et al., 2005), obtained equal to ~60-67 Pg-C yr^{-1}, but in the range of estimates from other studies (e.g., 23.9 - 49.1 Pg-C yr^{-1}; Steinacher et al., 2010). A more detailed comparison between satellite estimates (Behrenfeld et al., 2005) and model simulations of the global primary production is presented in Fig. S7. The simulated primary production reproduces the main features derived from satellite-based observations (Figs. S7a,d). The model, however, simulates relatively low rates (~200 mg-C m^{-2} day^{-1}) in the subtropical gyres and higher rates (> 500 mg-C m^{-2} day^{-1}) in upwelling regions, the North Atlantic and the Southern Ocean (Fig. S7g). Nevertheless, as also known from other modeling studies, the primary production in the tropics might be overestimated, whereas in the higher latitudes it might be underestimated (e.g., Steinacher

Deleted: .

Deleted: Figure 5 further compares the simulated surface phosphate concentration with an observation-based data set from WOA, for the summer and winter seasons. The global pattern of observed phosphate is mainly controlled by the ocean dynamics and it is well reproduced by the model. Hence, during winter enhanced wind mixing and convective mixing transport nutrient-rich deep water to the surface in the North Atlantic and North Pacific. At the same time, nutrient consumption by biological productivity in the high latitudes is weak due to low winter temperatures and reduced light conditions. The resulting maximum phosphate concentrations in the Atlantic and Pacific subpolar gyres, however, are somewhat underestimated (up to 1.5 mmol/m^3) by the model compared to the WOA data (Figs. 5a,b). This is also caused by a too shallow winter mixed layer depth simulated by the physical model NEMO as forced by the OMIP standard forcing.¶

Deleted: CTRL

Deleted: 6a

Deleted: 6a

Deleted: only

Deleted: increase (

Deleted: present-day nitrogen fixation rates compared to

Deleted: times

Deleted: increased

Deleted: also

Deleted: (

Deleted: the projected decrease of the global inorganic nitrogen and

Deleted: to result

Deleted: (

Deleted: %)

Deleted: 6c

Deleted: compared

Deleted: 6d

Deleted: On the contrary, a

Deleted: 6f

Deleted: A comparison between satellite estimates and model simulations of the global primary production is presented in Fig. 7. The present-day modelled globally integrated production (~47 Pg yr^{-1}) is lower compared to satellite-based estimates from SeaWiFS

Deleted: obtained equal to ~60-67 Pg yr^{-1}, but in the range of estimates from other studies (e.g., 50.7 ± 9.5 Pg yr^{-1}; Carr et al., 2006). The simulated primary production reproduces the main features derived from satellite-based observations (Behrenfeld et al., 2005). The model

Deleted: . However

Formatted: Justified

et al., 2010). High productivity in the open ocean areas is linked to upwelling areas such as the equatorial divergence zones or coastal upwellings, like at the west coasts of South Africa or northern South America. Primary productivity rates are also underestimated in the North Atlantic region (Fig. S7g), probably due to the low accumulation of nutrients during winter as already discussed. Figure S7 further illustrates the simulated primary production for the boreal winter (DJF) and summer (JJA), compared to the respective observation-based data. The model generally compares reasonably for both seasons; however, the modeled primary production rates (Figs. S7e,f, respectively) are calculated lower in the high latitudes. The pronounced seasonality due to light limitation and temperature of phytoplankton growth in the North Atlantic is well captured by the model. During the warm season, higher water temperatures and better light conditions increase primary production and nutrient consumption by phytoplankton growth in the high latitudes. This results in depleted nutrient concentrations in the North Atlantic during boreal summer. In the North Pacific, which is known as an HNLC region, nutrients remain at higher levels due to insufficient iron support. This is somewhat underestimated in the model as the simulated nitrate concentrations are too low (Fig. S4f), probably related to the slightly high iron concentrations in the upper 100 m North Pacific (Figs. S5d,f). The same biases mentioned for phosphate are likewise seen in the nitrate concentration as most features are mainly controlled by the model physics. Overall, only nitrogen fixation and denitrification can modulate the nitrate concentrations, apart from all other processes that also influence the phosphate in the same way (e.g., productivity, remineralization dissolution, etc.).

Deleted: ,

Deleted: ¶

Deleted: 7

Deleted: modelled

Deleted: 7e

Deleted: the

Deleted: still

Deleted: 3f

Deleted: 4d

3.3.1 Role of depositional nutrient elemental ratios

Despite the relatively strong changes in total atmospheric nutrient supply from PAST to FUTURE (Table 1), the impact of atmospheric nutrients on the global productivity rates remains low in the model. This is, nevertheless, not unexpected, as the atmospheric nutrient supply constitutes only a small fraction of the total ocean nutrient inventory. In addition, oceanic regions that are not nutrient-limited today are less sensitive to external nutrient supply. Finally, a large part of primary production is regenerated by remineralized nutrients from particulate organic matter (mainly detritus) in the upper ocean layer.

To further identify the oceanic regions that are particularly sensitive to changes in external nutrient inputs, the limiting factors for local productivity in the model are investigated. Figure 4a displays limitations due to nitrogen or phosphorus. High values, indicating low limitation, are seen in regions that are subject to intense upwelling, like in the equatorial divergence zones or the western margins of NW and southern Africa and South America (coastal upwelling). Accordingly, these regions are less sensitive to atmospheric deposition as nutrients are supplied from deep ocean layers. Lower nutrient limitation is likewise seen in the mid to high latitudes where limitations by temperature and light (Fig. 4b) limit the growth rates. Exceptions are the North Pacific, the Southern Ocean, and the equatorial Pacific where iron limitation matters (Fig. 4c). Consequently, the model's nutrient sensitivity is largest in the subtropics, in particular in the subtropical gyres where good light conditions and warm waters support high growth rates, paralleled by diminished nutrient supply from depth due to Ekman pumping. Furthermore, these regions are far from land nutrient sources and so, a major part of total primary production relates to regenerated production (i.e., with low rates of external nutrient supply) which is limited by nutrients as temperatures and light are sufficient. This makes productivity in the subtropical gyres sensitive to changes in the external atmospheric nutrient.

Formatted: Justified

In regions with significant macronutrient limitations, the elemental ratio of deposited N:P can be, however, important. To estimate the relative impact of the changes in this ratio, we calculated the modeled nitrogen concentrations relative to the model's Redfield ratio (Fig. 5a). For PRESENT, the model exhibits almost everywhere a deficiency with respect to nitrogen (except for some coastal areas). This is in good agreement with data from WOA which likewise indicates a predominant nitrogen deficiency almost everywhere (Fig. 5b). Next, the N:P ratio relative to the Redfield as supplied by atmospheric deposition for PRESENT (middle) together with the changes in PAST and FUTURE (Fig. S8b) is derived. Overall, a strong excess of N compared to P for modern times is indicated. As a consequence of the model's nitrogen deficiency (Fig. 5a), however, this atmospheric nitrogen excess maintains higher productivity than without the atmospheric supply. For preindustrial times, the atmospheric N:P ratio is almost everywhere reduced, increasing thus the N-deficiency. Hence, rather the lowered atmospheric nitrogen inputs than the lowered phosphorus inputs in PAST and FUTURE are responsible for the diminished productivity in these experiments. To further demonstrate this, we carried out an additional sensitivity simulation (namely PIP simulation) where the phosphorus atmospheric deposition fluxes kept constant at preindustrial levels, while the other studied atmospheric inputs (i.e., N and Fe) varied as for the STD simulation. As expected, the effect on phosphate concentrations (Fig. S9b) and productivity (Fig. S9d) in this sensitivity simulation remains extraordinarily low, i.e., the relative difference to STD is almost everywhere below 1%. This overall demonstrates that the changes in phosphorus do not play a significant role in marine productivity from preindustrial to future periods.

3.3.2 Global patterns of productivity change for preindustrial atmospheric deposition inputs

Model calculations demonstrate three major oceanic regions where the reductions in productivity are strongest in PAST, i.e. the subtropical gyres of the northern hemisphere Pacific, the Atlantic Ocean, and the northernmost North Pacific (Fig. 3d). The subtropical gyres, however, are the most sensitive to changes in nitrogen input and clearly show the strongest productivity reduction compared to PRESENT. Indeed, the nitrogen concentrations in the subtropics are not much affected (Fig. 2a). This is because good light conditions and warm waters persistently maintain high rates of nutrient consumption, so nitrogen concentrations are already very low in PRESENT. Thus, a change in external nutrient supply feeds immediately into productivity without a significant imprint on nitrogen concentrations.

In the northernmost Pacific, the strong productivity decline in PAST (Fig. 3d) is primarily related to the lowered availability of iron, although the reductions in iron deposition remain below 20% (Fig. 2d). However, besides light conditions, iron availability is the most important factor for limiting productivity in this region (Fig. 4c) compared to nitrogen and phosphorus (Fig. 4a). As a consequence, slight changes in iron supply will have a strong impact.

For most of the world ocean, productivity changes in FUTURE are in qualitative agreement with PAST, but less pronounced (Figs. 3d,f). This is mostly because both FUTURE and PAST experiments reflect reduced anthropogenic emissions and thus the same mechanisms are involved. The only exception is the western North Pacific where productivity is rather elevated in FUTURE (Fig. 3f) whereas it is strongly reduced in PAST (Fig. 3d). The different response is related to different iron inputs to the North Pacific (Figs 1d,f).

Formatted: Justified

3.3.3 Changes in phytoplankton composition

As already mentioned in Sect. 2, PISCES models two phytoplankton functional types, i.e., the nanophytoplankton producing calcareous shells and the diatoms producing siliceous shells (Aumont et al., 2015). In the high latitudes, a large part of productivity is related to siliceous diatoms (e.g., Malviya et al., 2016; Uitz et al., 2010) which is accounted for in the model by low nanophytoplankton to diatoms ratios (Fig. 6b). Accordingly, the overwhelming part of productivity reduction in the northernmost Pacific (Fig. 3d) is related to the decline of diatoms. This is well reflected by the increase of the nanophytoplankton to diatoms ratio for PAST relative to PRESENT (Fig. 6a). In turn, this leads to enhanced silicate concentrations in the North Pacific (Fig. 7a). Note that the Si atmospheric inputs are solely related to the dust deposition fluxes, and thus they do not have any interannual variability in the model. Part of the unutilized silicate is advected southward via the North Pacific Current and the California Current, leading also to elevated concentrations along the western coast of North America (Fig. 7a). A further consequence of the strongly diminished productivity is an accumulation of nitrogen in the subpolar gyre of the North Pacific (Fig. 2a). The nitrogen anomaly is strongest in the southwestern area of the gyre and part of the excess nitrogen is injected into the northern California Current. As a result, a strong positive and wedge-shaped productivity anomaly develops in front of western Canada in PAST (Fig. 3d). The positive anomaly is caused by the increased production of nanophytoplankton productivity (not shown) which dominates in this region, as indicated by higher nanophytoplankton to diatom ratios (Fig. 6b); i.e., north of the wedge lowered iron limits productivity, while south of the wedge nitrate is limiting. Altogether, this reflects a slight shift from diatom to nanophytoplankton production in the eastern Pacific (north of 40 °N), as indicated by a decline of ~10% of the nanophytoplankton to diatoms concentrations in the upper 20 m (Fig. 7b).

Apart from the northernmost Pacific, the decline in diatom production leads almost everywhere to slightly increased silicate concentrations in PAST (Fig. 7a). Productivity changes in the Southern Ocean remain low (Fig. 3d) for PAST. The reason for this is the strong light limitation around Antarctica (Fig. 4b) and the deep mixed layer which suppresses productivity and subsequently builds up a large pool of unutilized nutrients. Part of the unutilized nutrients is advected further north into the Southern Ocean, driving productivity there. Accordingly, the reduced deposition of nitrogen and iron in this area (Figs. 1a,d) have only a slight impact on productivity. Consequently, this region is relatively robust against external nutrient input maintaining stable productivity. A similar effect is seen for the North Atlantic where vigorous exchange with Arctic waters takes place across the Norwegian-Greenland Sea. By contrast, in the subpolar North Pacific, the import of unutilized nutrients from the Arctic is hampered, as the water exchange with polar waters is limited by the shallow Bering Strait and the Aleutian Arc. Therefore, the North Pacific appears the most sensitive to external nutrient inputs compared to other oceanic regions.

3.3.4 Global patterns of productivity change for future atmospheric deposition inputs according to the RCP8.5 emission scenario

For most parts of the global ocean, the changes in productivity in the FUTURE experiment are in qualitative agreement with PAST, but less pronounced. This is mostly because both FUTURE and PAST experiments reflect reduced anthropogenic emission and so the same mechanisms are involved. The only notable exception compared to PAST (Fig. 3d), is demonstrated

Formatted: Justified

in the eastern North Pacific where a strong negative wedge-shaped anomaly is seen in FUTURE (Fig. 3f). This opposite response is related to different iron inputs to the North Pacific. In FUTURE, the reduction of iron atmospheric inputs (Fig. 1f) is by far less strong and in the NE Pacific is even higher than today, thus the productivity increases in the NE Pacific subtropical gyre (Fig. 3f). As a result, more nitrogen is consumed in the subpolar gyre in FUTURE and no nitrogen accumulation takes place as in PAST (Figs. 2a,c). Accordingly, a strong negative nitrogen anomaly develops in the western North Pacific and nitrogen depleted waters are advected southward along the California Current (i.e., opposite to PAST). Altogether, these results imply an extreme sensitivity of the North Pacific against changes in atmospheric iron input. By contrast, the North Atlantic, which is less affected by iron limitation, reflects a widespread decline in productivity mainly controlled by reduced nitrogen inputs.

4 Biogeochemistry responses to atmospheric organic nutrients

Most marine biogeochemistry studies mainly account for the inorganic fraction as the most important pool of nutrients from the atmospheric pathway. However, state-of-the-art atmospheric chemistry models nowadays not only efficiently calculate the total dissolved nutrient atmospheric deposition fluxes, but they include the organic part as well, which turns out to be rather important for the total magnitude of the atmospheric input to the ocean (Fig. S3). Great uncertainty still exists concerning the importance of organic fraction on oceanic productivity. For this, we separated here the inorganic and organic fractions of the atmospheric nutrients to investigate the role of organic components in marine biogeochemistry. To estimate the response of the marine ecosystem to the contribution of the organic fraction in the atmospheric nutrient (N, P, and Fe) inputs, the differences in nitrogen fixation and primary production rates between the STD and the ORG simulations are presented in Fig. 8. Note that, as for the riverine organic fractions in the model (see Aumont et al., 2015), we assume here an instant transformation of the atmospheric dissolved organic nitrogen (DON) and organic phosphorus (DOP) inputs to the respective inorganic fractions in the water column.

When the organic fraction of the atmospheric nutrients is considered in the model, a modest decrease in the global nitrogen fixation rates of ~0.5 Tg-N yr^{-1} is calculated for present-day conditions (Table 1). The increased soluble Fe inputs (~25%) relative to the STD simulations - although smaller compared to relative increases of N (~45%) and P (~50%) - tend to reduce the Fe-limitation in diazotrophs. Consequently, the reduced Fe-limitations make the extra atmospheric inputs of ON to the ocean more effective, overall decreasing the global nitrogen fixation rates in the model (Fig. 8a). Note, however, that the nitrogen fixation is a rather energy-expensive process that is known to be inhibited in the excess of ammonium, in particular. In the tropical Pacific Ocean, the nitrogen fixation rates for the ORG simulation are significantly more intense compared to STD (up to ~90%) but suppressed (up to ~40%) elsewhere (Fig. 8b). For example, in the Indonesian throughflow and the eastern tropical Atlantic along central Africa, significantly reduced rates (more than 90%) are calculated for the ORG simulation. The lowered nitrogen fixation rates in these regions are mainly due to the additional ON deposition in the ocean. Nitrogen fixation is also decreased in the tropical Atlantic Ocean. On the other hand, increased soluble Fe inputs to the tropical

Formatted: Heading 1

Deleted: The differences of nitrogen fixation and primary production rates between the CTRL and the ORGF simulations are here used to estimate the response of the marine ecosystem to the contribution of the organic fraction in the atmospheric nutrient (N, P, and Fe) inputs. …ost marine biogeochemistry studies mainly account for the inorganic fraction of nutrients …s the most important pool on nitrogen…f nutrients from the atmospheric pathway. On the contrary, uncertainty still exists with respect to the organic fraction in atmospheric fluxes into the ocean. …owever, state-of-the-art atmospheric chemistry models can …owadays not only efficiently calculate the total dissolved nutrient atmospheric deposition fluxes including… but they include the organic part as well, which seems…urns out to be overall…rather important for the total magnitude of the atmospheric input to the ocean (see …ig. S1). To investigate ... [3]

Formatted: Default Paragraph Font, Underline color: Auto, Font color: Auto

Deleted: role

Formatted: Default Paragraph Font, Underline color: Auto, Font color: Auto

Deleted: components

Formatted: None

Deleted: isolate their contributions to the

Formatted ... [4]

Deleted: our approach is supported by the fact that PISCES, as also other biogeochemistry models, does not separately model the dissolved

Formatted: Font: Times New Roman, Font color: Black

Deleted: nitrogen (DON) and phosphorus (DOP), but all the dissolved organic matter is assumed to be instantaneously remineralized to the respective inorganic pools, i.e., the DIN and the DIP …ractions in the model (see Aumont et al., 2015).¶ ... [5]

Deleted: CTRL…TD simulations - although smaller compared to relative increases of N (~45%) and P (~50%) - tend to reduce the Fe-limitation in diazotrophs. Thus…onsequently, the reduced Fe- and P-limitations along with…ake the extra atmospheric inputs of ON to the the ocean more effective, overall decrease…ecreasing the global nitrogen fixation rates in the model (Fig. 8a). Note, however, that the nitrogen fixation is a rather energy-expensive process that is known to be inhibited in the excess of ammonium, in particular. Thus, the assumption of a rapid DON remineralization, considering also that the ON in the atmospheric particulate phase predominantly contains reduced nitrogen, may lead partially to an overestimation of the response of nitrogen fixation rates when accounting for the organic fraction of atmospheric nutrients. ... [6]

Deleted: Compared to CTRL…n the tropical Pacific Ocean, the nitrogen fixation rates for the ORGF…RG simulation are significantly more intense compared to STD (up to ~90%) in the tropical Pacific Ocean …ut suppressed (up to ~40%) in the tropical Atlantic Ocean…lsewhere (Fig. 8b). Especially…or example, in the Indonesian throughflow and in …he eastern tropical Atlantic along central Africa, significantly reduced rates (more than 90%) are ... [7]

Formatted: Justified

Pacific (Fig. S3d), partially lower the Fe limitation of diazotrophs and increase nitrogen fixation in these remote oceanic regions. Overall, compared to the STD, the present-day global nitrogen fixation rate for the ORG simulation leads to a net decrease by only ~0.4% (Table 1).

Primary production increases almost in all ocean basins for the ORG simulation (Fig. 8d), except some parts of the Subpolar Pacific Ocean. In particular, higher rates are calculated in the subpolar Atlantic Ocean (up to 15%). In the N-limited oceanic regions, the increased atmospheric nitrogen deposition (Fig. S3b) directly increases the production rates (Fig. 8d). Such a case is the western subtropical North Pacific, where atmospheric N deposition supports an extra production of up to 15%. The production rates are also increased in the subtropical South Pacific and Atlantic Oceans up to nearly 20%. In total, the primary production increased from ~46.7 Pg-C yr^{-1} for the STD to ~47.8 Pg-C yr^{-1} for the ORG (Table 1). Figure 8d points out to regions in the Pacific where production decreased. For the North Pacific, this represents the same mechanism as described above for the differences in primary production rates between PAST and PRESENT (Sect. 3.3). For the ORG simulation, the increased iron input in the Pacific subpolar gyre increases diatom production leading to higher consumption of nitrate (Fig. S10b). Subsequent transport of nitrogen diminished waters further to the south cause a decrease in productivity further south. The boundary between decreased and increased bands matches the sharp transition from iron limitation to nitrogen limitation (Figs. 4a,c). Increased iron input south of the boundary (i.e., where Fe limits) stimulates the production and diminishes nitrogen. However, the advective mixing of the N-diminished waters with waters further north decreases productivity north of the boundary (i.e., where N limits). Overall, the result is the dipole pattern as demonstrated in Fig. 8d.

5 Discussion

The main focus of this study is to investigate the effect of nutrient deposition on oceanic primary production. Hence, the presented experiments did not account for the impact of future climate change which could interact or may even mask the effect of changed atmospheric deposition fluxes considered here. Consequently, the here found effects are subject to some uncertainties related to the potential interaction with climate change. For example, climate-induced changes in the global wind system may not only alter atmospheric pathways for nutrients but also impact on oceanic up- and down-welling. Thus, shifts in the seasonal position of trade winds will likewise force shifts in the position of open-ocean and coastal upwelling. These regions are usually nutrient-rich and not particularly sensitive to varying atmospheric nutrient inputs. Displacements of these upwelling positions as a result of climate change can increase the sensitivity to external nutrient inputs in regions formerly impacted by upwelling.

Several studies have demonstrated that mid to high latitude areas, such as the North Atlantic and the Arctic, will be more stratified in a future warmer climate (Bindoff et al., 2019; Fu et al., 2016; Gröger et al., 2013; Sein et al., 2018; Steinacher et al., 2010), with negative feedback on vertical mixing and marine primary production due to reduced upward transport of nutrients into the photic zone. Accordingly, primary production in these regions will probably be more sensitive to changed atmospheric deposition rates in the future climate. Our results overall imply only marginal effects in polar regions like the

Deleted: S1d) for the ORGF simulation,

Deleted: decreased

Deleted: CTRL,

Deleted: simulated

Deleted: ORGF

Deleted:), although pronounced regional differences between the two simulations exist (Fig. 8b

Deleted: In contrast to the rather balanced nitrogen fixation rates, the primary production rates increased in the ORGF simulation (Fig. 8c), as the total atmospheric nitrogen inputs increased in the model (Fig. S1). According to global calculations, the primary production increased from ~46.7 Pg-C yr^{-1} for the CTRL to ~47.8 Pg-C yr^{-1} for the ORGF (Table 1). This increase may correspond to a modest decline of atmospheric pCO_2 of ~1.3 ppm, solely when accounting the organic fraction in atmospheric inputs in the model. The respective percentage differences compared to the CTRL simulation are presented in Fig. 8d.

Deleted: (

Deleted:) for the ORGF simulation. Moreover

Deleted: Subpolar

Deleted:

Deleted: ORGF

Deleted: S1b

Deleted: In

Deleted: the

Deleted: supported

Deleted: open

Deleted: % in the ORGF simulation.¶ ... [8]

Deleted: in space and time is also well in the range of satellite- ... [9]

Deleted: forced with bias-corrected forcing from the RCP8.5 ... [10]

Moved down [2]: in a global nitrogen-fixation rate of ~112 Tg-N

Deleted: This

Deleted: oceanic productivity was supported in the model by the ... [11]

Deleted: inputs (combustion sources and atmospheric processing of ... [12]

Deleted: were calculated for the modern subtropical Pacific and ... [13]

Deleted: **Another feature tested in the present**

Deleted: the contribution of organics to the atmospheric inputs to ... [14]

Deleted: Furthermore

Deleted: On the other hand, several studies have demonstrated that ... [15]

Moved down [3]: Accordingly, primary production in these

Moved (insertion) [3]

Deleted: Our results imply only marginal effects in cold regions ... [16]

Formatted: Justified

Arctic Ocean. This is certainly robust under the present climate when marine productivity is limited by temperature and sea-ice reducing light conditions in these regions. However, there is a large agreement that climate change will be most severe in the high latitudes, with strong increases in the water temperatures and substantially diminished sea ice cover in the Arctic (Collins et al., 2013). Temperature and sea-ice related light limitation will likely become less important in a future climate in this region and thus, more nutrients will be recycled in the polar region and less exported equatorward. Consequently, changes in atmospheric transport and deposition of the bioavailable nutrients may play a larger role in the future climate than today, especially under the high-emission climate scenarios. An example can be seen in the high latitudes of the Southern Ocean around Antarctica where the major amount of surplus DFe is deposited in our PAST and FUTURE experiments. As expected, the additional DFe availability has nearly no effect on productivity as convective mixing and extremely low water temperatures maintain sufficient nutrients and support low productivity under the present-day climate. This may, however, change with altered oceanographic conditions under a future warmer climate. In the northern hemisphere, namely the northernmost Pacific, known as an HNLC region where iron is the limiting factor, the increased supply of DFe clearly stimulates marine productivity in the PRESENT and FUTURE periods compared to PAST. However, this increase in productivity is likely overestimated since our experiments lack climate-induced changes in future stratification which would reduce the nutrient supply from the deep ocean.

The impact of atmospheric organic nutrients on the global oceanic productivity turns out as high (~1 Pg-C yr^{-1}; Table 1) as the increase in the present-day primary production since preindustrial times when only inorganic nutrients' supply is accounted for. However, all changes in nutrient deposition fluxes here accounted for, are solely driven by changes in the anthropogenic and biomass burning emissions, along with the changes in insoluble to soluble conversions rates due to atmospheric processing. Thus, the atmospheric deposition fields used in this study did not account for any changes in dust and bioaerosol emissions. Instead, they were kept constant to the present-day atmosphere (i.e., the year 2010), although several studies suggest that dust fluxes may be sensitive to climate change and the land-use changes (e.g., Ginoux et al., 2012; Mahowald et al., 2010; Prospero and Lamb, 2003), and thus could be an important driver of the atmospheric nutrient cycles.

6 Summary and conclusions

This study presents the implementation of state-of-the-art monthly mean atmospheric deposition fields in the global biogeochemistry model PISCES. The model is here run in offline modus, forced by dynamical physical outputs from the physical ocean model NEMO. The newly coupled atmospheric deposition fields considered for this work are all calculated based on a detailed representation of emissions of natural and combustion nutrient-containing aerosols, detailed atmospheric gas- and aqueous-phase chemical schemes, and mineral dissolution processes due to atmospheric acidity and organic ligands. Another feature tested in the present study is the contribution of organic components to the atmospheric inputs to the global ocean. Moreover, to effectively isolate here the impact of atmospheric deposition on the marine biogeochemistry parameters, the atmospheric CO_2 mixing ratio is set to the preindustrial values for all simulations.

Deleted: is

Deleted: . Thus, temperature and light limitation will likely become less important in a future climate in this region and thus, nutrient limitations will increase.

Deleted: such as RCP8.5.

Deleted: latitude

Deleted: had

Deleted: cold

Deleted: maintained

Deleted: northwestern

Deleted: stimulated

Deleted: experiment. This

Deleted: underestimated because

Deleted: lacked the

Deleted: Note also that

Deleted:

Deleted: , for this study the atmospheric CTM did not account for any changes in dust emissions for the preindustrial and future conditions, but they were kept constant to the present-day atmosphere (i.e., the year 2010).

Deleted: The combined effect of climate change

Formatted: Justified

For the present day, ~40 Tg-N yr^{-1}, ~0.28 Tg-Fe yr^{-1}, and ~0.10 Tg-P yr^{-1} of nitrogen, iron, and phosphorus atmospheric inputs to the global ocean, accounting for their inorganic fractions, are considered in PISCES. This results in a global nitrogen-fixation rate of ~112 Tg-N yr^{-1} and an integrated primary production of roughly 47 Pg-C yr^{-1}. Compared to present-day conditions, the lower preindustrial atmospheric nutrient inputs to the ocean result in a weakened primary production of ~2% globally. The decrease in oceanic productivity is supported by the preindustrial decrease in the soluble iron inputs, resulting from changes in combustion sources and the atmospheric processing of mineral aerosols along with the substantial decrease in atmospheric anthropogenic nitrogen inputs. The projected changes in air pollutants under the RCP8.5 emission scenario also result in a modest decrease in marine productivity compared to modern times. Global nitrogen-fixation rates present here a marginal variability, although some notable decreases are calculated for the modern subtropical Pacific and Atlantic gyres.

This work asserts the importance of an explicit representation of the atmospheric nutrients in the context of biogeochemistry modeling, providing also a first assessment of the contribution of another source of atmospheric nutrients than inorganics and, thus, the potential importance of organic nutrients on oceanic productivity. Overall, our main conclusions can be summarized as:

1) An overall low impact of atmospheric nutrient deposition scenarios on total marine primary production on a global scale. This is because much of modern productivity is driven by nutrients already recycled in the euphotic zone or by nutrient import from the deep ocean (such as in upwelling regions). Additionally, atmospheric transport appears rather important, as a significant part of nutrient deposition takes place in the northern high latitudes, where light conditions and temperature further limit productivity. Accordingly, even substantial reductions of nitrogen, phosphorus, and iron inputs, ranging between 36 and 51% during the preindustrial period, result in an only modest decline of primary production of about 3%.
2) Substantial local productivity changes of up to 20% are found in regions limited by nutrients. The strongest sensitivity against atmospheric nutrients is found for the oligotrophic subtropical gyres of the North Atlantic and the North Pacific, where good light conditions and warm temperatures together with low nutrient concentrations predominate. Additional atmospheric nutrient input to these regions immediately results in production by increasing the biogenic turnover.
3) The North Pacific turns out to be the most sensitive to iron deposition. For the preindustrial period, the lowered input of iron to this region leads to a strong decline of siliceous diatom production leading to an enrichment of silicate, nitrogen, and phosphorus. In turn, this leads to enhanced equatorward transport of nutrients resulting in elevated production rates of calcareous nanophytoplankton further southeast.
4) The North Pacific appears more sensitive to external nutrient atmospheric deposition compared to other oceanic regions mainly due to two reasons: the strongest deposition changes take place in the northern mid to high latitudes, and that compared to the Southern Ocean and the North Atlantic, the exchange with cold and nutrient-enriched polar waters is limited by land by the shallow Bering Strait and the Aleutian arc. By contrast, the southern high latitude ocean contains a large amount of unutilized nutrients that are advected further north (to mid-latitudes) making this

Moved (insertion) [2]

Deleted: is beyond the scope of the present study. However, this

Deleted: , i.e., the

Deleted: , and their potential impact on the oceanic productivity. Finally, despite the here discussed effects on nutrient-depleted ocean regions, the global ocean turned out to be notably robust with regard to the

Deleted: , against realistic scenarios for future and past atmospheric nutrient supply. The same

Deleted: likely be reached by other biogeochemistry models. This might be related to the large part of newly produced particular organic matter that is already remineralized within the ocean's mixed layer, so that nutrients formerly incorporated in the soft tissue becomes again rapidly bioavailable. Remineralization in state-of-the-art models, however, is parameterized according to present-day empirical relationships,

Deleted: well as the models' biogeochemistry and ocean dynamics are tuned against climatologies valid for the present-day climate. Furthermore, a more explicit representation of the nutrients' stoichiometric variability, rather than the fixed Redfield ratios routinely used in global biogeochemistry models, will allow a better representation of the marine productivity in protected climate forcings. Further investigations of the

Deleted: the

Deleted: inputs to the global oceanic

Deleted: are required under

Formatted: Justified

region more robust against changes in external nutrient input. In agreement, however, with observational evidence from WOA, PISCES exhibits a widespread surplus of nitrogen compared to phosphorus and with respect to the Redfield ratio. Therefore, the applied changes in phosphorus inputs have nearly no impact on primary production in the model. This applies even to the warm water regions, where reductions in atmospheric iron supply limit nitrogen fixation by diazotrophs in both PAST and FUTURE periods.

5) Finally, the effect of atmospheric organic nutrient deposition fluxes on the global primary production is calculated roughly as strong as the effect of the present-day increased emissions and atmospheric processing on the oceanic biogeochemistry since preindustrial times when only the inorganic fraction is considered in the model (~1 Pg-C yr^{-1}). Note that based on the Krishnamurthy et al. (2009) model estimations, an atmospheric pCO_2 declined of about 2.2 ppm due to the modern era's iron and nitrogen inputs to the global ocean can be supported. Accordingly, the here calculated increase in primary production related to the input of organic nutrients could correspond to a respective decrease in atmospheric pCO_2 of ~1.6 ppm. Although the overall impact of atmospheric organic nutrient deposition on a global scale is rather low, some stronger changes in regional oceanic productivity are clearly demonstrated in the oligotrophic subtropical gyres.

Formatted: Justified

Data availability. Atmospheric nutrient deposition data used for this study are available at Zenodo (doi: 10.5281/zenodo.4017209).

Author contribution. SM prepared the atmospheric input fields, performed the simulations, and the model evaluation. MG prepared the model forcing data. SM and MG wrote the manuscript. All authors contributed to the manuscript preparation.

Acknowledgments. Stelios Myriokefalitakis acknowledges financial support for this research from the European Union's Horizon 2020 research and innovation programme under the Marie Skłodowska-Curie grant agreement no. 705652 – ODEON. Matthias Gröger and Jenny Hieronymus acknowledge support from the European Commission's Horizon 2020 Framework Programme, under Grant Agreement number 641816, the "Coordinated Research in Earth Systems and Climate: Experiments, kNowledge, Dissemination and Outreach (CRESCENDO)". Stelios Myriokefalitakis acknowledges support from the Joint Group of Experts on the Scientific Aspects of Marine Environmental Protection (GESAMP; http://www.gesamp.org/), Working Group 38, the Atmospheric Input of Chemicals to the Ocean. The authors thank Alessandro Tagliabue for providing the dissolved iron oceanic concentration dataset. Model simulations were carried out on the Bi cluster operated by the Swedish National Supercomputer Centre (http://www.nsc.liu.se/) and data processing is supported by computational time granted by the Greek Research and Technology Network (GRNET) in the National HPC facility ARIS (https://hpc.grnet.gr/) under the project PR006002-ADIOS. The authors thank two anonymous reviewers for their comments that significantly helped to improve the final manuscript. The publication of this work was financed by the internal grant program of the National Observatory of Athens "Atmospheric deposition impacts on the ocean system" (number 5065).

Competing interests. The authors declare that they have no conflict of interest.

Deleted: climate change scenarios for the physical ocean and accounting for variable Redfield ratios in the marine environment.

Deleted: Page Break

Deleted: :

Deleted: preformed

Deleted: initialization fields.

Deleted: :

Deleted: acknowledges

Deleted: (https://hpc.grnet.gr/),

Deleted: programme

Deleted: :

Formatted: Font: Not Bold

Formatted: Justified

References

Aumont, O. and Bopp, L.: Globalizing results from ocean in situ iron fertilization studies, Global Biogeochem. Cycles, 20(2), GB2017, doi:10.1029/2005GB002591, 2006.

Aumont, O., Ethé, C., Tagliabue, A., Bopp, L. and Gehlen, M.: PISCES-v2: an ocean biogeochemical model for carbon and ecosystem studies, Geosci. Model Dev., 8(8), 2465–2513, doi:10.5194/gmd-8-2465-2015, 2015.

Barkley, A. E., Prospero, J. M., Mahowald, N., Hamilton, D. S., Popendorf, K. J., Oehlert, A. M., Pourmand, A., Gatineau, A., Panechou-Pulcherie, K., Blackwelder, P. and Gaston, C. J.: African biomass burning is a substantial source of phosphorus deposition to the Amazon, Tropical Atlantic Ocean, and Southern Ocean, Proc. Natl. Acad. Sci. U. S. A., 116(33), 16216–16221, doi:10.1073/pnas.1906091116, 2019.

Behrenfeld, M. J., Boss, E., Siegel, D. A. and Shea, D. M.: Carbon-based ocean productivity and phytoplankton physiology from space, Global Biogeochem. Cycles, 19(1), 1–14, doi:10.1029/2004GB002299, 2005.

Behrenfeld, M. J., O'Malley, R. T., Siegel, D. A., McClain, C. R., Sarmiento, J. L., Feldman, G. C., Milligan, A. J., Falkowski, P. G., Letelier, R. M. and Boss, E. S.: Climate-driven trends in contemporary ocean productivity, Nature, 444(7120), 752–755, doi:10.1038/nature05317, 2006.

Bindoff, N. L., Cheung, W. W. L., Kairo, J. G., Arístegui, J., Guinder, V. A., Hallberg, R., Hilmi, N., Jiao, N., Karim, M. S., Levin, L., O'Donoghue, S., Cuicapusa, S. R. P., Rinkevich, B., Suga, T., Tagliabue, A. and Williamson, P.: Changing Ocean, Marine Ecosystems, and Dependent Communities, IPCC Spec. Rep. Ocean Cryosph. a Chang. Clim. [H.-O. Pörtner, D.C. Roberts, V. Masson-Delmotte, P. Zhai, M. Tignor, E. Poloczanska, K. Mintenbeck, A. Alegría, M. Nicolai, A. Okem, J. Petzold, B. Rama, N.M. Weyer (eds.)]., 2019.

Camarero, L. and Catalan, J.: Atmospheric phosphorus deposition may cause lakes to revert from phosphorus limitation back to nitrogen limitation, Nat. Commun., 3, 1118, doi:10.1038/ncomms2125, 2012.

Christodoulaki, S., Petihakis, G., Kanakidou, M., Mihalopoulos, N., Tsiaras, K. and Triantafyllou, G.: Atmospheric deposition in the Eastern Mediterranean. A driving force for ecosystem dynamics, J. Mar. Syst., 109–110, 78–93, doi:10.1016/j.jmarsys.2012.07.007, 2013.

Christodoulaki, S., Petihakis, G., Mihalopoulos, N., Tsiaras, K., Triantafyllou, G. and Kanakidou, M.: Human-Driven Atmospheric Deposition of N and P Controls on the East Mediterranean Marine Ecosystem, J. Atmos. Sci., 73, 1611–1618, doi:10.1175/JAS-D-15-0241.1, 2016.

Collins, M., Knutti, R., Arblaster, J., Dufresne, J.-L., Fichefet, T., Friedlingstein, P., Gao, X., Gutowski, W. J., Johns, T., Krinner, G., Shongwe, M., Tebaldi, C., Weaver, A. J. and Wehner, M.: Intergovernmental Panel on Climate Change Working Group I. Climate Change 2013: The Physical Science Basis. Long-term Climate Change: Projections, Commitments and Irreversibility, in Climate Change 2013: The Physical Science Basis. Contribution of Working Group I to the Fifth Assessment Report of the Intergovernmental Panel on Climate Change, edited by T. F. Stocker, D. Qin, G.-K. Plattner, M. Tignor, S. K. Allen, J. Boschung, A. Nauels, Y. Xia, V. Bex, and P. M. Midgley, Cambridge University Press, Cambridge, United Kingdom

Formatted: Font: Times New Roman

Formatted: Font: Times New Roman

Deleted: Carr, M.-E., Friedrichs, M. A. M., Schmeltz, M., Noguchi Aita, M., Antoine, D., Arrigo, K. R., Asanuma, I., Aumont, O., Barber, R., Behrenfeld, M., Bidigare, R., Buitenhuis, E. T., Campbell, J., Ciotti, A., Dierssen, H., Dowell, M., Dunne, J., Esaias, W., Gentili, B., Gregg, W., Groom, S., Hoepffner, N., Ishizaka, J., Kameda, T., Le Quéré, C., Lohrenz, S., Marra, J., Mélin, F., Moore, K., Morel, A., Reddy, T. E., Ryan, J., Scardi, M., Smyth, T., Turpie, K., Tilstone, G., Waters, K. and Yamanaka, Y.: A comparison of global estimates of marine primary production from ocean color, Deep Sea Res. Part II Top. Stud. Oceanogr., 53(5–7), 741–770, doi:10.1016/j.dsr2.2006.01.028, 2006.¶

Formatted: Justified

and New York, NY, USA, Cambridge., 2013.

Dee, D. P., Uppala, S. M., Simmons, A. J., Berrisford, P., Poli, P., Kobayashi, S., Andrae, U., Balmaseda, M. A., Balsamo, G., Bauer, P., Bechtold, P., Beljaars, A. C. M., van de Berg, L., Bidlot, J., Bormann, N., Delsol, C., Dragani, R., Fuentes, M., Geer, A. J., Haimberger, L., Healy, S. B., Hersbach, H., Hólm, E. V, Isaksen, L., Kållberg, P., Köhler, M., Matricardi, M., McNally, A. P., Monge-Sanz, B. M., Morcrette, J.-J., Park, B.-K., Peubey, C., de Rosnay, P., Tavolato, C., Thépaut, J.-N., Vitart, F., Berg, L. Van De, Bidlot, J., Bormann, N., Delsol, C., Dragani, R., Fuentes, M., Geer, A. J. and Dee, D. P.: The ERA-Interim reanalysis: configuration and performance of the data assimilation system, Q. J. R. Meteorol. Soc., 137(656), 553–597, doi:10.1002/qj.828, 2011.

Duce, R. A., Liss, P. S., Merrill, J. T., Atlas, E. L., Hicks, B. B., Millertl, J. M., Prospero, J. M., Arimoto, R., Church, T. M., Ellis, W., Galloway, J. N., Hansen, L., Knap, A. H., Reinhardt, K. H., Soudine, A., Tsunogai, S., Wollast, R. and Zhou, M.: The atmospheric input of trace species to the world ocean, Global Biogeochem. Cycles, 5(3), 193–259, 1991.

Duce, R. A., LaRoche, J., Altieri, K., Arrigo, K. R., Baker, A. . R., Capone, D. G., Cornell, S., Dentener, F., Galloway, J., Ganeshram, R. S., Geider, R. J., Jickells, T. D., Kuypers, M. M., Langlois, R., Liss, P. S., Liu, S. M., Middelburg, J. J., Moore, C. M., Nickovic, S., Oschlies, A., Pedersen, T., Prospero, J., Schlitzer, R., Seitzinger, S., Sorensen, L. L., Uematsu, M., Ulloa, O., Voss, M., Ward, B. and Zamora, L.: Impacts of Atmospheric Anthropogenic Nitrogen on the Open Ocean, Science (80-.)., 320(5878), 893–897, doi:10.1126/science.1150369, 2008.

Falkowski, P. G., Scholes, R. J., Boyle, E., Canadell, J., Canfield, D., Elser, J., Gruber, N., Hibbard, K., Högberg, P., Linder, S., Mackenzie, F. T., Moore, B., Pedersen, T., Rosenthal, Y., Seitzinger, S., Smetacek, V. and Steffen, W.: The Global Carbon Cycle: A Test of Our Knowledge of Earth as a System, Science (80-.)., 290(5490), 291–296, doi:10.1126/science.290.5490.291, 2000.

Fountoukis, C. and Nenes, A.: ISORROPIA II: a computationally efficient thermodynamic equilibrium model for K+–Ca2+–Mg2+–NH4+–Na+–SO42−–NO3, Atmos. Chem. Phys., 7(17), 4639–4659, doi:10.5194/acp-7-4639-2007, 2007.

Fu, W., Randerson, J. T. and Moore, J. K.: Climate change impacts on net primary production (NPP) and export production (EP) regulated by increasing stratification and phytoplankton community structure in the CMIP5 models, Biogeosciences, 13(18), 5151–5170, doi:10.5194/bg-13-5151-2016, 2016.

Garcia, H., Locarnini, R., Boyer, T., Antonov, T., Baranova, O., Zweng, M. and Johnson, D.: WORLD OCEAN ATLAS 2009 Volume 3: Dissolved Oxygen, Apparent Oxygen Utilization, and Oxygen Saturation, U.S. Government Printing Office, Washington DC., 2010a.

Garcia, H. E., Locarnini, R. A., Boyer, T. P., Antonov, J. I., Zweng, M. M., Baranova, O. K. and Johnson, D. R.: WORLD OCEAN ATLAS 2009 Volume 4: Nutrients (phosphate, nitrate and silicate), U.S. Government Printing Office, Washington, D.C., 2010b.

Ginoux, P., Prospero, J. M., Gill, T. E., Hsu, N. C. and Zhao, M.: Global-scale attribution of anthropogenic and natural dust sources and their emission rates based on MODIS Deep Blue aerosol products, Rev. Geophys., 50(3), RG3005, doi:10.1029/2012RG000388, 2012.

Formatted: Font: Times New Roman

Formatted: Justified

Gröger, M., Maier-Reimer, E., Mikolajewicz, U., Moll, A. and Sein, D.: NW European shelf under climate warming: implications for open ocean exchange, primary production, and carbon absorption, Biogeosciences, 10(6), 3767–3792, doi:10.5194/bg-10-3767-2013, 2013.

Gruber, N.: The Dynamics of the Marine Nitrogen Cycle and its Influence on Atmospheric CO2 Variations, in The Ocean Carbon Cycle and Climate, pp. 97–148, Springer Netherlands, Dordrecht., 2004.

Gruber, N., Gloor, M., Mikaloff Fletcher, S. E., Doney, S. C., Dutkiewicz, S., Follows, M. J., Gerber, M., Jacobson, A. R., Joos, F., Lindsay, K., Menemenlis, D., Mouchet, A., Müller, S. A., Sarmiento, J. L. and Takahashi, T.: Oceanic sources, sinks, and transport of atmospheric CO2, Global Biogeochem. Cycles, 23(1), GB1005, doi:10.1029/2008GB003349, 2009.

Guieu, C., Dulac, F., Ridame, C. and Pondaven, P.: Introduction to project DUNE, a DUst experiment in a low Nutrient, low chlorophyll Ecosystem, Biogeosciences, 11(2), 425–442, doi:10.5194/bg-11-425-2014, 2014.

Hajima, T., Watanabe, M., Yamamoto, A., Tatebe, H., Noguchi, A., Abe, M., Ohgaito, R., Ito, A., Yamazaki, D., Okajima, H., Ito, A., Takata, K., Ogochi, K., Watanabe, S. and Kawamiya, M.: Description of the MIROC-ES2L Earth system model and evaluation of its climate-biogeochemical processes and feedbacks, Geosci. Model Dev. Discuss, doi:10.5194/gmd-2019-275, 2019.

Hamilton, D. S., Moore, J. K., Arneth, A., Bond, T. C., Carslaw, K. S., Hantson, S., Ito, A., Kaplan, J. O., Lindsay, K., Nieradzik, L., Rathod, S. D., Scanza, R. A. and Mahowald, N. M.: Impact of Changes to the Atmospheric Soluble Iron Deposition Flux on Ocean Biogeochemical Cycles in the Anthropocene, Global Biogeochem. Cycles, 34(3), doi:10.1029/2019GB006448, 2020.

Holt, J., Butenschön, M., Wakelin, S. L., Artioli, Y. and Allen, J. I.: Oceanic controls on the primary production of the northwest European continental shelf: model experiments under recent past conditions and a potential future scenario, Biogeosciences, 9(1), 97–117, doi:10.5194/bg-9-97-2012, 2012.

Huneeus, N., Schulz, M., Balkanski, Y., Griesfeller, J., Prospero, J., Kinne, S., Bauer, S., Boucher, O., Chin, M., Dentener, F., Diehl, T., Easter, R., Fillmore, D., Ghan, S., Ginoux, P., Grini, A., Horowitz, L., Koch, D., Krol, M. C., Landing, W., Liu, X., Mahowald, N., Miller, R., Morcrette, J.-J., Myhre, G., Penner, J., Perlwitz, J., Stier, P., Takemura, T. and Zender, C. S.: Global dust model intercomparison in AeroCom phase I, Atmos. Chem. Phys., 11(15), 7781–7816, doi:10.5194/acp-11-7781-2011, 2011.

Ito, A.: Global modeling study of potentially bioavailable iron input from shipboard aerosol sources to the ocean, Global Biogeochem. Cycles, 27(1), 1–10, doi:10.1029/2012GB004378, 2013.

Ito, A. and Xu, L.: Response of acid mobilization of iron-containing mineral dust to improvement of air quality projected in the future, Atmos. Chem. Phys., 14(7), 3441–3459, doi:10.5194/acp-14-3441-2014, 2014.

Ito, A., Myriokefalitakis, S., Kanakidou, M., Mahowald, N. M., Scanza, R. A., Hamilton, D. S., Baker, A. R., Jickells, T., Sarin, M., Bikkina, S., Gao, Y., Shelley, R. U., Buck, C. S., Landing, W. M., Bowie, A. R., Perron, M. M. G., Guieu, C., Meskhidze, N., Johnson, M. S., Feng, Y., Kok, J. F., Nenes, A. and Duce, R. A.: Pyrogenic iron: The missing link to high iron solubility in aerosols, Sci. Adv., 5(5), eaau7671, doi:10.1126/sciadv.aau7671, 2019a.

Deleted: &ndash; shelf

Formatted: Font: Times New Roman

Formatted: Font: Times New Roman

Formatted: Justified

Ito, A., Ye, Y., Yamamoto, A., Watanabe, M. and Aita, M. N.: Responses of ocean biogeochemistry to atmospheric supply of lithogenic and pyrogenic iron-containing aerosols, Geol. Mag., 1–16, doi:10.1017/S0016756819001080, 2019b.

Kanakidou, M., Duce, R. A., Prospero, J. M., Baker, A. R., Benitez-Nelson, C., Dentener, F. J., Hunter, K. A., Liss, P. S., Mahowald, N., Okin, G. S., Sarin, M., Tsigaridis, K., Uematsu, M., Zamora, L. M. and Zhu, T.: Atmospheric fluxes of organic N and P to the global ocean, Global Biogeochem. Cycles, 26(3), 2011GB004277, doi:10.1029/2011GB004277, 2012.

Kanakidou, M., Myriokefalitakis, S., Daskalakis, N., Fanourgakis, G., Nenes, A., Baker, A. R., Tsigaridis, K. and Mihalopoulos, N.: Past, Present, and Future Atmospheric Nitrogen Deposition, J. Atmos. Sci., 73(5), 2039–2047, doi:10.1175/JAS-D-15-0278.1, 2016.

Kanakidou, M., Myriokefalitakis, S. and Tsigaridis, K.: Aerosols in atmospheric chemistry and biogeochemical cycles of nutrients, Environ. Res. Lett., 13(6), 063004, doi:10.1088/1748-9326/aabcdb, 2018.

Kanakidou, M., Myriokefalitakis, S. and Tsagkaraki, M.: Atmospheric inputs of nutrients to the Mediterranean Sea, Deep Sea Res. Part II Top. Stud. Oceanogr., 171, 104606, doi:10.1016/j.dsr2.2019.06.014, 2020.

Key, R. M., Kozyr, A., Sabine, C. L., Lee, K., Wanninkhof, R., Bullister, J. L., Feely, R. A., Millero, F. J., Mordy, C. and Peng, T.-H.: A global ocean carbon climatology: Results from Global Data Analysis Project (GLODAP), Global Biogeochem. Cycles, 18(4), GB4031, doi:10.1029/2004GB002247, 2004.

Krishnamurthy, A., Moore, J. K., Zender, C. S. and Luo, C.: Effects of atmospheric inorganic nitrogen deposition on ocean biogeochemistry, J. Geophys. Res., 112(G2), G02019, doi:10.1029/2006JG000334, 2007.

Krishnamurthy, A., Moore, J. K., Mahowald, N., Luo, C., Doney, S. C., Lindsay, K. and Zender, C. S.: Impacts of increasing anthropogenic soluble iron and nitrogen deposition on ocean biogeochemistry, Global Biogeochem. Cycles, 23(3), GB3016, doi:10.1029/2008GB003440, 2009.

Krishnamurthy, A., Moore, J. K., Mahowald, N., Luo, C. and Zender, C. S.: Impacts of atmospheric nutrient inputs on marine biogeochemistry, J. Geophys. Res., 115(G1), G01006, doi:10.1029/2009JG001115, 2010.

Kustka, A., Carpenter, E. J. and Sañudo-Wilhelmy, S. A.: Iron and marine nitrogen fixation: progress and future directions, Res. Microbiol., 153(5), 255–262, doi:10.1016/S0923-2508(02)01325-6, 2002.

Lamarque, J.-F., Shindell, D. T., Josse, B., Young, P. J., Cionni, I., Eyring, V., Bergmann, D., Cameron-Smith, P., Collins, W. J., Doherty, R., Dalsoren, S., Faluvegi, G., Folberth, G., Ghan, S. J., Horowitz, L. W., Lee, Y. H., MacKenzie, I. A., Nagashima, T., Naik, V., Plummer, D., Righi, M., Rumbold, S. T., Schulz, M., Skeie, R. B., Stevenson, D. S., Strode, S., Sudo, K., Szopa, S., Voulgarakis, A. and Zeng, G.: The Atmospheric Chemistry and Climate Model Intercomparison Project (ACCMIP): overview and description of models, simulations and climate diagnostics, Geosci. Model Dev., 6(1), 179–206, doi:10.5194/gmd-6-179-2013, 2013.

Large, W. G. and Yeager, S. G.: The global climatology of an interannually varying air–sea flux data set, Clim. Dyn., 33(2–3), 341–364, doi:10.1007/s00382-008-0441-3, 2009.

Laufkötter, C., Vogt, M., Gruber, N., Aumont, O., Bopp, L., Doney, S. C., Dunne, J. P., Hauck, J., John, J. G., Lima, I. D., Seferian, R. and Völker, C.: Projected decreases in future marine export production: the role of the carbon flux through the

Formatted: Font: Times New Roman

Formatted: Font: Times New Roman

Formatted: Justified

upper ocean ecosystem, Biogeosciences, 13(13), 4023–4047, doi:10.5194/bg-13-4023-2016, 2016.

Locarnini, R. A., Mishonov, A. V., Antonov, J. I., Boyer, T. P., Garcia, H. E., Baranova, O. K., Zweng, M. M., Paver, C. R., Reagan, J. R., Johnson, D. R., Hamilton, M. and Seidov, D.: World Ocean Atlas 2013, Volume 1: Temperature, in World Ocean Atlas 2013, vol. 1, edited by E. S. Levitus and A. M. T. Ed., p. 40, NOAA Atlas NESDIS 73., 2013.

Luo, C., Mahowald, N., Bond, T., Chuang, P. Y., Artaxo, P., Siefert, R., Chen, Y. and Schauer, J.: Combustion iron distribution and deposition, Global Biogeochem. Cycles, 22(1), GB1012, doi:10.1029/2007GB002964, 2008.

Mahowald, N.: Aerosol Indirect Effect on Biogeochemical Cycles and Climate, Science (80-.)., 334(6057), 794–796, doi:10.1126/science.1207374, 2011.

Mahowald, N., Jickells, T. D., Baker, A. R., Artaxo, P., Benitez-Nelson, C. R., Bergametti, G., Bond, T. C., Chen, Y., Cohen, D. D., Herut, B., Kubilay, N., Losno, R., Luo, C., Maenhaut, W., McGee, K. A., Okin, G. S., Siefert, R. L. and Tsukuda, S.: Global distribution of atmospheric phosphorus sources, concentrations and deposition rates, and anthropogenic impacts, Global Biogeochem. Cycles, 22(4), GB4026, doi:10.1029/2008GB003240, 2008.

Mahowald, N. M., Engelstaedter, S., Luo, C., Sealy, A., Artaxo, P., Benitez-Nelson, C., Bonnet, S., Chen, Y., Chuang, P. Y., Cohen, D. D., Dulac, F., Herut, B., Johansen, A. M., Kubilay, N., Losno, R., Maenhaut, W., Paytan, A., Prospero, J. M., Shank, L. M. and Siefert, R. L.: Atmospheric iron deposition: global distribution, variability, and human perturbations., Ann. Rev. Mar. Sci., 1, 245–278, doi:10.1146/annurev.marine.010908.163727, 2009.

Mahowald, N. M., Kloster, S., Engelstaedter, S., Moore, J. K., Mukhopadhyay, S., McConnell, J. R., Albani, S., Doney, S. C., Bhattacharya, A., Curran, M. a J., Flanner, M. G., Hoffman, F. M., Lawrence, D. M., Lindsay, K., Mayewski, P. a., Neff, J., Rothenberg, D., Thomas, E., Thornton, P. E. and Zender, C. S.: Observed 20th century desert dust variability: impact on climate and biogeochemistry, Atmos. Chem. Phys., 10(22), 10875–10893, doi:10.5194/acp-10-10875-2010, 2010.

Mahowald, N. M., Scanza, R., Brahney, J., Goodale, C. L., Hess, P. G., Moore, J. K. and Neff, J.: Aerosol Deposition Impacts on Land and Ocean Carbon Cycles, Curr. Clim. Chang. Reports, 1–16, doi:10.1007/s40641-017-0056-z, 2017.

Malviya, S., Scalco, E., Audic, S., Vincent, F., Veluchamy, A., Poulain, J., Wincker, P., Iudicone, D., de Vargas, C., Bittner, L., Zingone, A. and Bowler, C.: Insights into global diatom distribution and diversity in the world's ocean, Proc. Natl. Acad. Sci., 113(11), E1516–E1525, doi:10.1073/pnas.1509523113, 2016.

Matsui, H., Mahowald, N. M., Moteki, N., Hamilton, D. S., Ohata, S., Yoshida, A., Koike, M., Scanza, R. A. and Flanner, M. G.: Anthropogenic combustion iron as a complex climate forcer, Nat. Commun., 9(1), 1593, doi:10.1038/s41467-018-03997-0, 2018.

Meskhidze, N., Völker, C., Al-Abadleh, H. A., Barbeau, K., Bressac, M., Buck, C., Bundy, R. M., Croot, P., Feng, Y., Ito, A., Johansen, A. M., Landing, W. M., Mao, J., Myriokefalitakis, S., Ohnemus, D., Pasquier, B. and Ye, Y.: Perspective on identifying and characterizing the processes controlling iron speciation and residence time at the atmosphere-ocean interface, Mar. Chem., 217, 103704, doi:10.1016/j.marchem.2019.103704, 2019.

Moore, C. M., Mills, M. M., Arrigo, K. R., Berman-Frank, I., Bopp, L., Boyd, P. W., Galbraith, E. D., Geider, R. J., Guieu, C., Jaccard, S. L., Jickells, T. D., La Roche, J., Lenton, T. M., Mahowald, N. M., Marañón, E., Marinov, I., Moore, J. K.,

Formatted: Font: Times New Roman

Formatted: Font: Times New Roman

Formatted: Justified

Nakatsuka, T., Oschlies, A., Saito, M. A., Thingstad, T. F., Tsuda, A. and Ulloa, O.: Processes and patterns of oceanic nutrient limitation, Nat. Geosci., 6(9), 701–710, doi:10.1038/ngeo1765, 2013a.

Moore, J. K. and Doney, S. C.: Iron availability limits the ocean nitrogen inventory stabilizing feedbacks between marine denitrification and nitrogen fixation, Global Biogeochem. Cycles, 21(2), GB2001, doi:10.1029/2006GB002762, 2007.

Moore, J. K., Doney, S. C., Glover, D. M. and Fung, I. Y.: Iron cycling and nutrient-limitation patterns in surface waters of the World Ocean, Deep Sea Res. Part II Top. Stud. Oceanogr., 49(1–3), 463–507, doi:10.1016/S0967-0645(01)00109-6, 2001.

Moore, J. K., Lindsay, K., Doney, S. C., Long, M. C. and Misumi, K.: Marine Ecosystem Dynamics and Biogeochemical Cycling in the Community Earth System Model [CESM1(BGC)]: Comparison of the 1990s with the 2090s under the RCP4.5 and RCP8.5 Scenarios, J. Clim., 26(23), 9291–9312, doi:10.1175/JCLI-D-12-00566.1, 2013b.

Myriokefalitakis, S., Vignati, E., Tsigaridis, K., Papadimas, C., Sciare, J., Mihalopoulos, N., Facchini, M. C., Rinaldi, M., Dentener, F. J., Ceburnis, D., Hatzianastasiou, N., O'Dowd, C. D., van Weele, M. and Kanakidou, M.: Global Modeling of the Oceanic Source of Organic Aerosols, Adv. Meteorol., 2010, 1–16, doi:10.1155/2010/939171, 2010.

Myriokefalitakis, S., Tsigaridis, K., Mihalopoulos, N., Sciare, J., Nenes, A., Kawamura, K., Segers, A. and Kanakidou, M.: In-cloud oxalate formation in the global troposphere: a 3-D modeling study, Atmos. Chem. Phys., 11(12), 5761–5782, doi:10.5194/acp-11-5761-2011, 2011.

Myriokefalitakis, S., Daskalakis, N., Mihalopoulos, N., Baker, A. R., Nenes, A. and Kanakidou, M.: Changes in dissolved iron deposition to the oceans driven by human activity: a 3-D global modelling study, Biogeosciences, 12(13), 3973–3992, doi:10.5194/bg-12-3973-2015, 2015.

Myriokefalitakis, S., Nenes, A., Baker, A. R. A. R., Mihalopoulos, N. and Kanakidou, M.: Bioavailable atmospheric phosphorous supply to the global ocean: a 3-D global modeling study, Biogeosciences, 13(24), 6519–6543, doi:10.5194/bg-13-6519-2016, 2016.

Myriokefalitakis, S., Fanourgakis, G. and Kanakidou, M.: The Contribution of Bioaerosols to the Organic Carbon Budget of the Atmosphere, in Perspectives on Atmospheric Sciences, edited by T. Karacostas, A. Bais, and P. T. Nastos, pp. 845–851, Springer International Publishing., 2017.

Myriokefalitakis, S., Ito, A., Kanakidou, M., Nenes, A., Krol, M. C., Mahowald, N. M., Scanza, R. A., Hamilton, D. S., Johnson, M. S., Meskhidze, N., Kok, J. F., Guieu, C., Baker, A. R., Jickells, T. D., Sarin, M. M., Bikkina, S., Shelley, R., Bowie, A., Perron, M. M. G. and Duce, R. A.: Reviews and syntheses: the GESAMP atmospheric iron deposition model intercomparison study, Biogeosciences, 15(21), 6659–6684, doi:10.5194/bg-15-6659-2018, 2018.

Nenes, A., Krom, M. D., Mihalopoulos, N., Van Cappellen, P., Shi, Z., Bougiatioti, A., Zarmpas, P. and Herut, B.: Atmospheric acidification of mineral aerosols: A source of bioavailable phosphorus for the oceans, Atmos. Chem. Phys., 11(13), 6265–6272, doi:10.5194/acp-11-6265-2011, 2011.

Nickovic, S., Vukovic, A., Vujadinovic, M., Djurdjevic, V. and Pejanovic, G.: Technical Note: High-resolution mineralogical database of dust-productive soils for atmospheric dust modeling, Atmos. Chem. Phys., 12(2), 845–855, doi:10.5194/acp-12-845-2012, 2012.

Formatted: Justified

Okin, G. S. G. S., Baker, A. R. A. R., Tegen, I., Mahowald, N. M. N. M., Dentener, F. J. F. J., Duce, R. A. R. A., Galloway, J. N. J. N., Hunter, K., Kanakidou, M., Kubilay, N., Prospero, J. M. J. M., Sarin, M., Surapipith, V., Uematsu, M. and Zhu, T.: Impacts of atmospheric nutrient deposition on marine productivity: Roles of nitrogen, phosphorus, and iron, Global Biogeochem. Cycles, 25(2), GB2022, doi:10.1029/2010GB003858, 2011.

Orr, J. C., Najjar, R. G., Aumont, O., Bopp, L., Bullister, J. L., Danabasoglu, G., Doney, S. C., Dunne, J. P., Dutay, J.-C., Graven, H., Griffies, S. M., John, J. G., Joos, F., Levin, I., Lindsay, K., Matear, R. J., McKinley, G. A., Mouchet, A., Oschlies, A., Romanou, A., Schlitzer, R., Tagliabue, A., Tanhua, T. and Yool, A.: Biogeochemical protocols and diagnostics for the CMIP6 Ocean Model Intercomparison Project (OMIP), Geosci. Model Dev., 10(6), 2169–2199, doi:10.5194/gmd-10-2169-2017, 2017.

Osman, M. B., Das, S. B., Trusel, L. D., Evans, M. J., Fischer, H., Grieman, M. M., Kipfstuhl, S., McConnell, J. R. and Saltzman, E. S.: Industrial-era decline in subarctic Atlantic productivity, Nature, 569(7757), 551–555, doi:10.1038/s41586-019-1181-8, 2019.

Paris, R. and Desboeufs, K. V.: Effect of atmospheric organic complexation on iron-bearing dust solubility, Atmos. Chem. Phys., 13(9), 4895–4905, doi:10.5194/acp-13-4895-2013, 2013.

Paris, R., Desboeufs, K. V. and Journet, E.: Variability of dust iron solubility in atmospheric waters: Investigation of the role of oxalate organic complexation, Atmos. Environ., 45(36), 6510–6517, doi:10.1016/j.atmosenv.2011.08.068, 2011.

Prospero, J. M. and Lamb, P. J.: African Droughts and Dust Transport to the Caribbean: Climate Change Implications, Science (80-.)., 302(5647), 1024–1027, doi:10.1126/science.1089915, 2003.

Le Quéré, C., Andres, R. J., Boden, T., Conway, T., Houghton, R. A., House, J. I., Marland, G., Peters, G. P., van der Werf, G. R., Ahlström, A., Andrew, R. M., Bopp, L., Canadell, J. G., Ciais, P., Doney, S. C., Enright, C., Friedlingstein, P., Huntingford, C., Jain, A. K., Jourdain, C., Kato, E., Keeling, R. F., Klein Goldewijk, K., Levis, S., Levy, P., Lomas, M., Poulter, B., Raupach, M. R., Schwinger, J., Sitch, S., Stocker, B. D., Viovy, N., Zaehle, S. and Zeng, N.: The global carbon budget 1959–2011, Earth Syst. Sci. Data, 5(1), 165–185, doi:10.5194/essd-5-165-2013, 2013.

Rubin, M., Berman-Frank, I. and Shaked, Y.: Dust- and mineral-iron utilization by the marine dinitrogen-fixer Trichodesmium, Nat. Geosci., 4(8), 529–534, doi:10.1038/ngeo1181, 2011.

Schneider, B., Bopp, L., Gehlen, M., Segschneider, J., Frölicher, T. L., Cadule, P., Friedlingstein, P., Doney, S. C., Behrenfeld, M. J. and Joos, F.: Climate-induced interannual variability of marine primary and export production in three global coupled climate carbon cycle models, Biogeosciences, 5(2), 597–614, doi:10.5194/bg-5-597-2008, 2008.

Schulz, M., Prospero, J. M., Baker, A. R., Dentener, F., Ickes, L., Liss, P. S., Mahowald, N. M., Nickovic, S., García-Pando, C. P., Rodríguez, S., Sarin, M., Tegen, I. and Duce, R. A.: Atmospheric Transport and Deposition of Mineral Dust to the Ocean: Implications for Research Needs, Environ. Sci. Technol., 46(19), 10390–10404, doi:10.1021/es300073u, 2012.

Sein, D. V., Koldunov, N. V., Danilov, S., Sidorenko, D., Wekerle, C., Cabos, W., Rackow, T., Scholz, P., Semmler, T., Wang, Q. and Jung, T.: The Relative Influence of Atmospheric and Oceanic Model Resolution on the Circulation of the North Atlantic Ocean in a Coupled Climate Model, J. Adv. Model. Earth Syst., 10(8), 2026–2041, doi:10.1029/2018MS001327, 2018.

Formatted: Justified

Shi, Z., Krom, M. D., Bonneville, S., Baker, A. R., Bristow, C., Drake, N., Mann, G., Carslaw, K., McQuaid, J. B., Jickells, T. and Benning, L. G.: Influence of chemical weathering and aging of iron oxides on the potential iron solubility of Saharan dust during simulated atmospheric processing, Global Biogeochem. Cycles, 25(2), GB2010, doi:10.1029/2010GB003837, 2011.

Skyllas, N., Bintanja, R., Buma, A. G. J., Brussaard, C. P. D., Gröger, M., Hieronymus, J. and van de Poll, W. H.: Validation of Stratification-Driven Phytoplankton Biomass and Nutrient Concentrations in the Northeast Atlantic Ocean as Simulated by EC-Earth, Geosciences, 9(10), 450, doi:10.3390/geosciences9100450, 2019.

Smith, H. J.: The state of ocean CO $_2$ uptake, edited by S. Hurtley, Science (80-.)., 363(6432), 1187.2-1187, doi:10.1126/science.363.6432.1187-b, 2019.

Steinacher, M., Joos, F., Frölicher, T. L., Bopp, L., Cadule, P., Cocco, V., Doney, S. C., Gehlen, M., Lindsay, K., Moore, J. K., Schneider, B. and Segschneider, J.: Projected 21st century decrease in marine productivity: a multi-model analysis, Biogeosciences, 7(3), 979–1005, doi:10.5194/bg-7-979-2010, 2010.

Tagliabue, A., Mtshali, T., Aumont, O., Bowie, A. R., Klunder, M. B., Roychoudhury, A. N. and Swart, S.: A global compilation of dissolved iron measurements: focus on distributions and processes in the Southern Ocean, Biogeosciences, 9(6), 2333–2349, doi:10.5194/bg-9-2333-2012, 2012.

Tagliabue, A., Aumont, O. and Bopp, L.: The impact of different external sources of iron on the global carbon cycle, Geophys. Res. Lett., 41(3), 920–926, doi:10.1002/2013GL059059, 2014.

Tagliabue, A., Aumont, O., Death, R., Dunne, J. P., Dutkiewicz, S., Galbraith, E., Misumi, K., Moore, J. K., Ridgwell, A., Sherman, E., Stock, C., Vichi, M., Völker, C. and Yool, A.: How well do global ocean biogeochemistry models simulate dissolved iron distributions?, Global Biogeochem. Cycles, 30(2), 149–174, doi:10.1002/2015GB005289, 2016.

Tagliabue, A., Bowie, A. R., Boyd, P. W., Buck, K. N., Johnson, K. S. and Saito, M. A.: The integral role of iron in ocean biogeochemistry, Nature, 543(7643), 51–59, doi:10.1038/nature21058, 2017.

Tegen, I., Harrison, S. P., Kohfeld, K., Prentice, I. C., Coe, M. and Heimann, M.: Impact of vegetation and preferential source areas on global dust aerosol: Results from a model study, J. Geophys. Res. Atmos., 107(D21), AAC 14-1-AAC 14-27, doi:10.1029/2001JD000963, 2002.

Tsigaridis, K., Krol, M., Dentener, F. J., Balkanski, Y., Lathière, J., Metzger, S., Hauglustaine, D. A. and Kanakidou, M.: Change in global aerosol composition since preindustrial times, Atmos. Chem. Phys., 6(12), 5143–5162, doi:10.5194/acp-6-5143-2006, 2006.

Uitz, J., Claustre, H., Gentili, B. and Stramski, D.: Phytoplankton class-specific primary production in the world's oceans: Seasonal and interannual variability from satellite observations, Global Biogeochem. Cycles, 24(3), GB3016, doi:10.1029/2009GB003680, 2010.

van Vuuren, D. P., Edmonds, J., Kainuma, M., Riahi, K., Thomson, A., Hibbard, K., Hurtt, G. C., Kram, T., Krey, V., Lamarque, J.-F., Masui, T., Meinshausen, M., Nakicenovic, N., Smith, S. J., Rose, S. K., Vuuren, D. P. Van, Edmonds, J., Kainuma, M., Riahi, K., Nakicenovic, N., Smith, S. J. and Rose, S. K.: The representative concentration pathways: an

Formatted: Font: Times New Roman

Formatted: Font: Times New Roman

Formatted: Justified

overview, Clim. Change, 109(1–2), 5–31, doi:10.1007/s10584-011-0148-z, 2011.

Wang, R., Balkanski, Y., Boucher, O., Ciais, P., Peñuelas, J. and Tao, S.: Significant contribution of combustion-related emissions to the atmospheric phosphorus budget, Nat. Geosci., 8(1), 48–54, doi:10.1038/ngeo2324, 2014.

Wang, R., Balkanski, Y., Bopp, L., Aumont, O., Boucher, O., Ciais, P., Gehlen, M., Peñuelas, J., Ethé, C., Hauglustaine, D., Li, B., Liu, J., Zhou, F. and Tao, S.: Influence of anthropogenic aerosol deposition on the relationship between oceanic productivity and warming, Geophys. Res. Lett., 42(24), 10745–10754, doi:10.1002/2015GL066753, 2015a.

Wang, R., Balkanski, Y., Boucher, O., Bopp, L., Chappell, A., Ciais, P., Hauglustaine, D., Peñuelas, J. and Tao, S.: Sources, transport and deposition of iron in the global atmosphere, Atmos. Chem. Phys., 15(11), 6247–6270, doi:10.5194/acp-15-6247-2015, 2015b.

Wang, W.-L., Moore, J. K., Martiny, A. C. and Primeau, F. W.: Convergent estimates of marine nitrogen fixation, Nature, 566(7743), 205–211, doi:10.1038/s41586-019-0911-2, 2019.

Wanninkhof, R.: Relationship between wind speed and gas exchange over the ocean, J. Geophys. Res., 97(C5), 7373, doi:10.1029/92JC00188, 1992.

Weber, R. J., Guo, H., Russell, A. G. and Nenes, A.: High aerosol acidity despite declining atmospheric sulfate concentrations over the past 15 years, Nat. Geosci., 9(4), 282–285, doi:10.1038/ngeo2665, 2016.

Wrightson, L. and Tagliabue, A.: Quantifying the Impact of Climate Change on Marine Diazotrophy: Insights From Earth System Models, Front. Mar. Sci., 7, 635, doi:10.3389/fmars.2020.00635, 2020.

Zweng, M. ., Reagan, J. R., Antonov, J. I., Locarnini, R. A., Mishonov, A. V., Boyer, T. P., Garcia, H. E., Baranova, O. K., Johnson, D. R., D.Seidov and Biddle, M. M.: World Ocean Atlas 2013, Volume 2: Salinity, edited by S. Levitus and A. M. Technical, p. 39, NOAA Atlas NESDIS 74., 2013.

Formatted: Justified

Tables and Figures

Table 1: Nutrients (N, Fe, P) atmospheric inputs (Tg yr^{-1}) considered in PISCES, nitrogen fixation (Tg-N yr^{-1}), and primary production (Pg-C yr^{-1}) as calculated by the STD and ORG simulations, for PAST (1851–1870 average), PRESENT (2001–2020 average) and FUTURE (2081–2100 average).

	Atmospheric Input Tg yr^{-1}			Nitrogen Fixation Tg-N yr^{-1}		Primary Production Pg-C yr^{-1}	
	Nutrient	STD	ORG	STD	ORG	STD	ORG
PAST	DN	19.74	34.47	111.62	112.22	45.46	46.43
	DFe	0.18	0.23				
	DP	0.06	0.11				
PRESENT	DN	40.01	58.01	111.87	111.41	46.65	47.75
	DFe	0.28	0.35				
	DP	0.10	0.15				
FUTURE	DN	34.62	51.08	110.75	110.65	46.36	47.42
	DFe	0.24	0.30				
	DP	0.08	0.13				

Deleted: the …itrogen fixation (Tg-N yr^{-1}), and the …rimary ... [18]
Deleted: Period
Formatted ... [19]
Formatted ... [20]
Deleted: CTRL
Deleted: ORGF
Deleted: CTRL
Deleted: ORGF
Deleted: ORGF
Formatted ... [21]
Deleted: CTRL
Formatted ... [22]
Formatted ... [23]
Formatted ... [24]
Formatted ... [25]
Formatted ... [26]
Deleted: 48
Formatted ... [29]
Formatted ... [27]
Formatted ... [28]
Deleted: 57
Formatted ... [30]
Deleted: 16
Formatted ... [31]
Deleted: 5
Formatted ... [32]
Deleted: 5
Formatted ... [33]
Deleted: 82
Formatted ... [36]
Deleted: 36
Formatted ... [37]
Deleted: 7
Formatted ... [38]
Deleted: 8
Formatted ... [34]
Formatted ... [39]
Formatted ... [35]
Formatted ... [40]
Formatted ... [41]
Deleted: 70
Formatted ... [42]
Deleted: 60
Formatted ... [43]
Deleted: 4
Formatted ... [44]
Deleted: 5
Formatted ... [45]
Formatted ... [17]

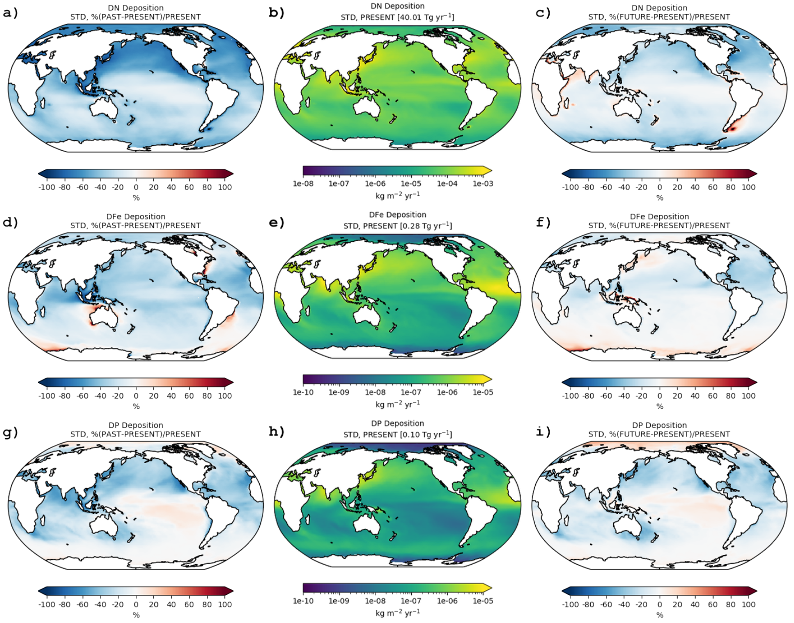

Figure 1: Atmospheric deposition fluxes into the ocean (kg m^{-2} yr^{-1}) of dissolved nitrogen (b), iron (e), and phosphorus (h) considered by the model for PRESENT (middle column) for the STD simulation, and the respective relative differences (%) to PAST (left column) and FUTURE (right column).

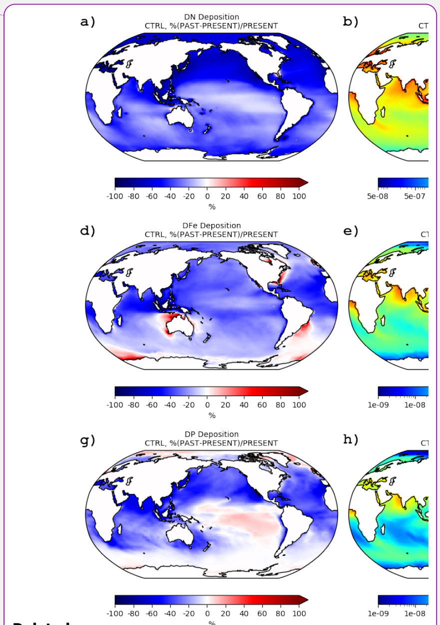

Deleted:

Deleted: a,

Deleted: ,c

Deleted: d,

Deleted: ,f)

Deleted: g,

Deleted: ,i

Deleted:),

Deleted:) for the CTRL simulation.

Formatted: Font: Not Bold

Formatted: Justified

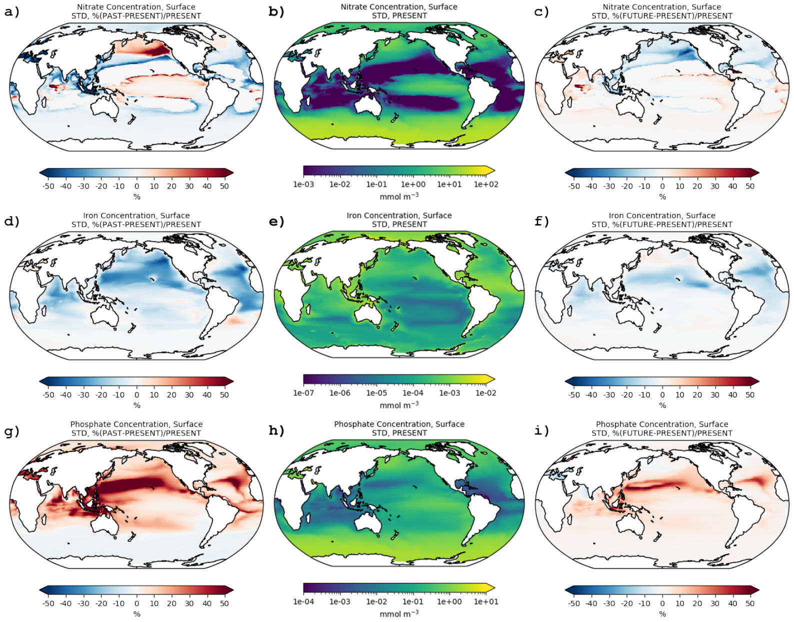

Figure 2: Surface oceanic concentrations (mmol m^{-3}) of nitrate (b), iron (e), and phosphate (h) as calculated by the model for PRESENT (middle column) for the STD simulation, and the respective relative differences (%) to PAST (left column) and FUTURE (right column).

Deleted:

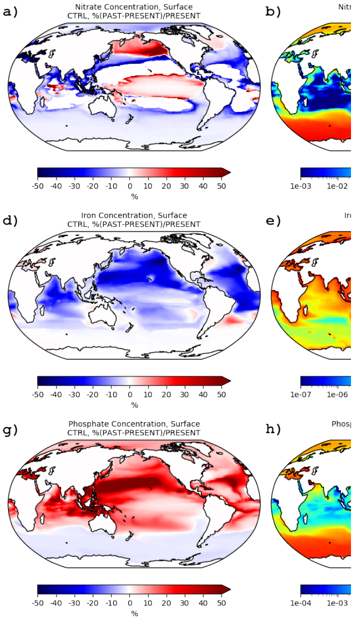

¶

Deleted: a,

Deleted: ,c

Deleted: d,

Deleted: ,f)

Deleted: g,

Deleted: ,i

Deleted:),

Deleted:) for the CTRL simulation.

Formatted: Font: Not Bold

Formatted: Justified

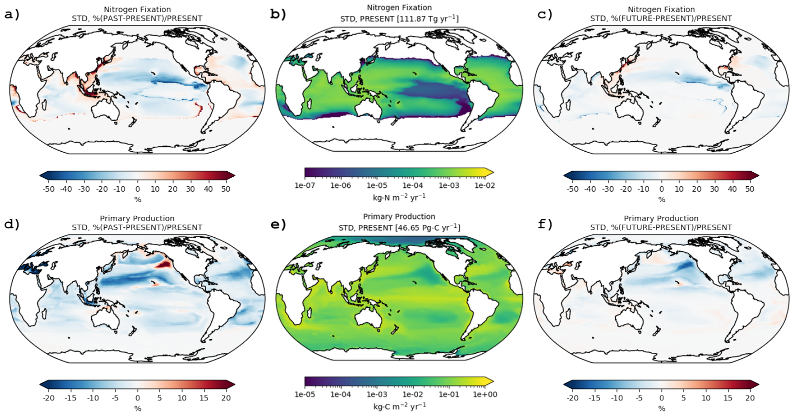

Figure 3: Nitrogen fixation (kg-N m^{-2} yr^{-1}) and primary production (kg-C m^{-2} yr^{-1}) rates as calculated by the model for PRESENT (b,e) for the STD simulation, and the respective relative differences (%) to PAST (a,d) and FUTURE (c,f).

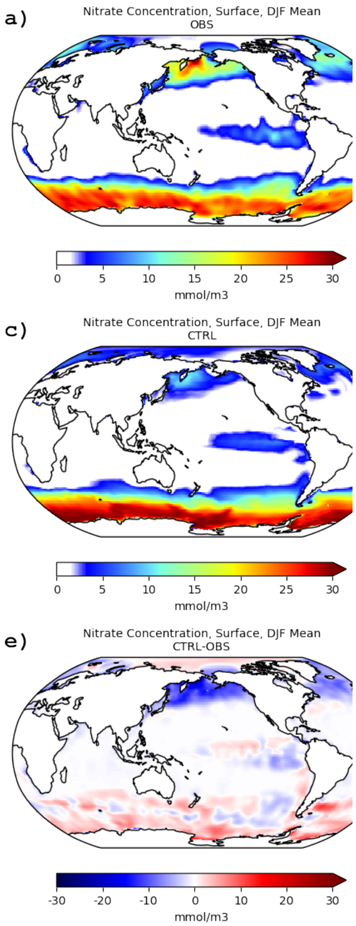

Deleted:

Deleted: : Surface nitrate concentrations (mmole m^{-3}) for the boreal winter (DJF; left column) and summer (JJA; right column) seasons as compiled from the World Ocean Atlas (WOA; Garcia et al., 2010b) (a,b), the simulated concentrations for PRESENT as simulated for CTRL (c,d), and the absolute differences compared to observations (e,f); observational and modelled data have been averaged over a 1°x1° horizontal resolution.¶

Page Break

¶ ... [46]

Formatted: Justified

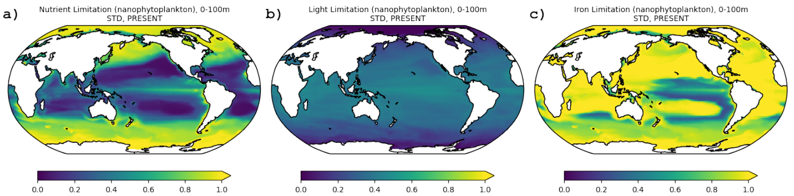

Figure 4: Limitation for nanophytoplankton production by nutrients (N and P; a), light (b), and iron (c). Low values indicate high limitation imposed by the respective property.

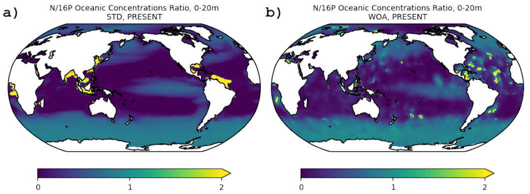

Figure 5: Molar oceanic ratios N:16P averaged in the upper 20m for PRESENT, as calculated by the model (a) for the STD simulation, and based on World Ocean Atlas (WOA; Garcia et al., 2010b) data (b). Values >1.0 denote overshoot of N vs P relative to the Redfield ratio (C:N:P =122:16:1); blue areas indicate a surplus of P or deficiency of N.

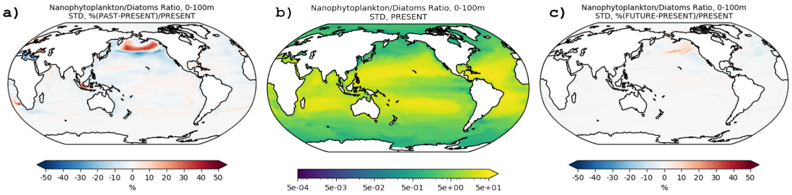

Figure 6: Nanophytoplankton to diatoms oceanic concentrations ratio averaged in the upper 100m for PRESENT (b) for the STD simulation, and the relative changes to PAST (a) and FUTURE (b).

Deleted: Surface phosphate concentrations (mmole m^{-3}) for the boreal winter (DJF; left column) and summer (JJA; right column) seasons as compiled from the

Deleted: (a,b), the simulated present day surface concentrations for PRESENT as simulated for CTRL (c,d), and the respective absolute differences (e,f); observational and modelled data have been averaged over a 1°x1° horizontal resolution.

Deleted: ----------Page Break----------

¶

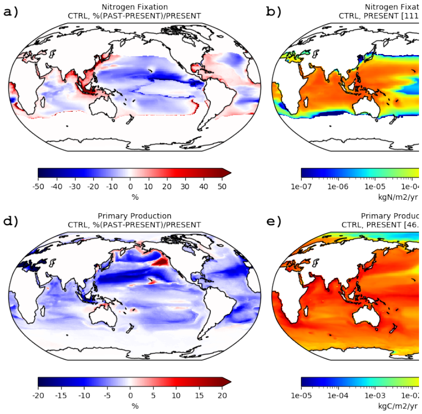

Deleted: Nitrogen fixation (kg-N m^{-2} yr^{-1}) and primary production (kg-C m^{-2} yr^{-1}) rates as calculated by the model for

Deleted: ,e),

Deleted: respective

Deleted: differences (%)

Deleted: ,d

Deleted: c,f) for the CTRL simulation.

Formatted: Font: Not Bold

Formatted: Justified

a)

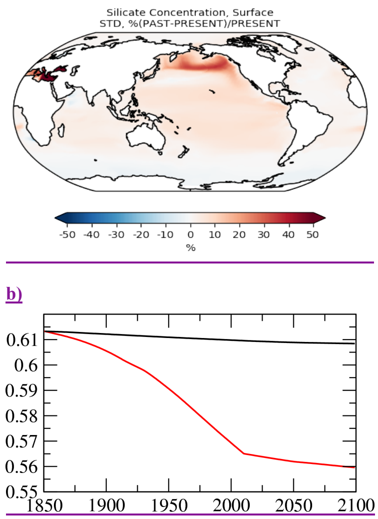

Figure 7: a) PAST to PRESENT relative differences (%) of silicate surface oceanic concentrations of as calculated by the model for the STD simulation; b) Seawater concentration ratio of nanophytoplankton to diatoms in the upper 20m, averaged over the NW Pacific (east of 200°E and north of 40°N). The red line indicates primary production rates for the STD simulation and the black line for the CTRL simulation, respectively.

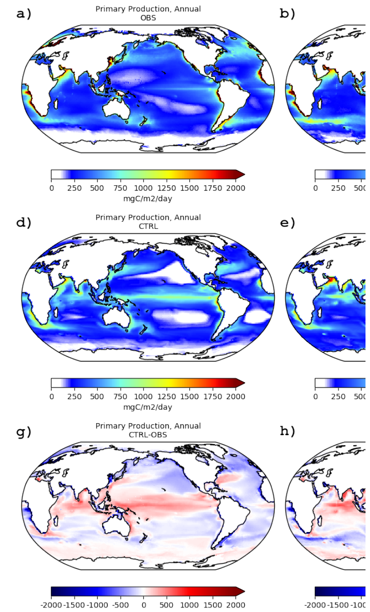

Deleted:

Deleted: : Primary production (mg-C m^{-2} day^{-1}) for annual (left column), boreal winter (DJF; middle column) and summer (JJA; right column) seasons, as derived based on satellite-based estimates from SeaWiFS (Behrenfeld et al., 2005) (a,b,c), the simulated integrated primary production for the CTRL simulation for PRESENT (d,e,f), and the respective absolute differences (g,h,i); satellite-based and modelled data have been averaged over a 1°x1° horizontal resolution.¶

Page Break

¶ ... [47]

Formatted: Justified

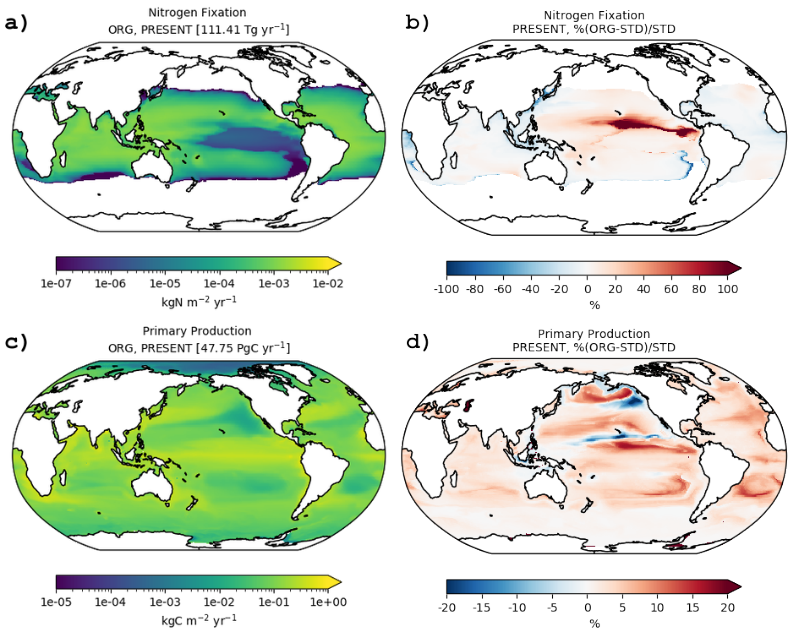

Figure 8: Nitrogen fixation (kg-N m^{-2} yr^{-1}) and primary production (kg-C m^{-2} yr^{-1}) rates as calculated by the model (a,c) for the ORG simulation for PRESENT, and the respective relative (%) differences (b,d) to the STD simulation.

Deleted: ORGF

Deleted: (2001–2020 average),

Deleted: compared

Deleted: CTRL

Formatted: Justified

Supplementary Tables

Table S1: Physical forcing fields provided at a daily time step.

Field	Units
Water flux into seawater	kg/m^2/s
Mixed layer depth	m
Surface net downward shortwave flux	W/m^2
Wind speed	m/s
Ice concentration	%
Water flux due to freezing/melting	kg/m^2/s
Tracer diffusive fluxes along the bottom boundary layer	m3/s
River runoff	kg/m^2/s
Ocean vertical salt diffusivity	m^2/s
Horizontal divergence transport	1/s
Seawater salinity	g/kg
Seawater potential temperature	°C
Effective ocean transports	m^3/s

Style Definition: List Paragraph

Style Definition: Normal1

Style Definition: Ohne

Deleted: Supplement

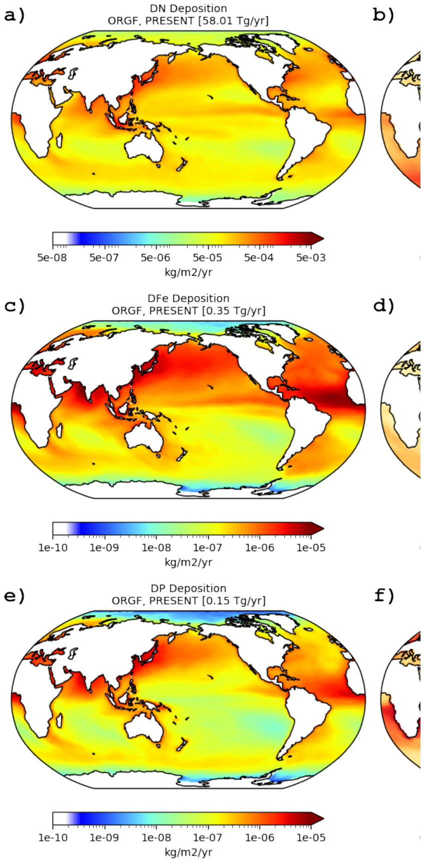

Supplementary Figures

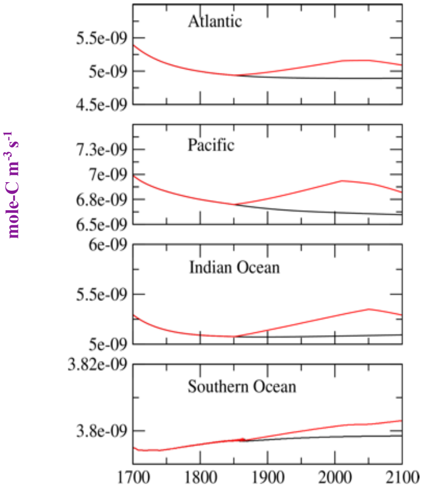

Figure S1: Area averaged annual mean primary production in mole C m^{-3} s^{-1} for the main ocean basins (Atlantic, Pacific, Indian and Southern Oceans). Red lines indicate primary production rates for the STD simulation and black lines for the CTRL simulation, respectively.

Formatted: English (UK)

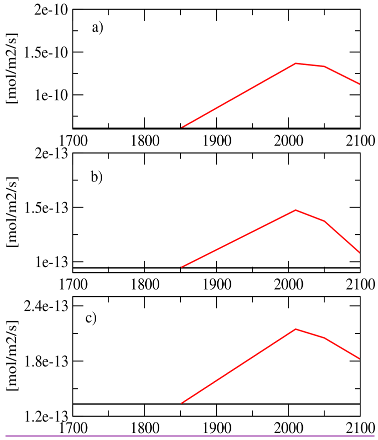

Figure S2: Globally averaged atmospheric deposition fluxes (red lines) of a) nitrogen, b) phosphorous, and c) iron in mol m^{-2} s^{-1}, as taken into account in PISCES. The black line indicates forcing for the control run under preindustrial conditions (i.e., year 1850).

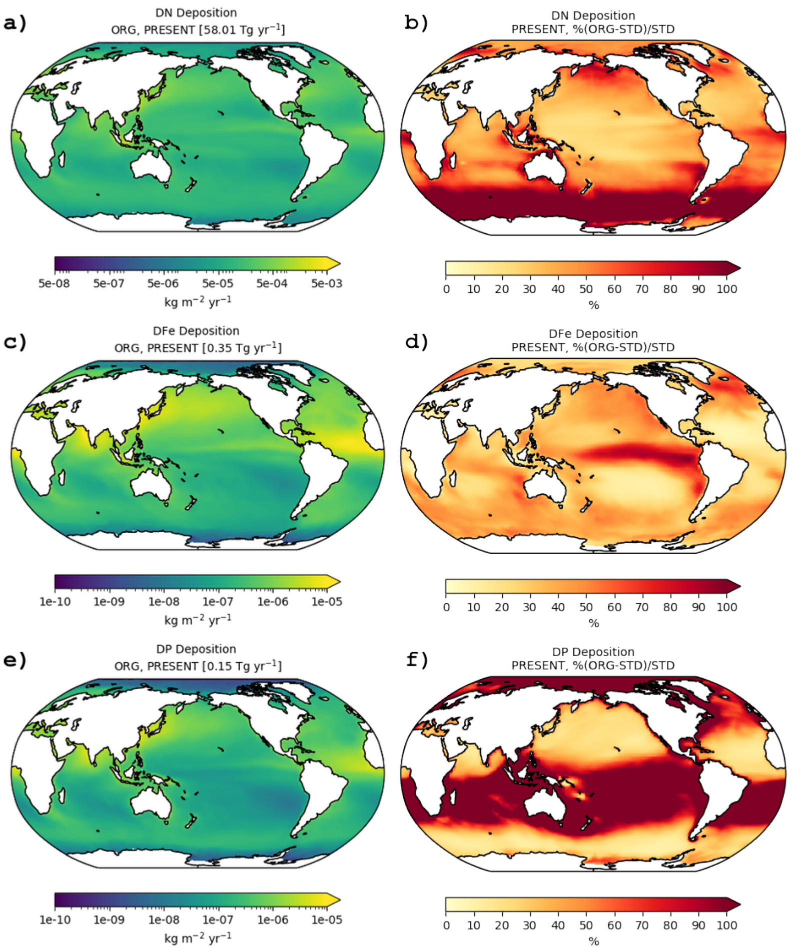

Figure S3: Atmospheric deposition fluxes (left column) into the ocean of dissolved nitrogen (a), iron (c), and phosphorus (e) considered by the model for the ORG simulation for PRESENT (2001–2020 average), and the respective percentage differences (b,d,f) compared to the STD simulation (right column).

Deleted:)

Deleted: ORGF

Deleted: CTRL

Formatted: Font: 10 pt, Not Bold

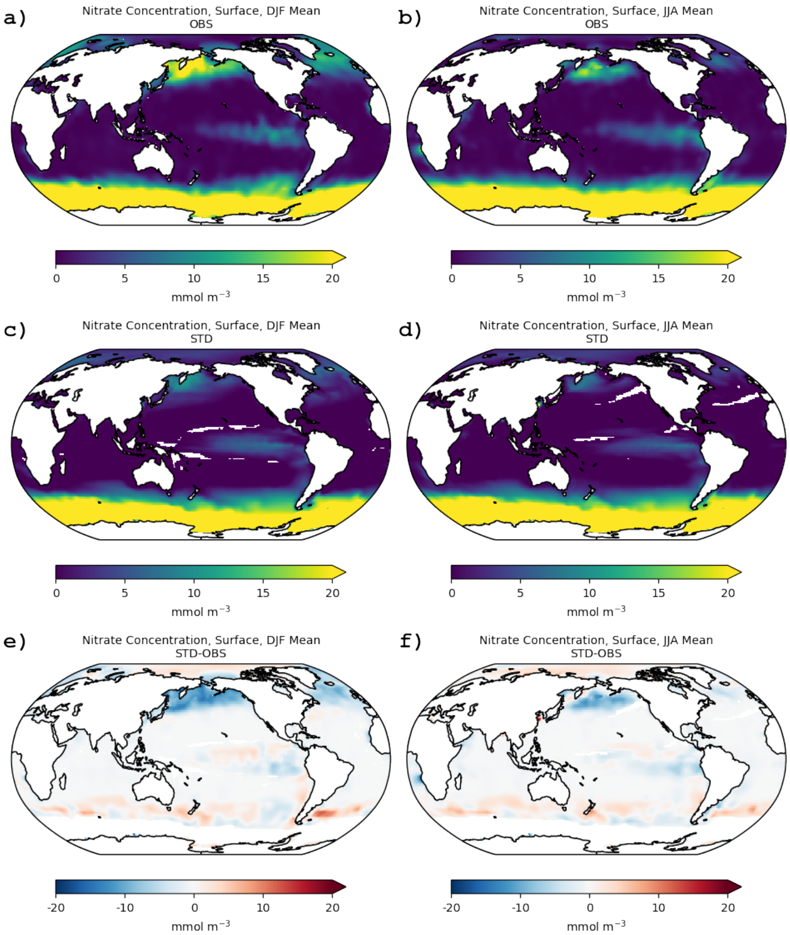

Figure S4: Surface nitrate concentrations (mmole m^{-3}) for the boreal winter (DJF; left column) and summer (JJA; right column) seasons as compiled from the World Ocean Atlas (WOA; Garcia et al., 2010b) (a,b), the simulated concentrations for PRESENT as simulated for STD (c,d), and the absolute differences compared to observations (e,f); observational and modeled data have been averaged over a 1°x1° horizontal resolution.

Deleted:

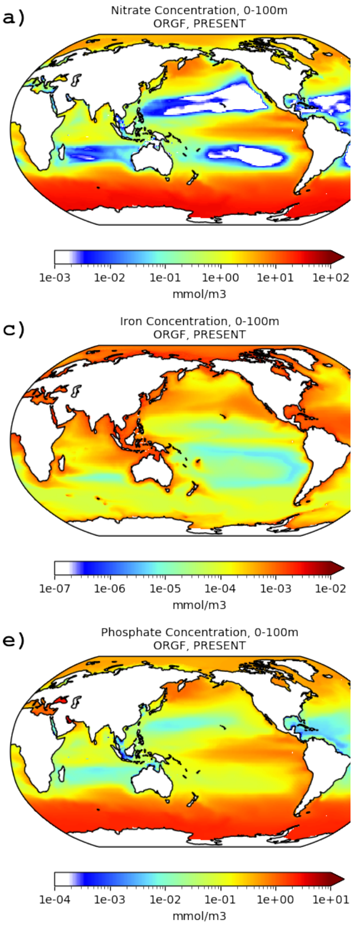

Figure S4 illustrates the comparison between the simulated present-day surface nitrate concentration and the compiled data from the World Ocean Atlas (WOA; Garcia et al., 2010b) for two seasons: the boreal winter (December, January, and February; DJF) and the boreal summer (June, July, and August; JJA). Generally, the model compares quite well with the nitrate surface observations. However, compared to the WOA compilation (Figs. S4a,b) the modeled nitrate concentrations (Figs. S4c,d, respectively) are lower in the northern high latitudes for both seasons (~5-10 mmol/m^3), especially in the Subpolar Pacific Ocean (up to 30 mmol/m^3) during DJF. This is likely related to the model's too shallow mixed layer thickness (not shown) and, as a consequence, the transport of nutrients and from deeper layers to the surface is likewise underestimated during the winter season. On the other hand, the surface nitrate concentrations are somewhat overestimated in the Southern Ocean for both seasons (Figs. S4e,f). This is also the case when the model uses PISCES defaults atmospheric deposition fields and it might be related to deficiencies in the model's abiotic processes. As also explained by Aumont et al. (2015), the WOA climatology may be, however, biased toward lower values since most of the observational data have been collected during the productive season in that region.

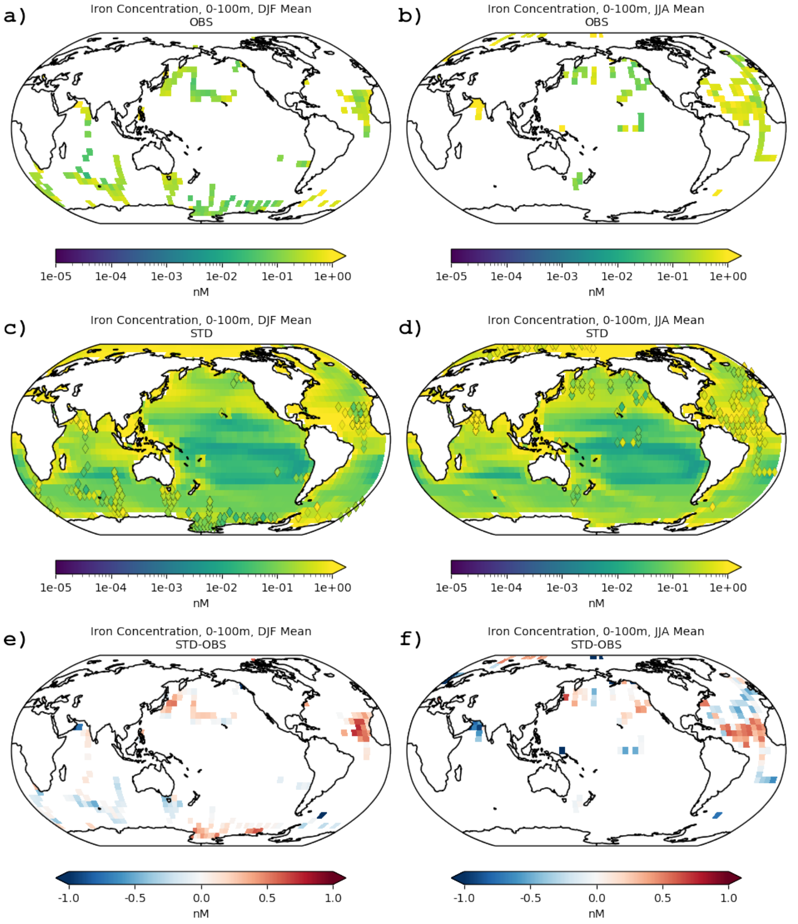

Figure S5: Iron concentrations (nM) averaged in the upper 100m for the boreal winter (DJF; left column) and summer (JJA; right column) seasons (a,b) as compiled by Tagliabue et al. (2012) (OBS), the respective simulated concentrations for PRESENT (c,d) as simulated for STD (diamond symbols represent observation data), and the respective absolute differences (e,f); observational and modeled data have been averaged over a 5°x5° horizontal resolution.

Figure S5 presents a comparison of the modeled with observed oceanic iron concentrations in the upper 100m, for two seasons (DJF and JJA). The DFe oceanic observation data (Figs. S5a,b) are taken from Tagliabue et al. (2012) (https://www.bodc.ac.uk/geotraces/data/historical/; last access 29/02/2020). The model simulates reasonably the observed oceanic iron concentrations for both seasons, for the STD simulation (Figs. S5c,d). The observed low oceanic DFe concentrations are well captured in most of the cases by the model, especially for boreal winter (Fig. S5d), but underestimated during boreal summer (Fig. S5d). Low dissolved iron concentrations of about 0.1 nM (i.e., 1nM = 10^{-9} moles per liter) are simulated and observed in the subtropical Atlantic and Pacific basins, especially in the HNLC regions. The high observed oceanic DFe concentrations (>1 nM) are also well simulated along the coasts and over the continental margins, as a result of sediment mobilization. In the vicinity of intense dust sources, such as the Sahara, the upper ocean in the model is strongly influenced by the atmospheric inputs, and some higher values compared to observations (up to 0.5 nM) are simulated in the North Atlantic Ocean, for both seasons. The model also slightly overestimates the observed DFe concentrations in the North Pacific, as well as in the subpolar Southern Ocean (Pacific sector) during the local summer season. This may be related to the too low consumption of nutrients, as the model may underestimate the biological production in this area (see Sect. 3). In the subtropical South Atlantic, the low DFe oceanic concentrations are well captured, although during boreal summer the model slightly underestimates the observations. In the Southern tropical Pacific during boreal summer, the low surface concentrations for the Fe-limited latitudes are also underestimated. Moreover, across the Southern Ocean (except for the subpolar sector) the model calculates lower values for the DFe concentrations.

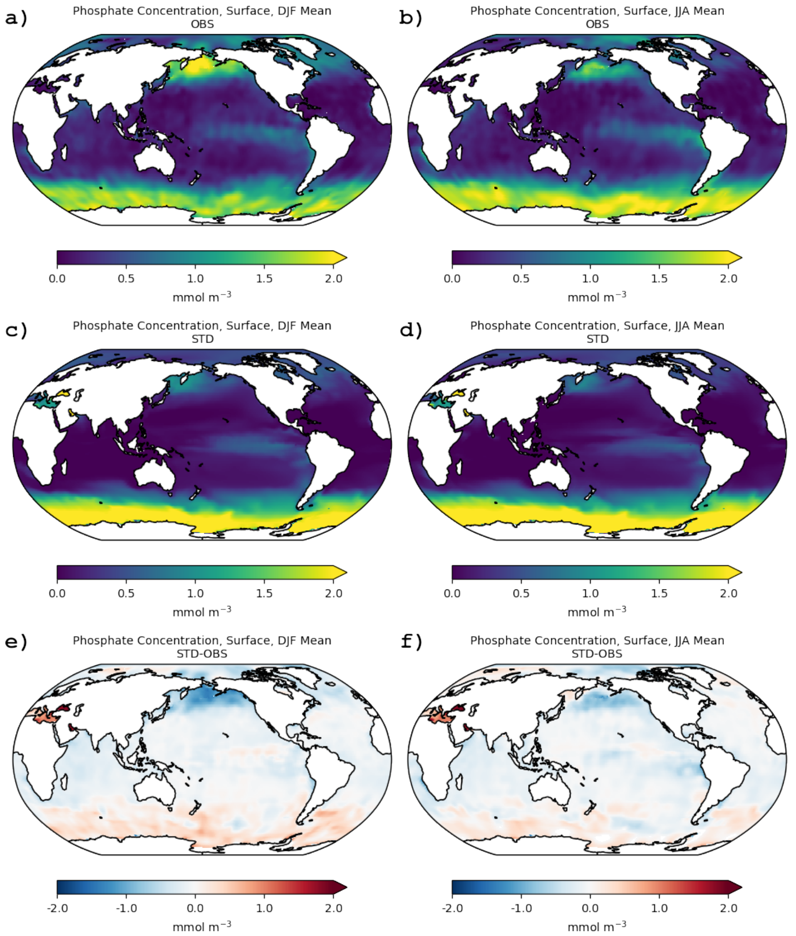

Figure S6: Surface phosphate concentrations (mmole m^{-3}) for the boreal winter (DJF; left column) and summer (JJA; right column) seasons as compiled from the World Ocean Atlas (WOA; Garcia et al., 2010b) (a,b), the simulated present-day surface concentrations for PRESENT as simulated for STD (c,d), and the respective absolute differences (e,f); observational and modeled data have been averaged over a 1°x1° horizontal resolution.

Figure S6 compares the simulated surface phosphate concentration with an observation-based data set from WOA, for the summer and winter seasons. The global pattern of observed phosphate is mainly controlled by the ocean dynamics and it is well reproduced by the model. Hence, during winter enhanced wind mixing and convective mixing transport nutrient-rich deep water to the surface in the North Atlantic and North Pacific. At the same time, nutrient consumption by biological productivity in the high latitudes is weak due to low winter temperatures and reduced light conditions. The resulting maximum phosphate concentrations in the Atlantic and Pacific subpolar gyres, however, are somewhat underestimated (up to 1.5 mmol m^{-3}) by the model compared to the WOA data (Figs. S6a,b). This is also caused by a too shallow winter mixed layer depth simulated by the physical model NEMO as forced by the OMIP standard forcing.

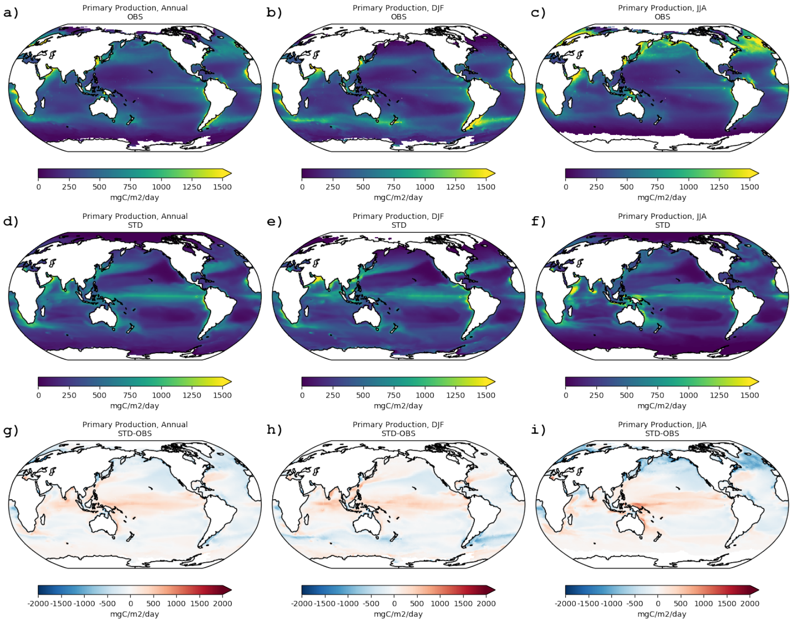

Figure S7: Primary production (mg-C m^{-2} day^{-1}) for annual (left column), boreal winter (DJF; middle column), and summer (JJA; right column) seasons, as derived based on satellite-based estimates from SeaWiFS (Behrenfeld et al., 2005) (a,b,c), the simulated integrated primary production for the STD simulation for PRESENT (d,e,f), and the respective absolute differences (g,h,i); satellite-based and modeled data have been averaged over a 1°x1° horizontal resolution.

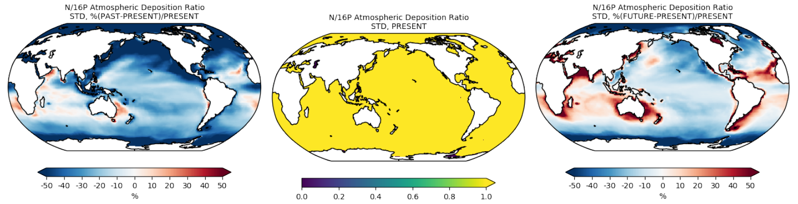

Figure S8: Atmospheric nutrient deposition fluxes relative to the Redfield ratio for PRESENT (middle) and the relative changes for PAST (left) and FUTURE (right) for the STD simulation; values >1.0 denotes excess of nitrogen compared to phosphorus.

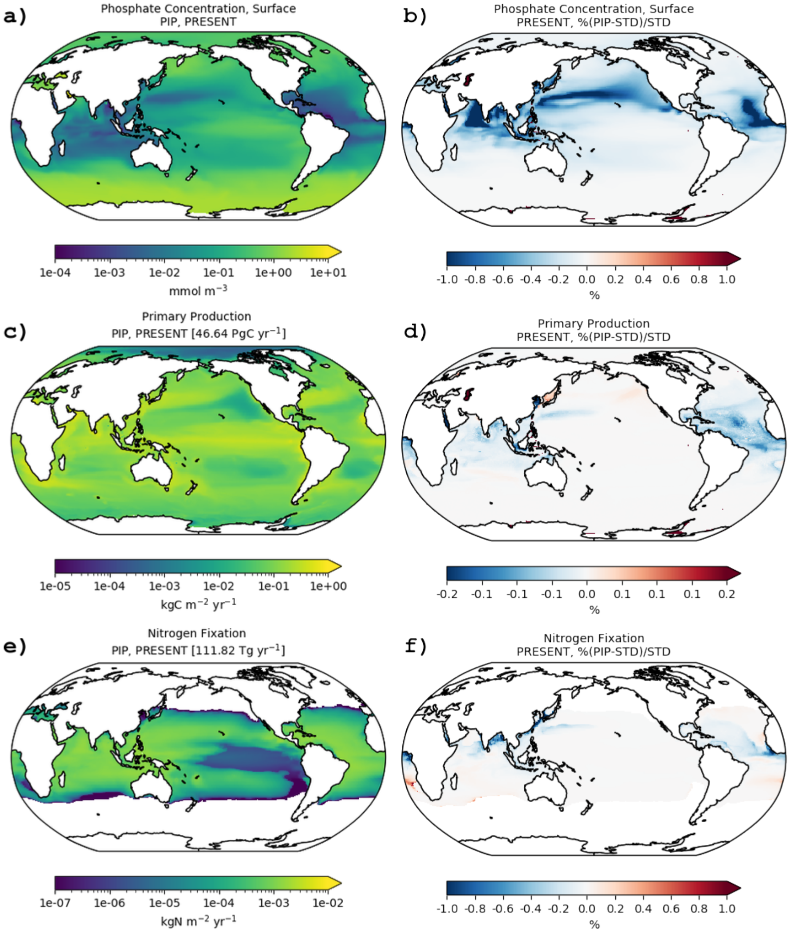

Figure S9: Surface oceanic concentrations (mmol m^{-3}) of phosphate (top row), primary production rates (kg-C m^{-2} yr^{-1}) (middle row), and nitrogen fixation (kg-N m^{-2} yr^{-1}) (bottom row), as calculated by the model for PRESENT for the sensitivity PIP simulation (i.e., as for STD, but keeping phosphorus atmospheric deposition to preindustrial levels) (left column), and the respective relative differences (%) to the STD simulation (right column).

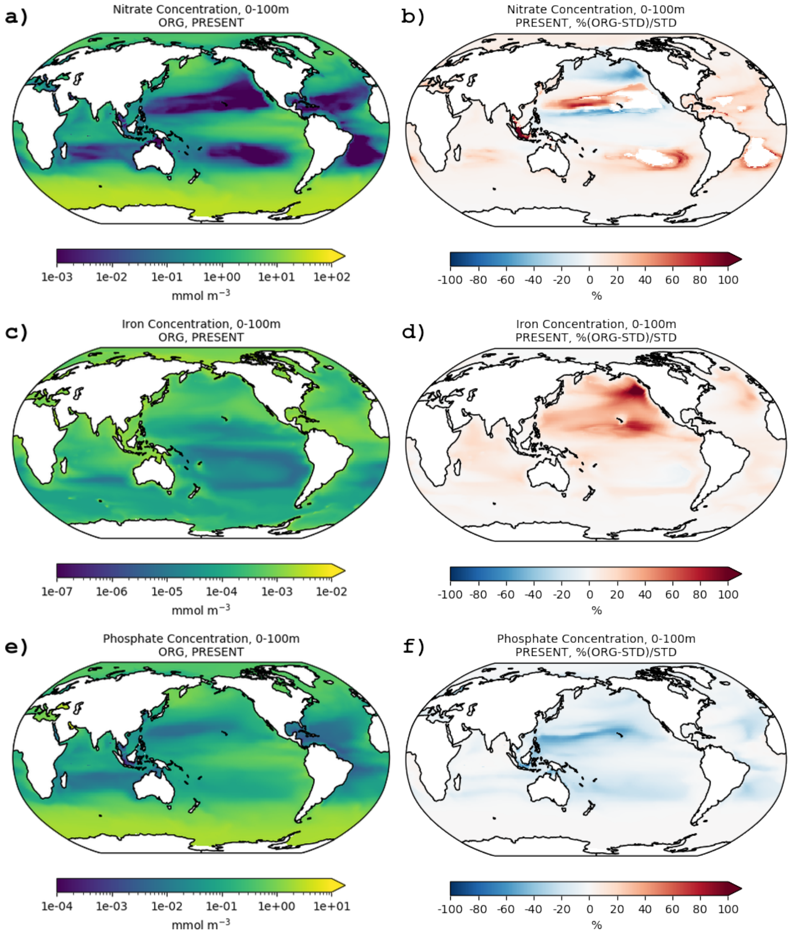

Figure S10: Oceanic concentrations averaged over the upper 100m (left column) of nitrate (a), iron (c) and phosphate (e) as calculated by the model for the ORG simulation for PRESENT (2001–2020 average), and the respective percentage differences (b,d,f) compared to the STD simulation (right column).

Deleted: ORGF

Deleted: CTRL

References

Aumont, O., Ethé, C., Tagliabue, A., Bopp, L. and Gehlen, M.: PISCES-v2: an ocean biogeochemical model for carbon and ecosystem studies, Geosci. Model Dev., 8(8), 2465–2513, doi:10.5194/gmd-8-2465-2015, 2015.

Behrenfeld, M. J., Boss, E., Siegel, D. A. and Shea, D. M.: Carbon-based ocean productivity and phytoplankton physiology from space, Global Biogeochem. Cycles, 19(1), 1–14, doi:10.1029/2004GB002299, 2005.

Garcia, H. E., Locarnini, R. A., Boyer, T. P., Antonov, J. I., Zweng, M. M., Baranova, O. K. and Johnson, D. R.: WORLD OCEAN ATLAS 2009 Volume 4: Nutrients (phosphate, nitrate and silicate), U.S. Government Printing Office, Washington, D.C., 2010.

Tagliabue, A., Mtshali, T., Aumont, O., Bowie, A. R., Klunder, M. B., Roychoudhury, A. N. and Swart, S.: A global compilation of dissolved iron measurements: focus on distributions and processes in the Southern Ocean, Biogeosciences, 9(6), 2333–2349, doi:10.5194/bg-9-2333-2012, 2012.

Formatted: Normal